Christoph Stangl

Non-destructive electrochemical investigations of Lithium Ion Batteries

Doctoral Thesis

Submitted in fulfillment for doctors degree of technical science

This work has been carried out under the supervision of

Univ.-Prof. Dipl.-Ing. Dr. techn. Franz Stelzer

at the

Graz University of Technology

Institute for Chemistry and Technology of Materials (ICTM)

In Cooperation with Magna E-Car Systems

2011

Deutsche Fassung:

Beschluss der Curricula-Kommission für Bachelor-, Master- und Diplomstudien vom 10.11.2008, Genehmigung des Senates am 01.12.2008

EIDESSTATTLICHE ERKLÄRUNG

Ich erkläre an Eides statt, dass ich die vorliegende Arbeit selbstständig verfasst, andere als die angegebenen Quellen/Hilfsmittel nicht benutzt, und die den benutzten Quellen wörtlich und inhaltlich entnommene Stellen als solche kenntlich gemacht habe.

Graz, am ………………………… ……………………………………………..

(Unterschrift)

Englische Fassung:

STATUTORY DECLARATION

I declare that I have authored this thesis independently, that I have not used other than the declared sources/resources, and that I have explicitly marked all material which has been quoted either literally or by content from the used sources.

……………………………… ……………………………………………..

date (signature)

Acknowledgement

First of all I am deeply grateful to my supervisor, the head of the Institute for Chemistry and Technology of Materials, Univ.-Prof. Dipl.-Ing. Dr.techn. Franz Stelzer for his guidance and support during the last three years and for giving me the opportunity to write this doctoral thesis and thereby to prove myself.

Dipl.-Ing. Dr. techn. Stefan Koller deserves special appreciation as well. His tenacity, dedication and guidance as project leader in the ChemLIB project and as chief executive officer of the Varta Micro Innovation GmbH were vital for the success of this work.

Additionally I want to thank Assoc.Prof. Dipl.-Ing. Dr.techn. Tanja Wrodnigg for her careful reading and valuable annotations on this doctoral thesis.

Generally, I have to thank the company Magna E-Car Systems and the FWF (Fonds zur Förderung der wissenschaftlichen Forschung), who funded the ChemLIB project, as well as VARTA Micro Innovation GmbH for financial support.

In this context I want to express my gratitude to the colleagues from Magna E-Car Systems, particularly Dipl.-Ing. Dr. techn. Nikolaus Hochgatterer and Dipl.-Ing. Heimo Kreimaier for their support and dedication within the ChemLIB project.

I am deeply and honestly grateful to my colleagues and friends at the Graz University of Technology and VARTA Micro Innovation GmbH. First of all I want to appreciate Dipl.-Ing. Cornelia Bayer and Dipl.-Ing Colin God, who shared with me a rental car in Canada, an office in Austria and countless memorable moments all over the world within the last four years. Furthermore, I want to thank especially Dipl.-Ing. Dr. techn. Bernd Fuchsbichler, Dipl.-Ing. Dr. techn. Harald Kren, Dipl.-Ing. Dr. techn. Barbara Rupp and Dipl.-Ing. Dr. techn.Martin Schmuck for their great friendship and collegiality.

I want to thank also my other working colleagues at the Graz University of Technology, who made my every day work enjoyable. Andrea Droisner, Dipl.-Ing. Laura Kaltenböck, Dipl.-Ing. Bsc. Michaela Scharfegger, and Stephania Toulis should be mentioned in this context. I would like to extend my thanks to all working colleagues, who were not mentioned here, as well as the non-scientific staff of the Institute for Chemistry and Technology of Materials.

I want to thank Karoline Kreuzthaler, who was the first to read and revise this doctoral thesis, but I am at least equally grateful to her support within the last months.

Finally, I have to thank my family, who supported me through all this years of study. Without you, this work would not have been possible.

Abstract

By now Lithium-ion batteries have acquired a dominant position in state-of-the-art energy storage systems. With the increasing demand for high power applications, especially caused by the automotive industry, a more precise knowledge of the processes inside of an industrially manufactured lithium ion battery is inevitable. Unfortunately, the 2-electrode assembly of a conventional battery disallows a separate investigation of the positive and the negative electrode, which would be very important to get information about the kinetics and balancing of the system and thus for optimization of the battery. Another point is to reveal positive and negative electrode processes and their interactions during battery cycling as well as the determination of aging effects either on the anode or on the cathode, which can't be distinguished in a normal battery system.

This work aimed to investigate commercial lithium ion batteries by non-destructive methods. To overcome the problem of distinction of anode and cathode effects, a third electrode, consisting of lithium metal, was inserted in industrially manufactured batteries to gain an additional reference electrode. Several electrochemical methods were used to determine the origin of cell ageing of the lithium ion batteries.

Kurzfassung

Mittlerweile haben Lithium Ionen Batterien eine dominante Position bei modernen Energiespeichersystemen eingenommen. Die steigende Nachfrage nach immer leistungsstärkeren Batterien, vor allem von Seiten der Automobilindustrie, macht eine genauere Kenntnis der Prozesse im Inneren einer industriell gefertigten Lithium Ionen Batterie unabdingbar. Leider erlaubt die Konstruktion einer konventionellen Batterie keine getrennte Betrachtung von positiver und negativer Elektrode. Diese Unterscheidung wäre jedoch von großer Bedeutung um Informationen zur kinetischen und kapazitiven Balancierung des Systems zu erhalten und die Zelle auf diese Weise zu optimieren. Generell würde eine separate Betrachtung nicht nur die Eigenschaften von Anode und Kathode, sowie ihre Interaktion während des Betriebs aufzeigen sondern auch wichtige Informationen zur Alterung von Lithium Ionen Batterien liefern.

Diese Arbeit zielte darauf ab, kommerziell erhältliche Lithium Ionen Batterien zerstörungsfrei zu untersuchen. Um eine Unterscheidung von Anoden- und Kathodeneffekten vornehmen zu können, wurde eine dritte Elektrode, bestehend aus Lithium Metall, in die industriell gefertigte Batterie eingebaut, um einen zusätzlichen Bezugspunkt zu schaffen. Verschiedene elektrochemische Methoden wurden im Anschluss angewendet, um den Ursprung der Zellalterung in Lithium Ionen Batterien zu untersuchen.

Table of Contents

1 INTRODUCTION

1.1 GENERAL ASPECTS

The use of energy plays a key role in the development of the human society by helping it to control and adapt to the environment. Managing the use of energy is one of the most important requirements in any functional society. In the industrialized world the development of energy resources has become essential for countless applications in agriculture, transportation, information technology or communications. The increasing use of energy since the industrial revolution has also brought with it a number of serious problems, some of which, such as global warming present potentially grave risks to the world (1). Therefore, a process of rethinking is triggered towards a more conserving and sustainable power generation by expediting renewable energies like solar, wind or geothermal energy systems. This is not least accounted for by rising crude oil prices and nearly exponentially increasing atmospheric carbon dioxide concentration.
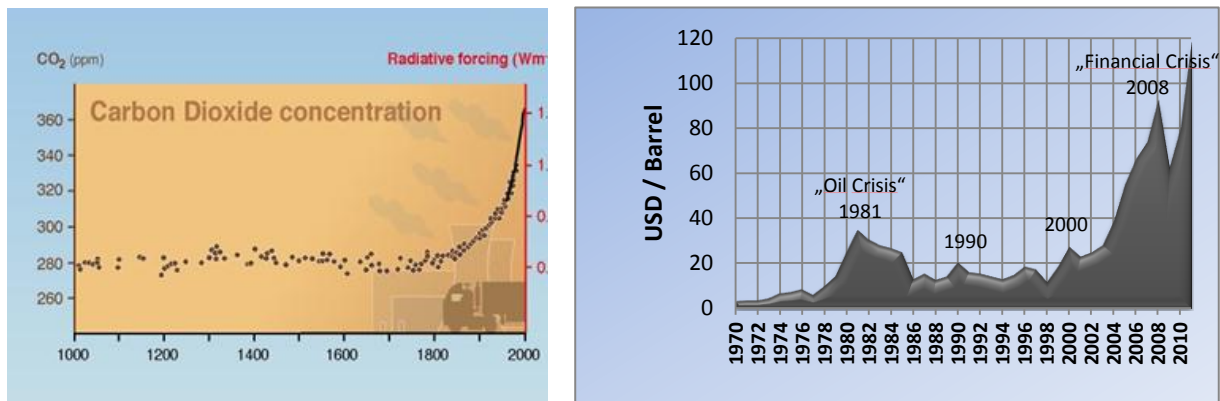
Figure 1: Atmospheric CO_2 Concentration (2) and development of crude oil price (3).

But not only the generation of energy but also its storage will receive a central significance in future. An efficient feasibility of storing energy will be essential especially in regard of transportation. According to the *European Council for Automotive R&D* (EUCAR) the future focus should be on the development of CO_2-neutral fuels from renewable energy sources, together with the vehicle technologies required for their efficient use. But also the electrification of vehicles shall play a key role in the medium- to long-term (4). The *European Commission* took the same line and published in

2001 the report "*Future Needs and Challenges for Non-Nuclear Energy Research in the European Union*", in which the lithium ion battery technology was described as one of the key enabling technologies in the facilitation of interactive energy networks with high power quality and security of service (5).

Indeed lithium ion batteries combine a relatively high energy density (Wh kg^{-1}) and power density (W kg^{-1}) compared to other energy storage systems, as can be inferred by the following Figure 2.
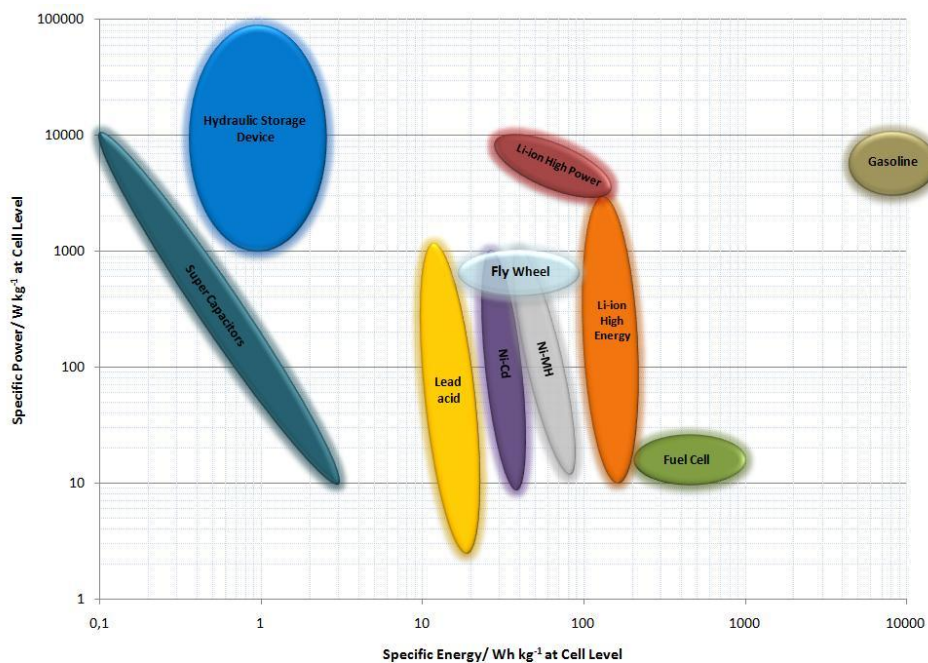
Figure 2: Ragone plot of current energy storage systems.

To return to the issue of vehicle electrification, it can be seen in Figure 2 that by now fuels achieve the highest energy per weight output. Conventional gasoline offers a specific energy of 44.4 MJ kg^{-1}(6), which is equal to about 12,000 Wh kg^{-1}. This is about 100 times more than lithium ion batteries are able to provide by now. Therefore, the prospective focus of research is on the improvement of state-of-the-art energy storage systems, especially of lithium ion batteries. The quantified targets that need to be met for future automotive batteries are listed in Table 1.

Table 1: Quantified targets for automotive lithium ion batteries until 2020 (7).

Year	2010	2015	2020
Range	>100 km	150km	200km
Energy density	>100 Wh kg^{-1}	150 Wh kg^{-1}	200 Wh kg^{-1}
Lifetime	N.A.	10 years	15 years
Cycle life	N.A.	4,000 cycles	5,000 cycles
Costs	>300€/kWh	<300€/kWh	<150€/kWh

The cell chemistry of state-of-the-art lithium ion batteries has not changed significantly during the last two decades. Most improvements, concerning energy density, rate capability or safety, have been achieved by adjusting the cell's inactive materials. But as a matter of fact, new active materials need to be found to fulfill the ambitious targets for automotive battery applications. Especially the enhancement of energy and/or power density with simultaneous decrease of costs proves difficult. The energy or power of a battery is determined by its potential and its capacity, which is the product of current and time. This relationship is displayed in Equation 1.

$$E_{el} = \int U \cdot I \cdot t = \int P \cdot t$$

Equation 1

E_{el}...   *electrical energy [Wh]*
U...   *voltage [V]*
I...   *current [A]*
t...   *time [h]*
P...   *power [W]*

As can be seen from this equation the screws that can be adjusted to enhance the overall electrical energy are either the cell's capacity or the cell voltage. Promising candidates for the next generation of lithium ion batteries are for example silicon-based electrodes, which offer a very high specific capacity of 4200 Ah kg^{-1} and therefore could replace the common graphitic anodes. On the other hand it is conceivable to replace state-of-the-art cathode materials by active materials that could provide higher redox-potentials and thus increase the cell voltage.

1.2 HISTORY OF RECHARGEABLE BATTERIES

Even though excavations near Baghdad, Iraq, suggest that ancient Parthians were already able to produce voltage in the so called "Baghdad Battery", which consisted of a copper cylinder and an iron rod in a terracotta pot, it is controversial if they really took advantage of the potential between these metals (8). Therefore, the history of battery probably starts in the late 18th century in Bologna, Italy, when Luigi Galvani (1737-1798) discovered the twitching of frosh legs whenever they came in contact with two different metals. He concluded erroneously that the twitching was evidence for the existence of "animal electricity" (9) and published his theory "*De viribus electricitatis in motu musculari commentarius* ("Commentary on the Force of Electricity on Muscular Motion") in 1791 (8). His theory was wrong but nevertheless it provided the basis for the research of Alessandro Cont di Volta (1745-1827), who interpreted Galvani's observations correctly and developed the first electric battery in 1800, called the "Voltaic pile". It consisted of alternating copper and zinc discs separated by cloth or cardboard soaked in brine to increase the electrolyte conductivity (10). With a voltage of about 1V per cell it was the first viable continuous electrical power source long way before the electric generator was invented.
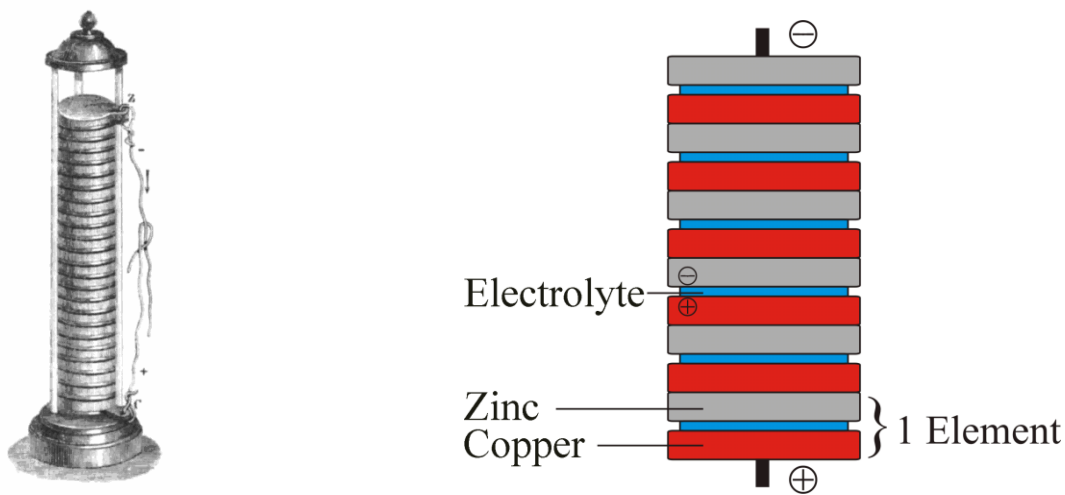
Figure 3: Historical Voltaic Pile and its composition.

The first rechargeable battery was developed by the German physicist Johann Wilhelm Ritter (1776-1810) in 1802. His pile consisted of 50 copper discs separated by cardboard discs, which were moistened by a salt solution (11). With the nascent industrialization a variety of developments emerged of which especially the lead-acid battery should be mentioned. The first rechargeable lead-acid battery was invented in 1859 by the French physicist Gaston Planté (1834-1889). Further developments made by the French engineer Camille Faure (1840–1898) (12) and the Luxembourgish

inventor Henri Tudor (1859 -1928) helped to achieve commercial success (13). Due to its low cost and good high-rate performance this battery system is even today widely used as provider of energy for engine starting, vehicle lighting and engine ignition in automobiles, boats or planes. Unfortunately, the lead-acid battery has also disadvantages like the relatively low cycle life or the limited specific energy of about 40 Wh kg^{-1} (14). In 1899, the Swedish scientist Waldemar Jungner (1869-1924) invented the rechargeable nickel-cadmium battery that consisted of nickel and cadmium electrodes in a potassium hydroxide solution. It should be the first battery that used an alkaline electrolyte. The nickel-cadmium system provided a significantly better specific energy than lead-acid batteries (up to 60 Wh kg^{-1}), but was much more expensive (12). Up to the 1990s NiCd-batteries were the most commonly used rechargeable batteries in the consumer area. In 1989 after twenty years of development the first consumer grade nickel metal-hydride rechargeable battery appeared on the market. Due to the fact that this type of battery used a hydrogen-absorbing alloy instead of toxic cadmium, it was more environmentally friendly, cost effective and provided a higher specific energy of up to 100 Wh kg^{-1} (15).

At that time it had been established for decades that lithium provided the lightest weight, highest voltage and greatest energy density of all metals. Therefore, lithium was of high interest as battery active material and several primary lithium cells were developed during the 1970s. Rechargeable systems, however, were not practical because of problems with the recharging of the metallic lithium anode (16). Ultimately cell failure could occur when deposited lithium grew unevenly and reached the positive electrode surface, leading to an internal short-circuit (17). It was the research work of J.B Goodenough and K. Mizushima (18) that meant a breakthrough, when they discovered the reversible intercalation of A_x-ion of the compound $A_xM_yO_2$, where A_x was an alkaline metal (lithium) and M_y was a transition metal (manganese, cobalt, nickel) (19). By the fact that this new type of cathode material contained available lithium, the use of graphite as anode material and subsequently waiving of metallic lithium became possible. Finally, in the year 1991, Sony used this patent and released the first lithium-ion rechargeable battery, using a $LiCoO_2$ cathode and a soft-carbon anode (19), leading to an unrivaled open-circuit voltage of 4.2 V and an operational voltage of 3.6V. Since then, there has been extraordinary amount of work on all aspects of lithium-ion chemistry, battery design, manufacture and application (16), but as already mentioned, the basic chemistry behind the lithium-ion battery, including the type of electrodes and electrolyte, has been hardly changed, apart from various additives that help to enhance the battery's performance.

1.3 RECHARGEABLE BATTERY MARKET PROSPECTIVE

In 2009 the estimated sales of primary and secondary battery devices amount up to $47.5 billion. According to experts the tendency is strongly upward, due to the growing demand for portable electronics and could lead to a $74 billion/year business in 2015 (20). In terms of rechargeable energy storage systems, a total volume of about 5 billion cells was produced; more than 50% of it related to lithium ion technologies (see Figure 4). Hence, lithium-ion batteries have acquired a dominant position in state-of-the-art energy storage systems by now.
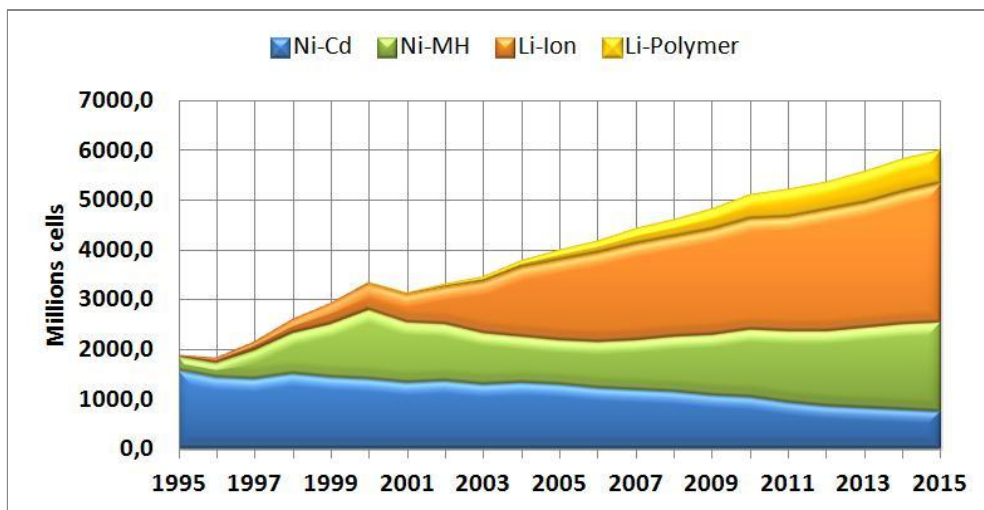
Figure 4: World-wide battery market (redrawn) (21).

Especially the Asian market benefits from this development, since all major manufactures of Lithium Ion Batteries are located either in Japan, Korea or China. In 2009 SANYO was world market leader, selling lithium ion batteries worth more than $3 billion, which is equivalent to approximately 26 % of world-wide sales. The Japanese companies SANYO, Sony and Panasonic achieve a market dominance of more than 50% in terms of world-wide sales, closely followed by Korean companies Samsung SDI and LG Chemical. US-Company EnerDel is the only Western company in this ranking, which can be seen in Figure 5, with a market share of only 0.4% (22). Europe is lagging far behind and is threatened to become just importer of lithium ion batteries (23).

Figure 5: Lithium ion battery market share (22).

The rate of growth amounts to several percent per year (24) and due to the fact that there is no equivalent energy storage system available, the end of this development is not in sight.

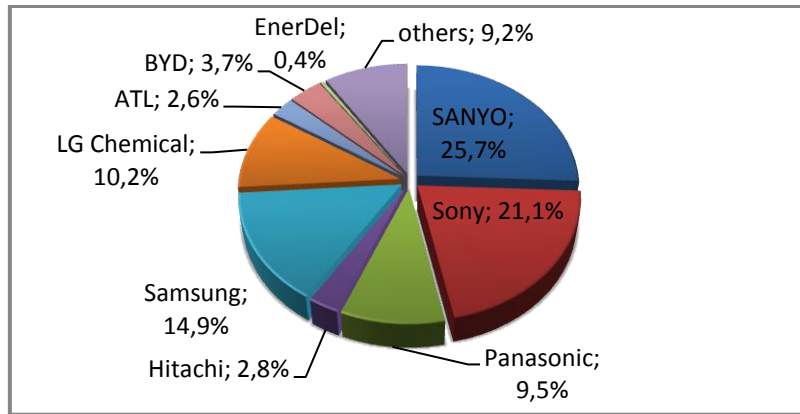If analysts are to be believed, the automotive branch will be another driving force for the expansion of lithium ion battery industry as well as for the development of more efficient, safer and cheaper lithium ion batteries (not necessarily in this order). Although the electrification of the power train gained great attention of media and of society itself within the last years, less than 5% of the total rechargeable battery production volume is referred to the automotive sector in 2010 (25).
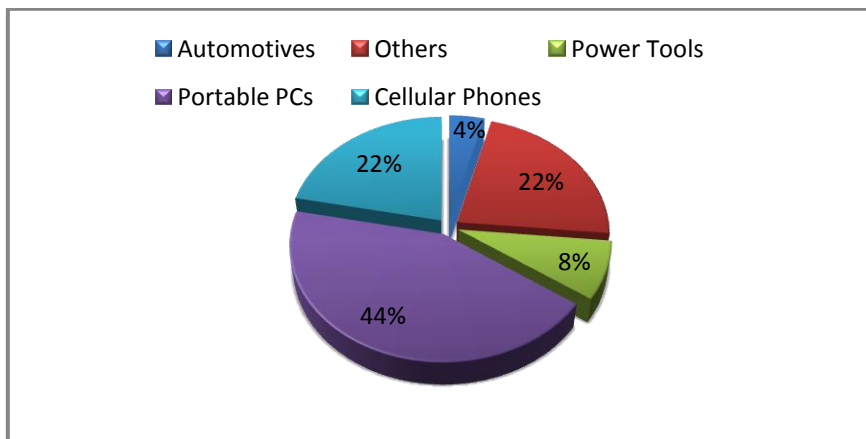
Figure 6: Distribution of worldwide rechargeable battery application in 2010 (25).

But it is estimated that the world EV market will grow from negligible levels in 2010 to about 250,000 units in 2015, and to about 500,000 units, which is still less than 1% of the anticipated 85 million annual new vehicle market. Meanwhile, the world market for plug-in electric vehicles (PHEVs) will increase from almost zero in 2010 to about 140,000 units in 2015 and 750,000 by 2020. The associated lithium ion automotive battery business (for EV, PHEV, and HEV) is projected to expand from $320 million in 2010, to $4 billion in 2015, and to $11 billion in 2020 (26).

2 THEORETICAL BASICS

2.1 ELECTROCHEMICAL POWER SOURCES

Electrochemical power sources convert chemical energy into electrical. As already mentioned in chapter 1, the amount of energy is equal to the product of voltage and capacity (see Equation 1). At least two reaction partners participate in the electrochemical oxidation and reduction reaction (22). This reaction involves the transfer of electrons from one material to another through an electric circuit, which is in contrast to other redox-reaction like the combustion of carbohydrates, where the electron transfer occurs directly. While the term "battery" is commonly used, the basic electrochemical unit being referred to be is the "galvanic cell" (27), which is also called galvanic element. Depending on the principle of operation, cells can be classified either in *primary cells*, in which the electrochemical reaction is irreversible, *secondary cells* (accumulators), which offer reversible redox-reactions and can be recharged several times or *fuel cells*, which in contrast operate in a continuous process and consume permanently reactants like hydrogen and oxygen (22). Since this doctoral thesis deals with rechargeable lithium ion batteries, subsequently the term "battery" or "cell" refers to a secondary cell, unless stated differently.

A galvanic cell usually consists of three major components (27), which will be later discussed in detail:

- The <u>anode</u> or negative electrode, which gives electrons to the external electric circuit and is for its part oxidized during the electrochemical discharge reaction.
- The <u>cathode</u> or positive electrode, which accepts electrons from the external electric circuit and is for its part reduced during the electrochemical discharge reaction.
- The <u>electrolyte</u>, which has to be an ionic conductor and provides the medium for ion transfer –and therefore charge transfer– inside the cell between the anode and the cathode. The electrolyte is typically liquid, with dissolved salts, acids or alkalis to impart ionic conductivity. But also gelatinous or even solid electrolytes are conceivable as long as they provide a good ionic conductivity.

The terms anode and cathode can be misleading due to the fact that they are normally coupled to oxidation/reduction processes. Although, in rechargeable batteries both electrodes are oxidized or reduced depending on whether the cell is charged or discharged. Therefore, it is agreed in the

community that the electrode providing the more negative potential and is oxidized during discharge, is called the anode, whereas the positive electrode is called the cathode.

2.1.1 THE GALVANIC CELL

To understand the mechanics of a galvanic cell, the buildup of the so-called Daniell Element, is shown in Figure 7. This simple galvanic cell consisted of a zinc- as well as of a copper-stick, which are dipped in an aqueous solution of their corresponding sulfates, and was invented by John Frederic Daniell (1790-1845) in 1836 (28). Due to the fact that two different electrolyte solutions are used, a salt bridge provides ion balancing and therefore prevents overpotential effects, which will be discussed later. When the cell is connected to an external load, electrons flow from the zinc anode to the copper cathode. The zinc anode is oxidized, meaning zinc ions are dissolved, whereas the copper ions are reduced at the cathode and copper is deposited.
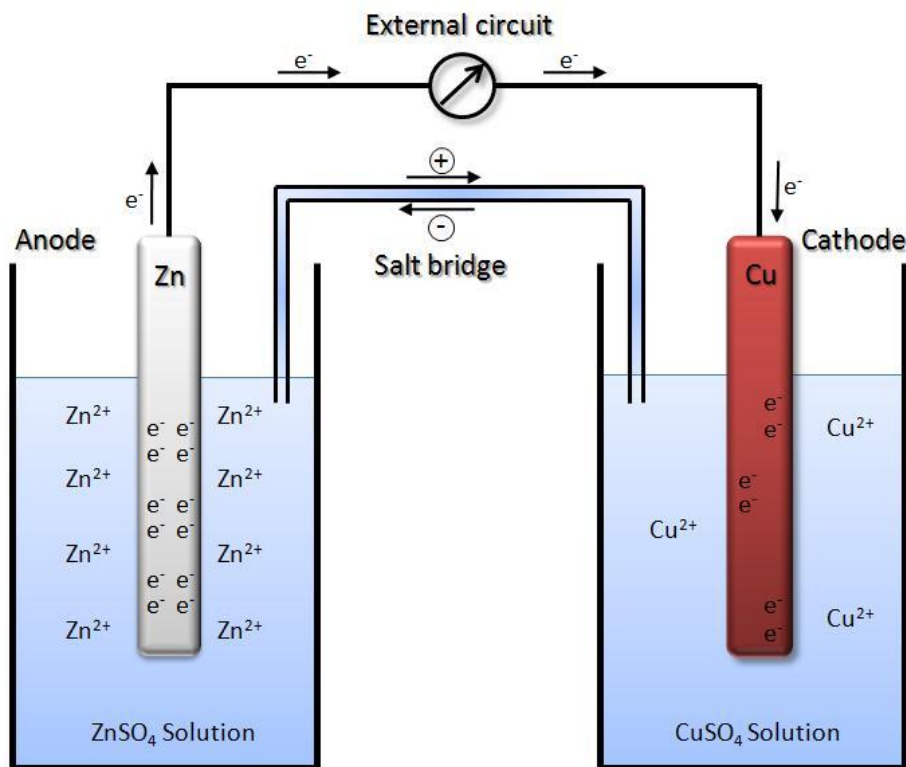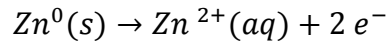

Figure 7: The Daniell-Element (redrawn) (28).

The overall reaction and the reactions of the single electrodes (half cell reactions) occurring during discharge of the Daniell Element are listed below (29):

- Negative Electrode:

$$Zn^0(s) \rightarrow Zn^{2+}(aq) + 2\ e^-$$

- Positive Electrode:

$$Cu^{2+}(aq) + 2\ e^- \rightarrow Cu^0(s)$$

- Overall reaction:

$$Zn^0(s) + Cu^{2+}(aq) \rightarrow Zn^{2+}(aq) + Cu^0(s)$$
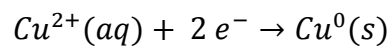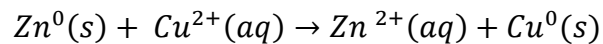
The standard potential E^0 of the cell is determined by its active materials and can be calculated from free-energy data or obtained experimentally (27).

$$E^0_{cell} = E^0_{cathode} - E^0_{anode}$$

Unfortunately, direct measurement of single electrode potentials is considered practically impossible. To establish a scale of standard potentials (half cell potentials) a reference potential is required (27). A listing of electrode potentials under standard conditions is given in Table 2. Data is normally related to the normal hydrogen electrode (NHE) but as a matter of fact, Li/Li$^+$ can be used as reference system as well, which is beneficial in case of lithium ion batteries because the zero grade of this Li/Li$^+$ scale corresponds to the anode potential in fully charged state. Therefore both reference systems are listed in Table 2.

Table 2: Electrochemical series, electrode reactions and potentials vs. H/H$^+$ and Li/Li$^+$ (27)(30) at 25°C.

Electrode		Electrode reaction	E_0 vs. H/H$^+$ [V]	E vs. Li/Li$^+$ [V]
F	Fluorine	$F_2 \rightleftharpoons 2F^-$	+2.87	5.92
O	Oxygen	$H_2O_2 \rightleftharpoons 2H_2O$	+1.78	4.83
Au	Gold	$Au^+ \rightleftharpoons Au$	+1.69	4.74
Cr	Chromium	$Cr^{6+} \rightleftharpoons Cr^{3+}$	+1.33	4.38
Pt	Platinum	$Pt^{2+} \rightleftharpoons Pt$	+1.2	4.25
Ag	Silver	$Ag^+ \rightleftharpoons Ag$	+0.8	3.85
Cu	Copper	$Cu^{2+} \rightleftharpoons Cu$	+0.34	3.40
H	Hydrogen	$2H^+ \rightleftharpoons H_2$	0	3.05
Pb	Lead	$Pb^{2+} \rightleftharpoons Pb$	-0.13	2.92
Sn	Tin	$Sn^{2+} \rightleftharpoons Sn$	-0.14	2.91
Ni	Nickel	$Ni^{2+} \rightleftharpoons Ni$	-0.23	2.82
Co	Cobalt	$Co^{2+} \rightleftharpoons Co$	-0.27	2.78
Cd	Cadmium	$Cd^{2+} \rightleftharpoons Cd$	-0.4	2.65
Fe	Iron	$Fe^{2+} \rightleftharpoons Fe$	-0.44	2.61
S	Sulphur	$S \rightleftharpoons S^{2-}$	-0.48	2.57
Zn	Zinc	$Zn^{2+} \rightleftharpoons Zn$	-0.76	2.29
H$_2$O	Water	$H_2O \rightleftharpoons ½ H_2 + OH^-$	-0.83	2.22
Mn	Manganese	$Mn^{2+} \rightleftharpoons Mn$	-1.05	2.00
Ti	Titanium	$Ti^{3+} \rightleftharpoons Ti$	-1.21	1.84
Al	Aluminum	$Al^{3+} \rightleftharpoons Al$	-1.66	1.39
Mg	Magnesium	$Mg^{2+} \rightleftharpoons Mg$	-2.38	0.67
Na	Sodium	$Na^+ \rightleftharpoons Na$	-2.71	0.34
K	Potassium	$K^+ \rightleftharpoons K$	-2.92	0.13
Li	Lithium	$Li^+ \rightleftharpoons Li$	-3.05	0

Using the data from Table 2, this implies a theoretical potential of 1.10V for the Daniell Element:

$$Zn^0(s) \rightarrow Zn^{2+}(aq) + 2\,e^- \qquad\qquad \text{- (-0.76) V}$$

$$Cu^{2+}(aq) + 2\,e^- \rightarrow Cu^0(s) \qquad\qquad \text{+0.34 V}$$

$$Zn^0(s) + Cu^{2+}(aq) \rightarrow Zn^{2+}(aq) + Cu^0(s) \qquad\qquad \underline{\textbf{1.10 V}}$$
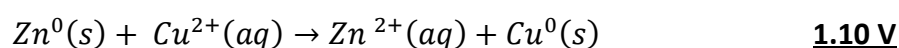
Equation 6

This voltage of 1.10V refers to equilibrium conditions, which means in general that no current flow occurs and hence it is called equilibrium cell voltage.

While describing batteries, the term open-circuit voltage **OCV** or **V$_{oc}$** is often used. The open-circuit voltage is defined as the difference of the electrical potential between the two terminals of a device, when no current flow occurs (31). On that account it is the experimentally obtained equilibrium cell voltage, which should in theory be identical to the calculated equilibrium cell voltage. In practice, however, values less than those expected are always encountered, due, for example, to the restricted ability of the electrodes to attain equilibrium or to the presence of parasitic side reaction in the cell (32).

2.1.2 THERMODYNAMIC BASICS

The driving force that enables a battery to deliver electric energy to an external circuit is the change of free energy **ΔG** (27), also known as Gibbs free energy or free reaction enthalpy. From thermodynamic point of view, ΔG can be expressed by the Gibbs-Helmholtz relation, shown in Equation 7.

$$\Delta G = \Delta H - T \cdot \Delta S$$

Equation 7

ΔG…   free energy
ΔH…   reaction enthalpy
T…   temperature
ΔS…   entropy

The terms ΔG, ΔH, and ΔS are state functions and depend only on the identity of the materials and the initial and final states of the reaction (33). In regard to electrochemical cell reaction ΔG connotes the utilizable electric energy, whereas ΔH is the theoretical available energy of the system. They differ in the product of temperature and the entropy, which corresponds to the amount of heat consumed or released during the reaction (22). While ΔG^0 is negative, the process is voluntary and happens spontaneously and work can be done until the chemical equilibrium is reached (see Figure 8).

1. $\Delta_R G = 0$ and $E = 0$ $\rightarrow$ cell is located in equilibrium
2. $\Delta_R G < 0$ and $E > 0$ $\rightarrow$ exergonic/voluntary reaction (e.g. galvanic cell)
3. $\Delta_R G > 0$ and $E < 0$ $\rightarrow$ endergonic/forced reaction (e.g. electrolysis)
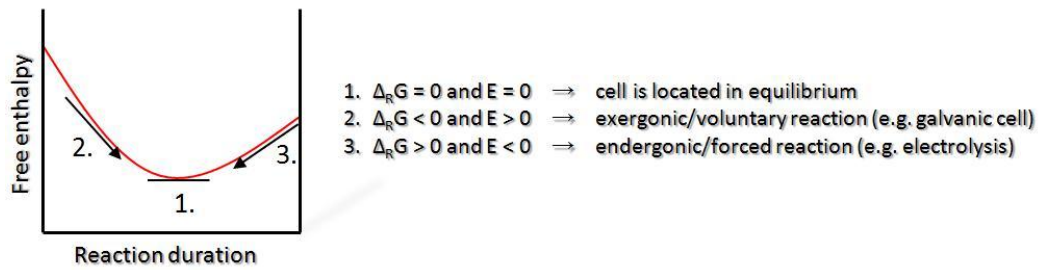
Figure 8: Difference of galvanic and electrolysis cell in terms of free enthalpy and reaction duration (redrawn) (29).

On condition that the process is isotherm and isobar, the maximum work that the system is able to perform is given by ΔG_R (29).

$$w_{e,max} = \Delta G_R$$

ΔG_R...   *free energy*
$w_{e,max}$...   *maximum of work*

If the reactants and products of the cell reaction are in their standard conditions, then the free energy is denoted by the standard value ΔG_R^0 and can also be expressed as

$$\Delta G_R^0 = -z \cdot F \cdot E^0 \text{ (32).}$$

ΔG_R^0...   *standard free energy*
z...   *number of electrons involved*
F...   *Faraday constant ($96,487$ C mol^{-1}= 26.8 Ah mol^{-1})*
E^0...   *standard electrode potential or standard electromotive force*

The Faraday constant, which is used in Equation 9, is the product of the elementary charge *e* (1.602 x 10^{-19} C mol⁻¹) and the Avogadro constant N_A (6.023 x 10^{23} mol⁻¹) (22).

$$F = \frac{I \cdot t}{n} = \frac{Q}{n} = N_A \cdot e$$

Equation 10

F…	*Faraday constant*
n…	*number of electrons involved*
I…	*current*
t…	*time*
Q…	*quantity of electricity (electric charge)*

It also plays an important role in the relationship of the electronic current I and the mass m of the substance, which donates electrons. This relationship, shown in Equation 11, is also known as Faraday's first law (22).

$$Q = I \cdot t = n \cdot z \cdot F = \frac{m}{M} \cdot z \cdot F$$

Equation 11

m...	*mass of active material*
M...	*molar mass*
n...	*molar amount*
z...	*number of electrons involved*
I...	*electronic current*
t...	*time*

Closely related to the free energy G is the chemical potential **μ** (32).

$$\mu_i = \frac{\partial G}{\partial v_i}$$

μ_i chemical potential of species i
G...   free energy
v_i...   stoichiometric factors of species i

In the presence of an electric potential E the chemical potential μ results consequently in the electrochemical potential $\overline{\mu}$. Therefore, every species inside a battery, e.g. anode, cathode or electrolyte, has its own electrochemical potential.

$$\overline{\mu_i} = \mu_i + z_i \cdot F \cdot E$$

$\overline{\mu_i}$...   electrochemical potential of species i
μ_i...   chemical potential of species i
z...   number of electrons involved
F...   Faraday constant
E...   electrode potential

All previous derivations relate to standard states but there can be other conditions, which need to be discussed additionally.

2.1.2.1 Concentration Dependence of the Equilibrium Cell Voltage

The chemical potential of one half-cell depends on the concentration c_i of the compounds, which react at the electrode (32):

$$\mu_i = \mu_{i,0} + R \cdot T \cdot \ln c_i$$

μ_i	*chemical potential of species i*
$\mu_{i,0}$	*chemical potential of species I at standard state*
$R...$	*ideal gas constant (8.314 J mol^{-1} K^1)*
$T...$	*temperature*
$c_i...$	*concentration of species i*

As a consequence, the equilibrium voltage E of a cell is also dependent on the concentration of its compounds. Combining Equation 9, Equation 12 and Equation 14 leads to one of the most important electrochemical relations, the so called Nernst equation (22):

$$E_{cell} = E_{cell}^0 - \frac{R \cdot T}{z \cdot F} \sum v_i \cdot \ln c_i$$

$E^0...$	*standard electrode potential or standard electromotive force*
$z...$	*number of electrons involved*
$F...$	*Faraday constant*
$R...$	*ideal gas constant*
$T...$	*temperature*
$v_i...$	*stoichiometric factors of species i*
$c_i...$	*concentration of species i*

2.1.2.2 Temperature Dependence of the Equilibrium Cell Voltage

The temperature dependence of the cell voltage E results from Equation 9 by partial differentiation at constant cell pressure. This ends up in Equation 16.

$$\left(\frac{\partial \Delta E}{\partial T}\right)_p = -\frac{1}{z \cdot F} \cdot \left(\frac{\partial \Delta G}{\partial T}\right)_p$$

<div align="right">*Equation 16*</div>

E…   electrode potential
z…   number of electrons involved
F…   Faraday constant
T…   temperature
G…   free energy

Combining of Equation 7 and Equation 16 finally leads to Equation 17 (32).

$$\left(\frac{\partial \Delta E}{\partial T}\right)_p = -\frac{1}{z \cdot F} \cdot \left(-\Delta S\right)_p$$

<div align="right">*Equation 17*</div>

E…   electrode potential
z…   number of electrons involved
F…   Faraday constant
T…   temperature
S…   entropy

This simply means that the reversible heat of a cell, which is the product of temperature and entropy, also influences the equilibrium potential of the cell and is well known as Peltier effect (22). If, for example, the entropy decreases during the cell reaction and therefore the state of order of the system increases in the course of reaction, then the equilibrium cell voltage will decrease with increasing temperature (32).

2.1.3 FROM GALVANI POTENTIAL TO THE ELECTROCHEMICAL DOUBLE LAYER

As a consequence of Equation 13, every species inside a battery has its own electrochemical potential. The difference in inner potentials between two phases, e.g. electrode and electrolyte, is referred to as the Galvani potential difference **Δφ** (32).
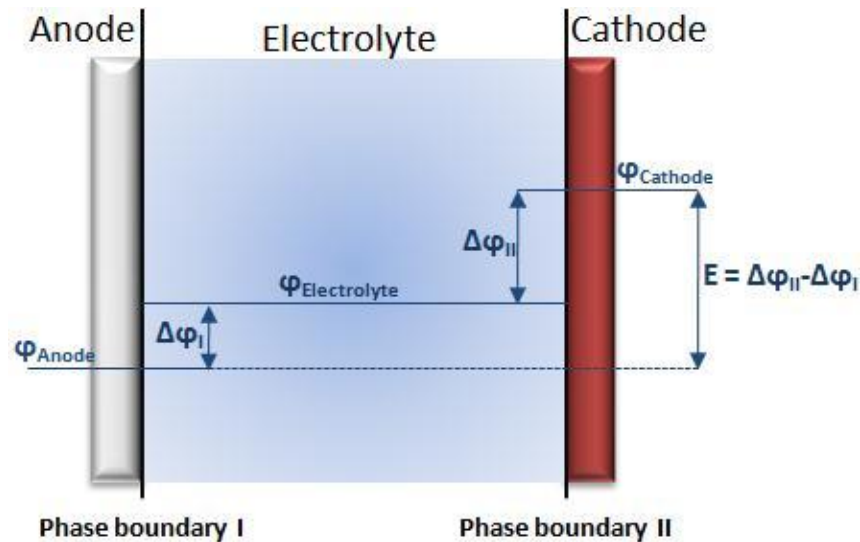

Figure 9: Galvani potentials at phase boundaries (redrawn)(32).

It has to be noticed that the direct measurement of the Galvani potential difference $\Delta\varphi_I$ und $\Delta\varphi_{II}$ is not possible, due to the fact that any device to measure this potential would create a new phase boundary with a new Galvani potential, once it would be in contact with one of the other phases.

This stage-model for the inner potentials, shown in Figure 9, fits well for a macroscopic point of view. However, close to the phase boundary the electrically charged electrode interacts with ions of opposite charge in the electrolyte and aligns the solvent dipoles. Consequently, a charged layer in the electrode as well as a layer of charge in the electrolyte is formed, henceforth referred to as electrochemical double layer (EDL) (27).

The simplest model to describe this double layer are two parallel layers of charge, one on the electrode surface and one comprising counter-ions at the distance of closest approach. This model was termed by Helmholtz the compact double layer and is nowadays known as the Helmholtz layer model (32). The Helmholtz model is redolent of a plate capacitor but is undoubtedly incomplete, because it ignores the interfering effects of thermal motion of the ions (29). Gouy and Chapman were the first, who considered the effect of thermal motion on the ions near an electrode

surface (32). Their model is comprised of a diffuse double layer and can best be compared to the well known Debye-Hückel Theory, which describes the electrostatic interaction of ions in electrolytes. The only difference is the consideration of a plane geometry at the electrode-electrolyte boundary instead of a radially symmetrical (34). The diffuse layer model, however, neglects the existence of a compact double layer and is thus incomplete as well. It was Otto Stern (1888-1969), who pointed out the most realistic model of the electrode surface. Actually his Stern-model combines the Helmholtz model and the Gouy-Chapman model. The three models are shown in Figure 10.
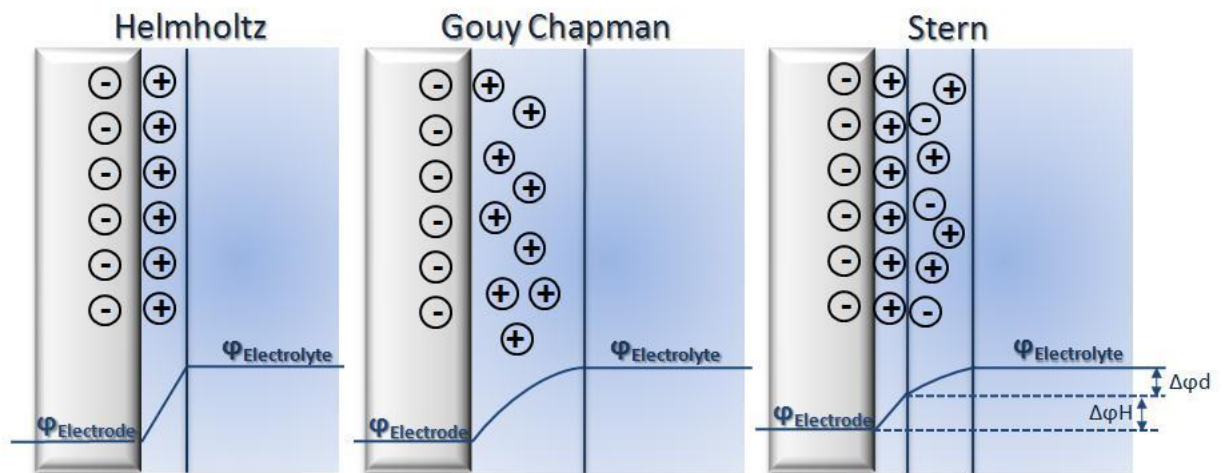

Figure 10: Helmholtz model, Gouy Chapman model and Stern model (redrawn) (32) (35).

Using the Stern model the potential drop $\Delta\varphi$ between the inner electrode and the inner electrolyte can be divided into two contributions $\Delta\varphi H$ and $\Delta\varphi d$. $\Delta\varphi H$ is the potential drop caused by the inner Helmholtz layer, whereas $\Delta\varphi d$ refers to the diffuse layer, which is also known as Nernst layer. The potential drop $\Delta\varphi d$ is also called Zeta-potential (32). The thickness of the charged layer amounts to about 0.1 nm in metals and up to 10 nm in the solvent. While the electron density is responsible for the thickness of the layer inside the metal, inside the solvent it depends predominantly on the ionic strength of the solvated ions (36). Therefore, the concentration, the activity of the ion respectively, as well as the ionic conductivity of the solvent play a primary role on the formation of the double layer.

2.1.3.1 Double Layer Capacity

As already mentioned, the electrochemical double layer can be considered as a parallel plate capacitor. As a matter of fact, there is a linear relationship between the potential between the plates, already determined as Δφ, and the charge **Q** on the plates. This constant of proportionality is also known as capacitance **C** (32).

$$Q = C \cdot \Delta\varphi \quad \text{or} \quad C = \frac{Q}{\Delta\varphi}$$

Equation 18

Q…   charge at the electrode surface
C…   capacitance
Δφ…   Galvani potential difference

Thus the capacitance describes the ability of an electrochemical double layer to hold a charge or to be precise, it is a measure of the amount of electrical energy stored (or separated) for a given potential Δφ. The capacitance of a plate capacitor is directly proportional to the surface area of the conductor plates, or, as in case of an electrochemical double layer, to the area of the electrode/electrolyte interface (37). Furthermore, the capacitance depends on the distance between the two charged layers. Its SI-Unit is farad **F**, whereas one farad is equal to one coulomb per volt.

2.1.4 *Kinetic Basics*

The thermodynamic treatment of electrochemical processes describes the equilibrium condition of a galvanic cell but does not provide information on non-equilibrium conditions such as they occur while a current flow (27). If for example a battery is discharged, a shift in the potential of the single half-cell is measured.

This deviation is on the one side due to the ohmic resistance, which is specific for every single material. On the other side there are several polarization effects, occurring during a charge flow. The sum of these effects ends up in a potential drop, which is known as the over-potential **ŋ**.

$$\eta = E - E_R$$

$\eta...$ *over-potential*
$E...$ *cell potential*
$E_R...$ *equilibrium cell potential*

The impact of overpotentials on the voltage curve of an electrode is displayed in Figure 11.
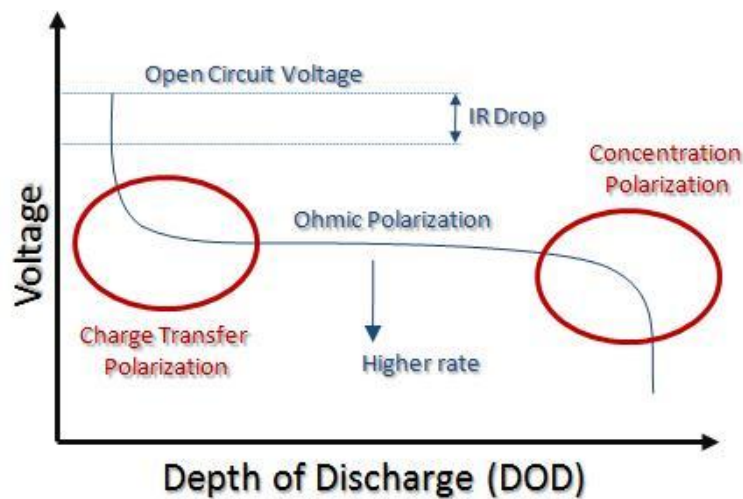
Figure 11: Overpotential effects for an electrode (redrawn) (38).

Depending on their origin, a distinction has to be made between few different types of polarization (22). Beside the ohmic polarization, the charge-transfer overpotential and the concentration overpotential are of fundamental importance for rechargeable battery applications. As it can be seen in Figure 11, these effects occur especially at very high or very low depth of discharge (DOD), meaning at the very begin and end of a charge or discharge process. Several overpotential effects are subsequently discussed in detail.

2.1.4.1 Ohmic Polarization

Nearly all materials counter the electricity transport with electric resistance. For a wide variety of materials and conditions, the electrical resistance R is constant for a given temperature and follows the Ohm's law (39) (40), which displays a relationship between current, potential difference across two points and the resistance. Due to this relationship the electric resistance results in a potential drop inside a battery as soon as the current flows.

$$\Delta E = I \cdot R_\Omega$$

<div align="right">*Equation 20*</div>

ΔE…	*Ohmic voltage drop or IR-drop*
I…	*Current*
R_Ω…	*Ohmic resistance*

The IR-drop depends on following factors (41):

- The current and potential distribution in the electrolyte and therefore the geometry of the cell
- The conductivity of the electrode as well as of the electrolyte solution
- If present, the position of the reference electrode with respect of the working electrode (If the voltage is measured exactly at the electrode surface, then the ohmic drop is zero)

2.1.4.2 Charge-transfer Overpotential

The charge-transfer overpotential or electron transfer overpotential is caused by a limitation on the speed of the charge transfer through the electrode/electrolyte phase-boundary. The kinetics of the charge-transfer is generally dependent on the nature of the electrode components as well as conditions in the electrolyte. This kind of overpotential can be described by the Butler-Volmer equation (22).

$$I = A \cdot i_0 \cdot \left\{ exp^{\frac{(1-\alpha)\cdot z \cdot F}{R \cdot T}(E - E_0)} - exp^{-\frac{\alpha \cdot z \cdot F}{R \cdot T}(E - E_0)} \right\}$$

<div align="right">Equation 21</div>

I...	current
A...	reactive surface (m^2)
i_0...	exchange current density ($A\ m^{-2}$)
α...	symmetry factor, no dimension
z...	number of electrons involved
F...	Faraday constant
E...	Cell Voltage
E_0...	Equilibrium potential

However, the Butler-Volmer equation is not valid for low over-voltage conditions, when the cell voltage and the equilibrium potential are nearly equal. Furthermore, the Butler-Volmer equation has to be replaced by the Tafel equation at high over-potential regions.

$$I = i_0 \cdot exp^{-\frac{z \cdot F}{R \cdot T}(E - E_0)}$$

<div align="right">Equation 22</div>

I...	current
i_0...	exchange current density
z...	number of electrons involved
F...	Faraday constant
E...	Cell Voltage
E_0...	Equilibrium potential

2.1.4.3 Diffusion overpotential

The diffusion or concentration overpotential concerns especially high current densities, when an impoverishment of reaction substances can occur. In the case that not enough charge carrier are present at the phase boundary, the voltage rises, whereas the limiting factor is the kinetics of the diffusion processes through the Nernst layer (22). The uneven contribution of charge carriers in the electrolyte can also influence the ionic conduction and the resistance of the liquid, respectively, (32) and hence has to be taken into account.

2.1.4.4 Reaction Overpotential

Reaction overpotential can be a result of the fact that a chemical reaction, which is coupled to the electron transfer step, is unable to keep pace. Usually this kind of overpotential is of less fundamental importance than the above mentioned representatives.

2.1.4.5 Crystallization Overpotential

The crystallization overpotential, however, is absolutely relevant for rechargeable battery systems. This overpotential exists as a result of the inhibited intercalation of metal ions into their lattice (22). Especially the charging process of metal electrodes, meaning the metal deposition on the negative electrode suffers from this overpotential (22). In case of the lithium ion battery, this concerns for instance the possible lithium plating at the negative electrode. This hazardous deposition is impeded and would occur approximately 0.1 V below the potential metallic lithium (42).

2.2 LITHIUM ION BATTERIES - THEORETICAL BASICS

Like all rechargeable batteries, the lithium ion battery is able to store energy and subsequently to provide it over duration of time. However, the amount of energy that can be stored can be led back to the amount of lithium ions that are inserted into or extracted from the so called lithium insertion compounds. As already mentioned in chapter 41.2 the commercial breakthrough of lithium ion batteries did not happen until the discovery of these insertion compounds, also known as host matrices, which were able to reversibly insert and extract lithium ions into vacancies in their structure. It is important to mention that the lithium ion in rechargeable lithium ion batteries is no redox-active species and hence just responsible for the charge transport from the anode to the cathode and vice versa. Lithium ion batteries especially stand out due to their high specific energy and energy density, which is mainly caused by the high cell voltage of more than 3 V.

State-of-the-art lithium ion batteries are in discharged state, when constructed, which is in contrast to most other battery assemblies. At the start the positive electrode material contains most of the

cell's lithium and therefore serves as lithium source. During first charge lithium ions move through the electrolyte from the cathode to the anode. This is driven by an applied external voltage. While the potential of the positive electrode rises with constant lithium extraction, the potential of the negative electrode is lowered by the continuous lithium insertion and therefore the cell voltage becomes higher (43).

At first sight, the electrochemical process of the system appears quite simple (44). The lithium insertion/extraction process occurring with a flow of lithium ions through the electrolyte is accompanied by a reduction/oxidation of the lithium insertion compound.

Simultaneously, the released electrons first pass through the current collector that consists of copper and aluminum, respectively. Both metals are excellent electronic conductors but as a matter of fact, copper can just serve as current collector on the negative electrode, because the high oxidative conditions at the positive side would cause copper dissolution, derived from Table 2. This limits the lifetime as well as the safety of the battery. Aluminum, however, is passivated by electrolyte components and hence protected against further corrosion. This will be discussed more in detail in chapter 2.2.3. Unfortunately, aluminum cannot serve as current collector for the negative electrode, because lithium and aluminum begin to form a very brittle intermetallic phase at a potential of about 2 V versus Li/Li^+. In theory this would be advantageous, because the amount of lithium uptake would be increased. In practice, however, this alloy formation is accompanied by high volume changes, which leads to micro-cracks within the current collector and hence destroys the structural integrity of the electrode (45).

Finally, after passing the current collector the electrons flow through the external circuit (46). A schematic drawing of a lithium ion battery is shown in Figure 12.
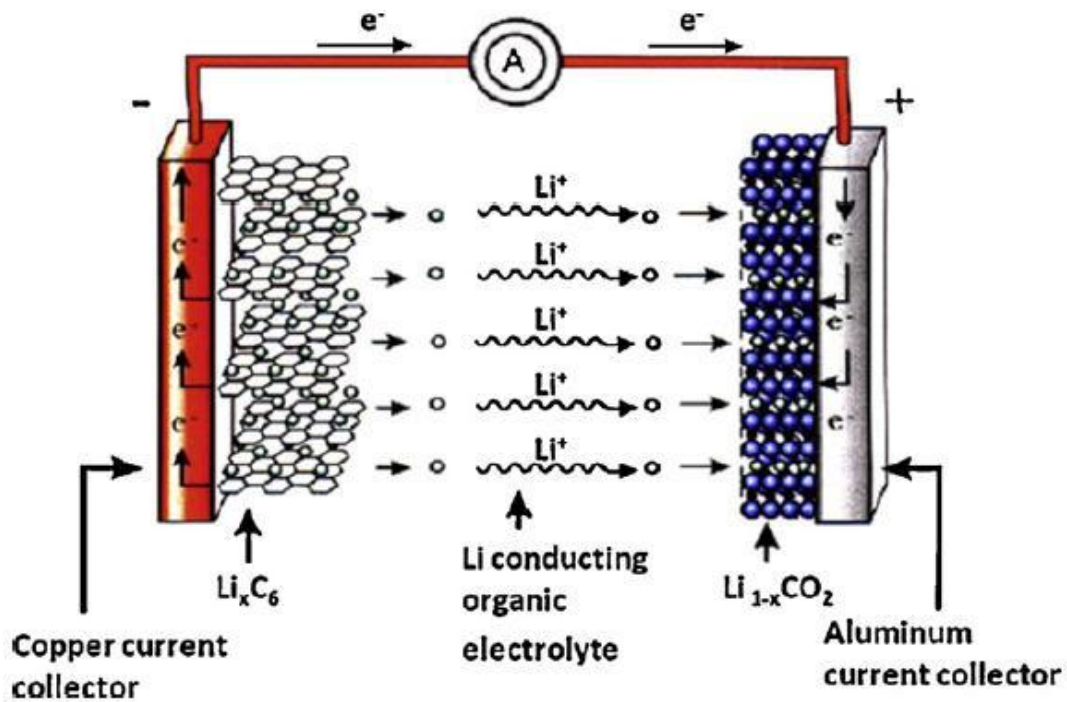
Figure 12: Schematic drawing of a lithium ion battery (44).

As described in previous chapters the maximum energy of a cell is determined by the cell voltage, meaning the difference of electrochemical potential of negative and positive electrode and the amount of charges that can be stored or provided from the battery, thus the capacity. The electrochemical potential of lithium storage compounds refers to the potential that is required for spontaneous reversible lithium intercalation and therefore is called lithium chemical potential μ_{Li}. It is obvious that electrode materials should provide a large difference regarding to lithium chemical potential to enhance the overall cell voltage and as a result also the energy. The factors that determine μ_{Li} vary in principle. In carbon anodes for example, the lithium chemical potential corresponds to the Fermi energy in an itinerant-electron band, while the energy of a redox couple of a transition-metal cation determines μ_{Li} in common cathode materials (47).

By the fact that state-of-the-art anode materials operate at potentials just about the potential of metallic lithium, which represents the negative maximum of the electrochemical series (see Table 2), the voltage increase has to be caused by the choice of the cathode material. In general, this means that the transition metal ion M^{n+} in the $Li_xM_yX_z$ compound should have a high oxidation state (46). By distinguishing cathode materials regarding their electrochemical potential versus lithium, a classification can be made into 3 V, 4 V and 5 V materials. This will be discussed in detail in chapter 2.2.2.

Moreover, both host materials should offer a large number of available sites for lithium insertion and the accessibility of multiple valences for the redox-active compound to enhance the amount of stored lithium ions and therefore to improve capacity (46). The number of available lithium sites as well as the velocity of lithium ion diffusion within the host material is determined by the structure of the insertion compound. A classification can be made on the base of their structure into one-, two- or three-dimensional host matrices. The three possibilities are schematically represented in Figure 13.
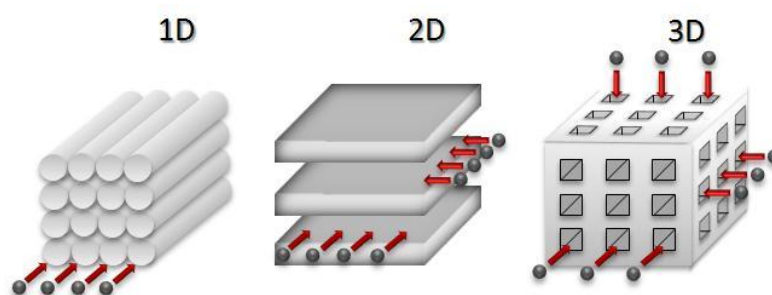
Figure 13: Lithium ion insertion into one-, two-, and three-dimensional host materials (redrawn) (48).

Both electrochemical potential and lithium storage capacity are material-specific properties. There are several additional requirements for lithium storage compounds, which are listed below (46):

- The compound should have a good structural stability without breaking any M-X bonds in order to provide a good cycle life for the cells. For that reason the host structure should hardly change over the entire range x of lithium insertion/extraction. Furthermore, it should be chemically stable without undergoing any reaction with the electrolyte.

- Lithium-ion conductivity σ_{Li} is one main cause of overpotential in lithium ion batteries and thus should be as high as possible. Simultaneously, a good electronic conductivity is important to ensure the transport of electrons to/from the external circuit.

- From a commercial point of view, the insertion compound should be inexpensive, environmentally benign and provide a good specific energy and energy density, so volume and weight should be as low as possible.

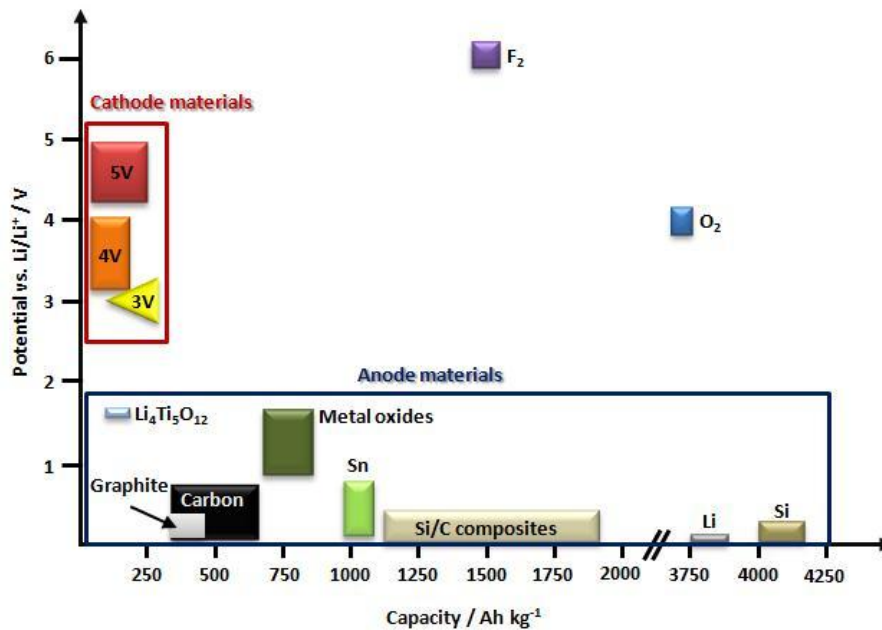A pool of possible active materials is illustrated in Figure 14.

Figure 14: Anode and Cathode materials for lithium ion batteries (redrawn) (49).

To realize an entire electrode for a lithium ion battery, however, adhesion of the active material particles to the current collector as well as among themselves has to be guaranteed. Therefore, electrodes contain binder systems that are responsible for this adhesion. State-of-the-art binder system is polyvinylidendifluoride (PVdF), which is soluble only in organic media. There have been approaches to replace this binder by aqueous soluble polymers like styrene-butadiene rubber (SBR) or sodium carboxymethylcellulose (Na-CMC), especially in regard to silicon anodes (50). Due to the fact, that these polymers can't conduct electrons, the addition of binder molecules leads to a decrease of electronic conductivity of the overall electrode. Hence, conducting agents like carbon black have to be added to prevent power loss traced back to bad electronic conductivity.

In the following chapters the most important components of a lithium ion battery, including anode materials, cathode materials as well as electrolyte components, are discussed in detail.

2.2.1 THE NEGATIVE ELECTRODE

In state-of-the-art lithium ion batteries the use of graphite or other carbonaceous materials as active mass of the negative electrode is commonly applied. The reasons behind the commercial success of carbon-based anodes include low inherent cost of carbon, the excellent reversibility of lithium insertion (17) accompanied with its extremely negative electrochemical potential close to that of metallic lithium (51). The charge and discharge reactions can be simply described as

$$C_n + x \cdot Li^+ + x \cdot e^- \rightleftharpoons Li_x C_n$$
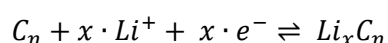
The electrochemical lithium insertion properties of carbonaceous materials mainly depend on the crystallinity and morphology of the host material. This affects the current/voltage characteristics of the electrochemical insertion reaction and possible side reactions (42). Considering that plenty of possible materials exist, a classification is inevitable. A rough distinction can be made by classifying the carbon based materials as graphitic (ordered) or non-graphitic (disordered). Due to the fact that most measurements in this doctoral thesis have reference to graphitic carbon, this anode material is subsequently discussed in detail.

2.2.1.1 Graphite as Negative Electrode Material

Graphite is a typically layered compound, which means, in respect of Figure 13, it is a two-dimensional host material that consists of hexagonal graphene sheets of sp^2-hybridized carbon atoms. In this context, term "intercalation" is often used, which means the insertion of lithium ions into the interlayer gaps of a layered host (42). The layers, the graphene sheets respectively, are bonded together by relatively weak Van der Waals forces into an AB – stacking sequence (hexagonal graphite or α-phase) along the x-axis, as shown in Figure 15 (51). The distance between two layers A and B in this stacking order amounts to 3.354 angstrom **Å** or 0.3354 nm respectively.
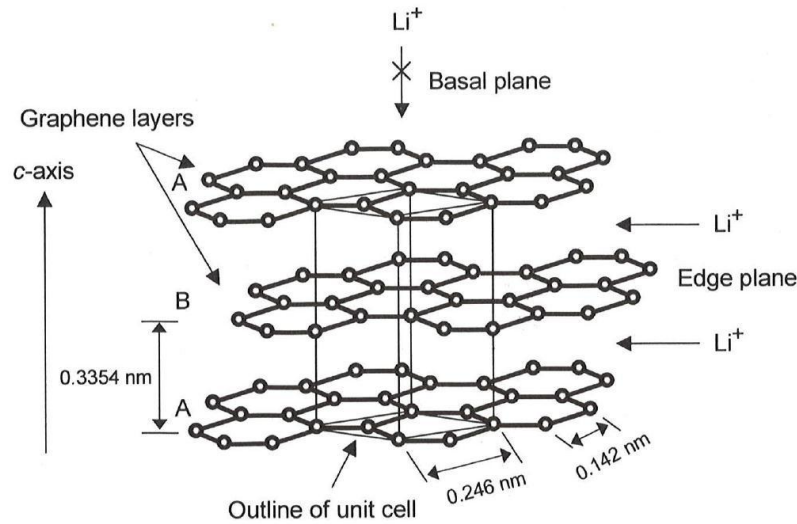
Figure 15: Crystal structure of hexagonal graphite showing the AB – stacking of graphene sheets and the unit cell (51).

Instead of the ABAB – stacking order, an ABC – stacking order (rhombohedral graphite or β-phase) is possible as well. Due to the small energy for transformation of AB into ABC stacking (and vice versa), mixed-type graphite can easily occur (42). It is apparent in Figure 15 that graphite has two distinct surfaces present, the basal plane and the edge or prismatic plane (52) and it is well known that those two planes show a different electrochemical behavior in many respects. Regarding the intercalation of lithium ions, insertion proceeds solely via the edge plane surface (42). During intercalation the stacking order of the carbon layers shifts to AA, while simultaneously the interlayer distance between the graphene layers increases moderately to 0.370 nm, which corresponds to an increase of volume of about 10% (48).
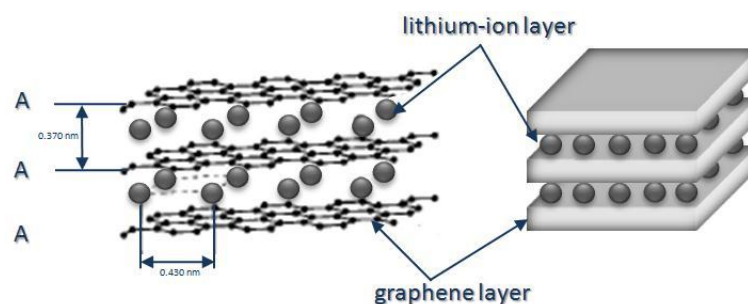
Figure 16: Schematic drawing showing the AA layer stacking sequence of carbon with intercalated lithium (redrawn) (48)

In general, the intercalation of lithium in graphitic carbons occurs in stages, meaning a periodic array of occupied and unoccupied layers is formed at low concentrations of the guest species. This stageing is a thermodynamic phenomenon due to the fact that few but highly occupied van der Waals gaps are energetically favored over a random distribution of lithium ions. The stepwise intercalation of

lithium as well as the degree of insertion can be easily observed during electrochemical reduction of carbons in Li$^+$ containing electrolytes (42) (48).
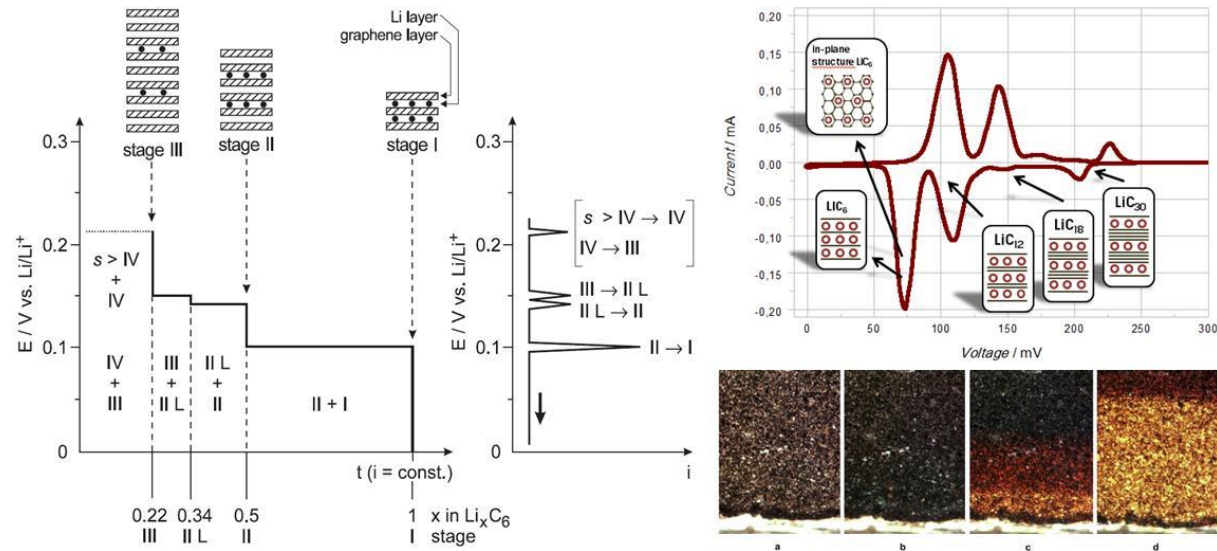

Figure 17: Stage formation during electrochemical intercalation of lithium into graphite. Schematic galvanostatic curve (left), schematic voltammetric curve (middle) (48), cylcovoltammetric measurement provided by S. Koller (upper right) and a sequence of four optical micrographs showing the time-evolution of color in the electrode (lower right) (53), modified by H. Kren and C. God.

The stepwise intercalation of lithium ions into the interlayer gaps of graphite is illustrated in Figure 17. Considering Equation 23, no lithium ions are intercalated at begin of the charge, so the stoichiometry of the Li$_x$C$_6$ compound is defined by x=0. In succession a Li$_{0.2}$C$_6$ compound is formed at a potential of about 0.21 V vs. Li/Li$^+$ (51). Due to the fact that the chemical potential of Li in coexisting phases is equal, coexisting phase regions appear as plateaus in plots of the voltage V$_{(x,T)}$ of Li/Li$_x$C$_6$ cells versus x at constant temperature (54), while under potentiodynamic control current peaks indicate two phase regions (see Figure 17). The charging proceeds with the formation of a Li$_{0.3}$C$_6$ phase at about 0.15V vs. Li/Li$^+$ and a Li$_{0.5}$C$_6$ phase at about 0.12V vs. Li/Li$^+$ (51). The maximum lithium content that can be stored amounts to one lithium ion per six carbon host atoms, leading to the last phase, which is equal to a LiC$_6$ stoichiometry (48)(55). As a matter of fact there are no sharp discontinuities between the two-phase regions due to slightly varying packing densities of Li$_x$C$_6$ and various types of overpotential, which leads to plateau sloping in galvanostatic measurements and peak broadening in voltammetric measurements, respectively (48). Using Equation 11 the theoretical capacity of these compounds can be calculated.
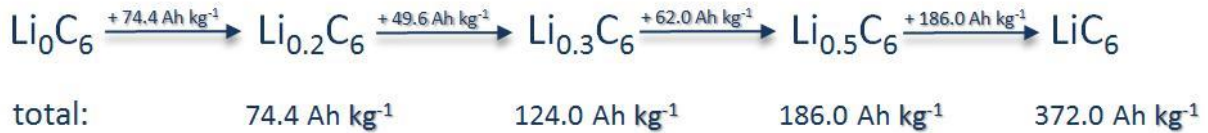
$$\text{Li}_0\text{C}_6 \xrightarrow{+\,74.4\ \text{Ah kg}^{-1}} \text{Li}_{0.2}\text{C}_6 \xrightarrow{+\,49.6\ \text{Ah kg}^{-1}} \text{Li}_{0.3}\text{C}_6 \xrightarrow{+\,62.0\ \text{Ah kg}^{-1}} \text{Li}_{0.5}\text{C}_6 \xrightarrow{+\,186.0\ \text{Ah kg}^{-1}} \text{LiC}_6$$

| total: | 74.4 Ah kg^{-1} | 124.0 Ah kg^{-1} | 186.0 Ah kg^{-1} | 372.0 Ah kg^{-1} |

Figure 18: Calculation of the theoretical capacities of Li$_x$C$_6$ compounds.

In practice, however, the consumed capacity during the first charge exceeds the theoretical specific capacity of 372 Ah kg^{-1} by far. In the subsequent discharge step, the lithium ion recovery amounts to about 80-95% of this capacity. In the following cycles the charge consumption during intercalation is lower and matches well with the assumed theoretical data. Besides the charge recovery is close to 100%.
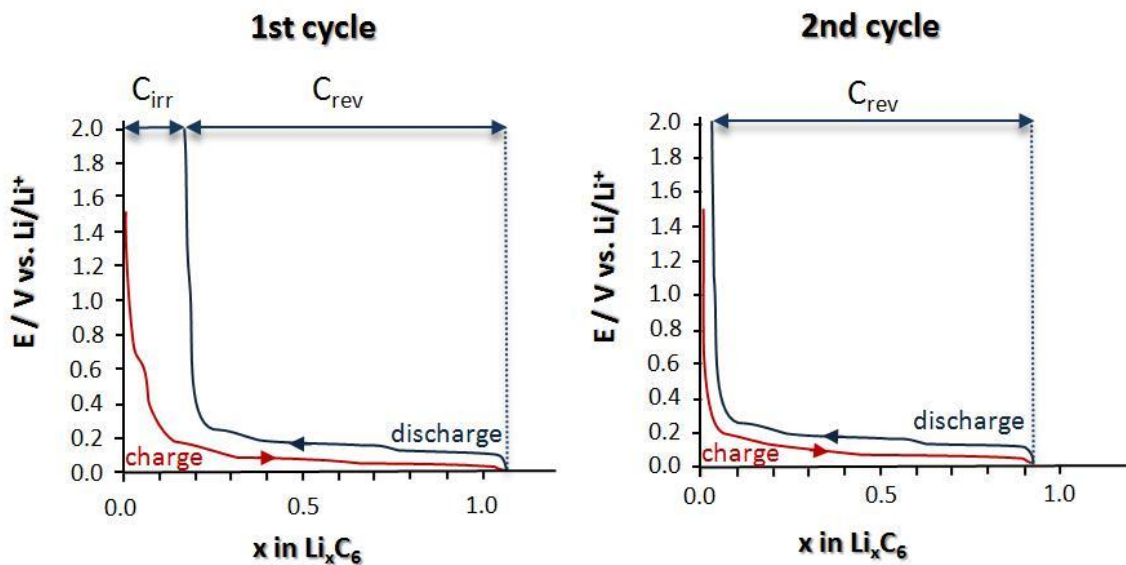
Figure 19: Constant current charge/discharge curves of 1st and 2nd cycle of Timrex KS44 graphite (redrawn) (48).

This excess charge, which is irreversibly lost in the first cycle, is generally ascribed to the formation of the so called "solid electrolyte interphase" (SEI) together with corrosion-like reactions of Li$_x$C$_6$ (42). The SEI is the result of thermodynamic instability of the electrolyte towards the highly reductive potential at the surface of the negative electrode and will be discussed in detail in chapter 2.2.3.

2.2.2 THE POSITIVE ELECTRODE

Countless cathode materials have been proposed for rechargeable lithium ion batteries within the last 20 years. Winter et al. classify these materials into three main groups: i) inorganic transition-metal oxides and chalcogenides, ii) organic molecules, and iii) polymers, whereas the latter two groups have gained only subordinate importance compared to the enormous amount of research work that has been done on this topic (42).

Within the inorganic transition metal oxides another classification can be made by the distinction of the achievable overall cell voltage, which is dependent of the lithium chemical potential of the positive electrode. There are materials known that operate averagely at 3 V, 4 V and even 5 V vs. Li/Li^+. Materials operating at 3V usually contain no lithium after synthesis and hence cannot serve as lithium ion source. Representatives of this class of cathode materials are TiS_2, MoS_2 or MnO_2 (56). Due to the fact that the anode has to contain lithium, when using one of these materials, their commercial importance narrows down to primary lithium metal batteries. State-of-the-art lithium ion batteries, however, use 4 V cathode materials, which include available lithium in their structure and hence are assembled in discharged state. Most common cathode materials, comprising compounds with the formula of $LiMO_2$ (M: Mn, Co, and Ni), can be assigned to the group of 4 V materials. Recently, materials with even higher lithium chemical potential were introduced, e.g. $LiNiPO_4$ with a theoretical redox-potential of 5.1 V, which was proved to lie practically between 5.1 V and 5.3 V (57) (58). These materials can be classified as 5 V materials and due to their high potential they offer much more energy in a rechargeable battery assembly. Unfortunately, there are drawbacks that inhibit a commercial breakthrough by now. Besides a required optimization in terms of electronic conductivity and lithium ion diffusion the thermodynamic instability of most electrolyte systems at these potentials is a major obstacle. Additionally, cathode materials can be distinguished by its structure (see Figure 13). The three major classes of cathode materials and their most important representatives are discussed subsequently.

2.2.2.1 Layered Transition-metal Oxides

Layered, and hence two-dimensional, lithium transition-metal oxides arguably represent the most successful category of positive electrode materials. In the ideal layered $LiMO_2$ structure, the Li^+ and the M^{3+} ions occupy octahedral sites in alternate layers between cubic close packed oxygen layers (59). The cations in this so called α-$NaFeO_2$ structure order in alternating (111) planes (46). This topology offers highly accessible lithium ion diffusion pathways (60). The layered structured is displayed in Figure 20.
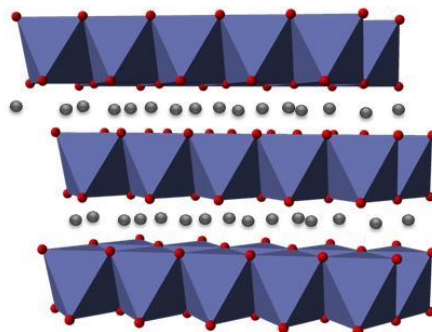
Figure 20: The two-dimensional pathway structure of $LiMO_2$ (61).

Among these layered compounds, lithium cobalt oxide (**$LiCoO_2$**) is not only the first material used as cathode in a commercial lithium ion battery (see chapter 1.2), but also the material of choice in many state-of-the-art assemblies. $Li_{1-x}CoO_2$ offers a relatively high theoretical capacity of 274 Ah kg^{-1} and a relatively high lithium diffusion rate of about $5x10^{-9}$ cm^2 s^{-1}. The electronic conductivity, however, changes dramatically with its composition, behaving like a metal at x=0.6 and like a semiconductor at x=1.1 (62). $LiCoO_2$ involves some more drawbacks. Cobalt is not only environmentally critical but more expensive than other transition metals, like manganese, nickel or iron. Simultaneously, the theoretical capacity of $Li_{1-x}CoO_2$ cannot be achieved by far, because the structure undergoes a phase transition at about x=0.5, which is accompanied by a release oxygen from the oxide (63) and progressive electrolyte decomposition due to the high electrochemical potential of the electrode (64). Consequently, $LiCoO_2$ is highly sensitive to overcharge conditions (65).

2.2.2.2 Spinel-structured Transition-metals

Electrodes with the typical spinel-type structure, $A[B_2]X_4$, have been in focus over the past 20 years (59). This can be explained by the fact that on the one hand many spinel compounds exist in nature and furthermore there are a plenty of considerable types of cations and valences. The most common and hence most studied representative of this group is lithium manganese oxide (**LiMn$_2$O$_4$**). The anion lattice of this compound is, similar to layered structures, related to α-NaFeO$_2$ with cubic close-packed oxygen ions. The only difference concerns the distribution of the cations among the available octahedral and tetrahedral sites (62). This leads to cross-linked channels that allow lithium diffusion in three dimensions (48) (66).
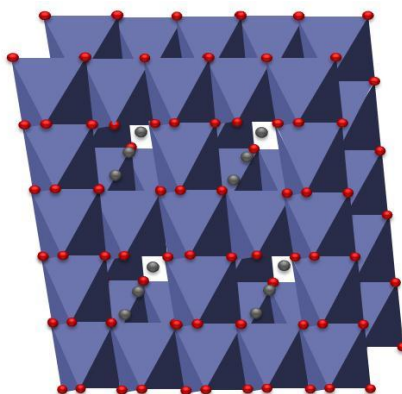
Figure 21: The three-dimensional pathway structure of LiMn$_2$O$_4$ (redrawn) (59).

Due to this three-dimensional framework structure and depending on the route of synthesis and its conditions as well as the measurement techniques, chemical diffusion coefficients in the range of $10^{-8} - 10^{-10}\,cm^2\,s^{-1}$ could be obtained (48) (67). The theoretical capacity of the compound, obtained from Equation 11, amounts 148 Ah kg^{-1}. With a flat operating voltage curve of 3.95 V-4.1 V vs. Li/Li$^+$ (68) LiMn$_2$O$_4$ would be predestinated to replace LiCoO$_2$ in state-of-the-art lithium ion battery applications, particularly since manganese is abundant, inexpensive and environmentally benign. However, structural changes in the material occur in the 3 V region and cause a 6.5% increase in unit cell volume. Subsequently a loss in structural integrity and a rapid capacity fade is the result. Therefore, LiMn$_2$O$_4$ could be used only in the 4 V region, which limits the capacity to a practical level of about 120 Ah kg^{-1}(46). Additionally, manganese can dissolute at the end of discharge, when the concentration of the Mn^{3+} ion is at the highest level. Mn^{3+} is believed to undergo a disproportionation reaction and form solid Mn^{4+} and soluble Mn^{2+} (59). Subsequently the dissolved manganese tends to poison the surface of the anode during cycling (63). Basic approaches have been

made to overcome this structural problems that lead to an inacceptable capacity fade. For instance the partial substitution of manganese by nickel or lithium can help to prevent manganese dissolution (69).

2.2.2.3 Olivine-type Cathode Materials

In 1996 Padhi et al. reported a new type of lithium insertion materials: olivine-structured polyanionic cathodes (70). In analogy to the spinel framework, the general formula of this compounds account to AB_2X_4 and olivines are quite abundant in nature as well. The most popular representative of this group is lithium iron phosphate (**LiFePO$_4$** or **LFP**), which can be found in nature as tryphilite. The charged $FePO_4$ on the other hand is referred to the heterosite structure (71) (72). The non toxicity and the low cost of materials and synthesis as well as the high theoretical capacity of 170 Ah kg^{-1} make this compound a very promising candidate for the use in industrial lithium ion batteries (73). Additionally, the phosphate positive-electrode is less susceptible to heat an overcharge conditions and therefore demonstrates greater safety characteristics than $LiCoO_2$-based systems (68).

$LiFePO_4$ is isostructural with the common mineral peridot ($Mg_{2-x}Fe_xSiO_4$), where the phosphor atoms substitute for the silicon atoms while the lithium atoms replace magnesium. The structure may be regarded as layered, due to the fact that layers of Fe^{2+} and P^{5+} ions alternate with layers of Li^+ ions in a direction perpendicular to the close-packed oxygen. Here the P^{5+} ions form a PO_4 tetrahedra, while the Fe^{2+} ions form an edge-shared FeO_6 octahedra. A second octahedral site is formed by lithium and the edges of the PO_4 tetrahedra. Thus, in the olivine structure of $LiFePO_4$ there are two crystallographically independent octahedral sites. Both, however, are energetically unfavorable for additional Li occupation because they share several faces with neighboring, occupied polyhedral (74). This connectivity has a special impact on both electronic and ionic conductivity in lithium iron phosphate (73). The structure of the compound is shown in Figure 22.
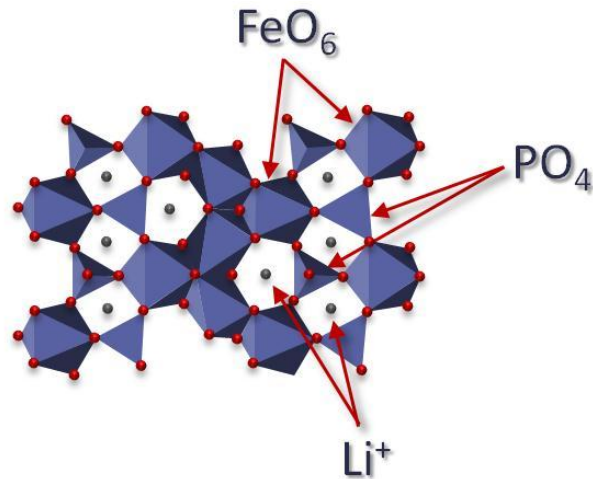
Figure 22: The one-dimensional pathway structure of LiFePO$_4$ (redrawn) (75).

The change of tryphilite to heterosite and vice versa, so the lithiation/delithiation during charging/discharging is a small first-order displacive mechanism and gives a two-phase separation over most of the solid-solution range 0>x>1 of Li$_{1-x}$FePO$_4$. This results in a very flat voltage curve with one insertion plateau at about 3.4 V (76). It was assumed by Goodenough et al. that the lithium insertion proceeds from the surface of the particle moving inward behind a two-phase interface. Consequentially, the surface area of the interface shrinks with proceeding insertion. Hence, the lithium-transport gets diffusion-limited, when the available surface area reaches a critical level and is not able to sustain the current anymore (71). A schematic illustration of this process is shown in Figure 23.
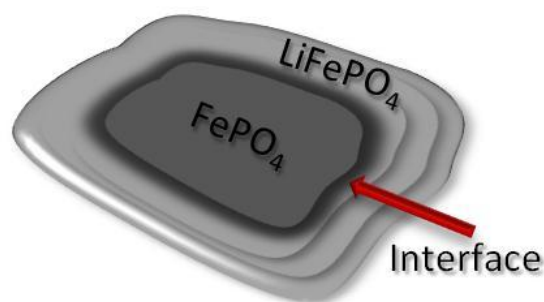
Figure 23: Illustrated motion of the LiFePO$_4$/FePO$_4$ interface on lithium insertion to a particle of FePO$_4$ (redrawn) (71).

As a matter of fact, lithium ion diffusion through the FeO$_6$-layers is blocked, but there are still two spatial directions conceivable. But although 2D- diffusion pathways through the particles are available (76), it was proved that the lithium ion motion is just one-dimensional (77) (78). This can be

explained by the fact that one path is energetically unfavored and the lithium ions perform a so called stenmark-rotation to move along the path that requires a minimum energy (78).

In peridot, the manganese and iron ions can partially change positions. In case of lithium iron phosphate an exchange of iron and lithium would be disadvantageous because any Fe^{2+} ion within the lithium layers would reduce not only the Li^+ ion conductivity but also the ease of extracting the entire lithium from the olivine framework (74). Structural inhomogeneity in olivine compounds is much more critical than structural defects in layered or spinel frameworks because the blockage in 1D diffusion pathways is fundamentally different from blockages in 2D and 3D diffusion paths, where ions can move around blocked sites (77). Hence, the theoretical maximum capacity of 170 Ah kg^{-1} cannot be achieved, so the conditions of synthesis have to be carefully controlled to guarantee an as ideal structure as possible (74).

Beside the relatively low cell voltage that can be obtained when using $LiFePO_4$- cathodes the low electronic conductivity of 10^{-9} $S \cdot cm^{-1}$ and the associated poor rate capability of the material is another major drawback. Improvements of rate capability have been achieved by synthesizing nano-scaled particles (79) as well as by an electronic conductive particle coating (80) (81).

2.2.3 THE ELECTROLYTE

Electrolytes for battery applications usually consist of a conducting salt that is dissolved in one or several solvents. The basic requirements of such an electrolyte system in any electrochemical device can be simply summarized to high ionic conductivity, low melting and high boiling point, chemical and electrochemical stability and safety. In regard to an applicable system, low cost and environmental friendliness have to be added to this list.

In general, potential classes of electrolytes for lithium ion batteries can be divided into liquid electrolytes, ionic liquids, solid polymer electrolytes and hybrid electrolyte systems (47). Due to the fact that liquid electrolytes, especially organic liquid electrolytes, represent the most common and hence most important class and furthermore complete measurements within this work refer to liquid electrolytes, they are subsequently discussed in detail.

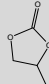### 2.2.3.1 Organic Liquid Electrolytes

Because of the high cell voltage and the associated high reduction and oxidation potential at the surface of the electrodes, aqueous as well as protic electrolyte systems seem to be inappropriate for an assignment in lithium ion batteries. Indeed, there are just a few organic compounds that can tolerate such a wide voltage range of about 4 V without being oxidized (82).

High ionic conductivity and a low ohmic resistance, respectively, are essential in lithium ion batteries, because high internal resistance would lead to unwanted heating of the cell, especially at high current rates. Hence, an ionic conductivity of $>10^{-3}$ S cm^{-1} is required, which is still two orders of magnitude lower than conductivities of aqueous electrolytes. Simultaneously, a wide temperature range of -40°C to 90°C is desired and the lithium transference number has to be as high as possible to minimize concentration polarization effects (83).

To fulfill these requirements, the choice of the inorganic conducting salt is of key importance. The first issue that has to be regarded is the sufficient solubility of the conducting salt. In order to dissolve a conducting salt in a solvent several factors have to be considered. For example, the interaction energies between solvent molecules, including the all-electrostatic, polarization, and dispersion energies as well as the lattice energy of the conducting salt, need to be overcome (82). Beside the permittivity also called dielectric constant ϵ of the solvent, which should be as high as possible, it can be generally assumed that the solubility of the salt depends on its anion. Small anions, like chloride, would be preferable in terms of conductivity but unfortunately salts like lithium chloride (LiCl) have a very high lattice energy, which impedes the dissolution of the molecules. Alternatively large monovalent anions like ClO_4^- or PF_6^- are used, which offer a good solubility and ionic conductivity. For that reason the high molar mass and property to increase the viscosity of the electrolyte are tolerated (84). This deliberation limits the possible variants for solvents as well as for salts. From the very beginning of lithium ion battery development lithium hexafluorophosphate (LiPF$_6$) has been the standard salt in more or less any application (85) and until now it is the conducting salt of choice. LiPF$_6$ is not only unstable at higher temperatures, but also corrosive and harmful, when swallowed (86) Due to that reason, tremendous efforts have been made to replace it by other molecules like lithium perchlorate (LiClO$_4$) or lithium tetrafluoroborate (LiBF$_4$) (87). Unfortunately, these components suffer from other serious disadvantages. LiClO$_4$, for instance, is thermally unstable and shows explosion risks, especially, when solved in ethers, while LiBF$_4$ offers just moderate ionic conductivity (88). So concerning the performance of the battery LiPF$_6$ is the best compromise and there seems to be no way to get past it within the next years.

As already mentioned, a high dielectric constant is necessary to dissolve $LiPF_6$. Hence, compounds are needed, which tolerate the wide potential window of lithium ion batteries, and on the other hand offer polar groups such as carbonyl (C=O), nitrile (C≡N), sulfonyl (S=O) and ether-linkage (-O-) (87). For that reason organic carbonates are of key importance (82) and commonly used as solvents in state-of-the-art lithium ion batteries (89). These compounds combine high oxidation stability and acceptable dielectric constants, as can be seen in Table 3. One of their major drawbacks, however, is their high flammability, which can be critical in terms of safety (see chapter 2.2.7).

Table 3: Electrolyte oxidation potentials and dielectric constant for organic solvents used in lithium battery applications (1M LiPF$_6$) (82) (87).

Solvent	Structure	Abbreviation	Oxidation Potential (V)	Dielectric constant
Propylene Carbonate		PC	4.3	64.9
Ethylene Carbonate		EC	5.2	89.8
Dimethyl Carbonate		DMC	5.1	3.1
Diethyl Carbonate		DEC	5.2	2.8
Ethyl methyl Carbonate		EMC	5.2	3.0
γ-Butyrolactone		GBL	5.2	39.1(90)

Considering the data in Table 3, it is obvious that ethylene carbonate (EC) and propylene carbonate (PC) offer good values for permittivity and oxidative stability. Therefore, both compounds would represent potential electrolyte components in lithium ion batteries. Indeed, the first commercialized rechargeable battery used an EC/PC mixture as electrolyte (87). The high permittivity, however, is associated with a high viscosity, which is impedimental for charge transfer. For that reason the high viscosity component has to be mixed with others to improve especially the low temperature performance. Addition of linear carbonates with high fluidity, like for instance diethyl carbonate (DEC), enhances the ionic conductivity of multi-solvent state-of-the-art electrolytes (82).

Unfortunately, all of the listed solvents are thermodynamically unstable against the high reduction potential of metallic lithium and in further consequence also against the potential of charged carbon anodes (82). The effects of the electrolyte decomposition caused by the reduction at the anode are discussed below.

2.2.3.2   Effects of Electrolyte Reduction – The Solid Electrolyte Interphase (SEI)

The decomposition of alkyl carbonates occurs at potentials below 1.5 V vs. Li/Li$^+$ in the presence of lithium ions (16) and means an irreversible consumption of material (lithium as well as electrolyte) (48). As mentioned in chapter 2.2.1.1 the observed irreversible capacity within the first cycle of a graphite anode can be lead back to the charge that is consumed for electrolyte reduction. The onset potential of the decomposition is not a fixed value, but dependent on a number of factors, like nature and composition of electrolyte, nature of additives used in the electrolyte, sweep rates or nature and morphology of the anode material (91).

This decomposition is definitely undesirable due to the associated loss of material, but it is advantageous in a way, since the decomposition products of some electrolyte components, like EC, form an effective protective film on the surface of the electrode that prevents any sustained electrolyte reduction. This also explains the unique position of EC as a lithium ion battery electrolyte, due to the fact that PC is not able to form this kind of protective layer (87). Peled was the first to describe this very essential layer, calling it "*Solid Electrolyte Interphase*" (SEI), since that the layer acts as an interphase between the electrode and the electrolyte solution and has the properties of a solid electrolyte (92). Due to the fact that the layer is electronically insulating, further electrolyte decomposition is impeded. The layer is permeable for lithium ions but not for solvating molecules, so the interphase acts like a "sieve" (92) and prevents the exfoliation of the graphene planes due to solvent co-intercalation (87).

The formation and composition of the SEI was subject of numerous investigations and it is still controversial. Peled et al. assume that there is a competition among many reduction reactions of salts, solvents and impurities, the rates of which depend on the current exchange density i_0 and the overpotential η for each process (93). Decomposition of the conducting salt results in the formation of inorganic precipitates such as LiF, LiCl, Li_2O, whereas the partial or complete reduction of solvents produces, beside gaseous products like CO_2, ethylene or hydrogen (94), mainly solid Li_2CO_3, $LiCO_2R$, alkoxides and polymeric compounds (95). Hence, the lithium is irreversibly consumed during the

formation of the SEI and leads to a decrease of the overall cell capacity. All mentioned materials get simultaneously reduced and precipitate on the electrode as a mosaic of microphases (95) or form separate layers (93). Due to the fact that Li_2CO_3 is thermodynamically unstable with respect to lithium, it is assumed, that solid carbonates do not appear directly onto the electrode surface, but are reduced to Li_2O and Li_2C (95)(96). Lithium oxide and lithium fluoride microphases, however, are stable versus lithium and hence can precipitate onto the surface. As a consequence, the surface of the graphite electrode is mainly coated by microphases of LiF and Li_2O, whereas the side facing towards the electrolyte basically consists of organic decomposition products. The thickness of these phases may vary from a few Å up to several hundred Å. Due to the fact that some of the components are partially soluble in the electrolyte, a distinct measurement of the SEI thickness proves difficult (91). A simplified model of the electrode/electrolyte phase boundary, including the SEI, is shown in Figure 24.
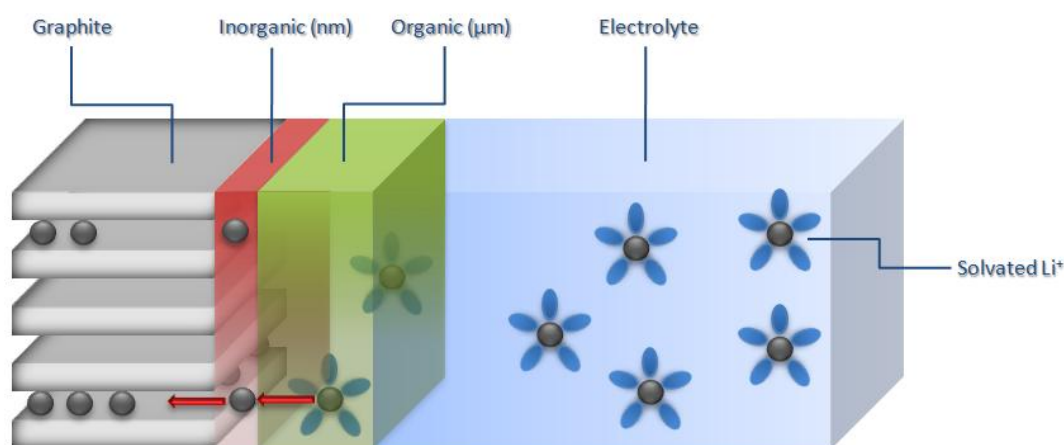
Figure 24: Illustration of films at the graphite-electrolyte phase boundary (redrawn) (97).

The organic components of the SEI are mainly composed of semicarbonates and oligomers, typically polyolephines, which is an important issue concerning the long-term cycling performance of lithium ion batteries. On the one hand polyolephines can add flexibility to the SEI and fill void volumes, but on the other hand they are ion-nonconducting substances and hence can block lithium ion migration. On that account oligomers can cause uneven current distribution and consequently uneven lithium intercalation. Furthermore, the polymers may dissolve in the electrolyte, especially at elevated temperatures, and thus cause discontinuity in the SEI (95).

On the account that the composition and properties of the SEI is dependent on the surface of the electrode as well as on the components and impurities of the electrolyte, it could be very

advantageous to design an ideal SEI. This interphase should have a minimum electronic and a maximum ionic conductivity. Furthermore, the SEI should be formed fast and before the onset of Li^+ intercalation, so the formation potential should be more positive than the Li^+ intercalation potential. Moreover, an ideal SEI should provide a homogenous composition and morphology and should consist rather of Li_2CO_3, than of metastable, partially soluble semicarbonates. The compact layer of the SEI should adhere well to the carbon and simultaneously a flexible or elastic property is desired to accommodate non-uniform electrochemical behavior and active material breathing (91). An optimization of the SEI towards these requirements would be essential not only concerning the high/low temperature and long-term performance of a lithium ion battery, but also its safety. One promising approach is the usage of so called film forming additives, which are compounds that help to improve the properties of the SEI. Among the various additives tested, vinylene carbonate (VC) might be the most famous in the lithium ion research community and its importance can be evidenced by the number of companies that vied for its patent rights (87). As a matter of fact the SEI composition changes drastically, when VC is used as additive, providing a higher polymeric content due to the reductive polymerization of VC. It was proven in several studies that VC presence improves cycle life performance and reduces the irreversible loss of capacity within the first cycle (87) (98).

2.2.3.3 Effects of Electrolyte Oxidation – Cathode Surface Films

As a matter of fact, all transition metal oxide cathodes are covered by a native surface film, mainly composed of Li_2CO_3, which arises from the precursors used for synthesis or, more likely, from the reaction between the metal oxides and the atmospheric CO_2 during the processing of these strongly oxidizing materials (87). For that reason, study of oxidation reactions of electrolyte components onto the surface of cathode has come into focus only within the last years particularly due to the research and development of lithium ion batteries with cathode redox potentials as high as 5 V (99). But it should be noted, that alkyl carbonates can be oxidized already at potentials below 4 V (100). These surface films are generally unstable, so the electrolyte is not protected from further oxidation on subsequent cycling (47). It was proved by *Electrochemical Impedance Spectroscopy* (EIS) techniques that the observed resistance increase on cycling of a common Li_xMO_2 could be traced back to the formation of a surface film. For $LiFePO_4$, however, this differs slightly. The lower potential of the $LiFePO_4$ compound prevents solvent oxidation and hence the surface film is only composed of inorganic salt-based reaction products, mainly lithium, fluorine and phosphor (101). One of the main

driving forces for the film formation onto the cathode surface is the reaction of the conducting salt $LiPF_6$ with traces of water, which can originate from contaminated electrolyte or electrode components (89).
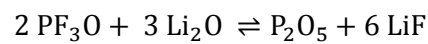
$$LiPF_6 \rightleftharpoons LiF \downarrow + PF_5$$

$$PF_5 + H_2O \rightleftharpoons PF_3O + 2\,HF$$
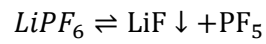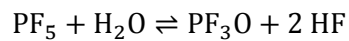
The presence of HF as well as of PF_5, which is a strong Lewis acid, leads inevitably to corrosion of the electrode material and subsequently to dissolution of the transition metal. Furthermore, PF_3O can react with Li_2O, forming LiF and P_2O_5 (101).

$$2\,PF_3O + 3\,Li_2O \rightleftharpoons P_2O_5 + 6\,LiF$$

Recapitulating a postulated model for the cathode-electrolyte phase boundary of a manganese spinel is displayed in Figure 25.
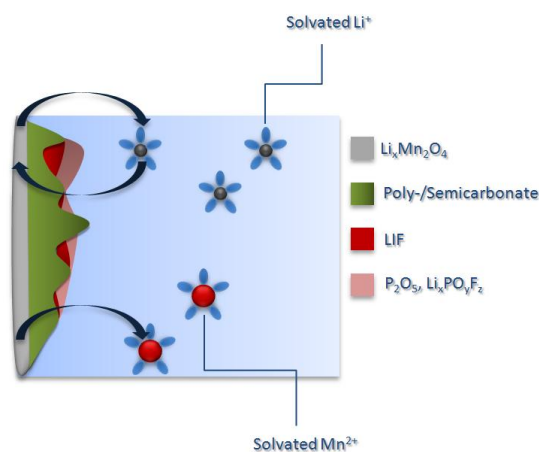
Figure 25: A proposed model for the surface layer formed on a LiMn$_2$O$_4$ electrode (redrawn) (101).

2.2.4 THE SEPARATOR

All of the previous remarks concern individual components of a battery and principally all essential components are listed earlier. To operate battery systems safely, however, another passive element is necessary to keep the distance between the positive and the negative electrode, namely the separator. As a passive element that does not participate in any electrochemical reaction, it has naturally attracted only little scientific interest (102).

As indicated, the essential function of the separator is the prevention of electronic contact between anode and cathode and hence to eliminate the hazard of an internal short-circuit. Simultaneously, the ionic transport has to be enabled through the microporous structure of the separator. In lithium ion batteries, microporous polypropylene and polyethylene membranes are commonly applied. These materials are chemically and electrochemically stable in the potential window of the electrodes, which is one basic requirement for the use of a separator (103). Some other requirements, which need to be fulfilled, are listed in Table 4.

Table 4: General Requirements of Lithium Ion Battery Separator (103)

Parameter	Requirement
Thickness	<25 μm
Electrical resistance	< 2 Ω cm^{-2}
Pore size	<1 μm
Porosity	~40%
Shrinkage	<5%
Tensile strength	<2% offset at 1,000 psi
Shutdown temperature	~130° C
Melting Point	>150°C
Wettability	Complete wet out in standard electrolytes
Chemical stability	Stable in battery for long period of time
Dimensional stability	Should lay flat, be stable in electrolyte
Skew	<0.2 mm m^{-1}

2.2.5 AGEING OF LITHIUM ION BATTERIES

Generally, ageing of a battery means the modification of its properties with time and use, where the essential properties are the available energy and power as well as cell mechanical integrity. While the decrease of available energy is mostly caused by the loss of active material, either on the anode or the cathode side, and the loss of mobile lithium, respectively, the loss of available power is mainly attributed to a rise of impedance. Most of the time, both phenomena are jointly observed (104).

Especially the imminent electrification of the power train and the associated requirements in terms of calendar and cycle life-time (see Table 1) lead to intensified investigations concerning the ageing of lithium ion batteries. In this context, cycle life-time concerns ageing during cycling, while calendar life-time is in regard to ageing during storage. Lithium ion batteries are complex systems to understand, and the processes of their ageing are even more complicated (105). The possibilities for a qualified monitoring of ageing effects include the validation of capacity fade, impedance rise or potential change. But as a matter of fact, several different mechanisms can cause, for instance, capacity fading and a distinction is very difficult. Most of the time, it isn't even possible to distinguish anode and cathode ageing effects at all. Ageing mechanisms occurring at anodes and cathodes, however, differ significantly and are therefore separately discussed.

2.2.5.1 Anode Ageing Mechanisms

In fact there are more or less three relevant ageing scenarios that influence the performance of an anode over time. One reason could be any effects related to the structural changes of active material, therefore graphite. These effects, however, are considered to be minor, for the reason that the volume changes of graphite during uptake and removal of lithium ions are not drastic (typically in the order of 10%) (105). On point that has to be noticed, however, is the possible exfoliation of graphite caused by solvent co-intercalation and gas evolution inside the graphene sheets, respectively. These reactions can lead to a rapid degradation of the electrode (42). Changes of porosity of the electrode can have major influence as well, due to the fact that a good electrolyte access is a key feature for a good anode performance (105).

Secondly changes of inactive parts of the anode compound, like binder or conductive agents are conceivable causes for a worse cell performance. It can be generally assumed that the loss of either mechanical or electronic contact within an electrode compound results in higher cell impedance.

Again volume changes are one possible reason for the loss of contact between carbon particles, binder and carbon, current collector and carbon or binder and current collector (106). A degradation of the binder itself is considerable as well, since it is widely accepted that fluorine-containing polymer-binder like PVdF do exothermically react with anodes at a high state of charge (SOC) and form LiF (105) (107). Furthermore, the possible corrosion of the current collector and the dissolution of copper at high depth of discharge (DOD) have to be taken into account. Both effects, the degradation of the binder and of the current collector can cause mechanical disintegration.

Finally, and probably most important is the fact that ageing can be caused by changes at the electrode/electrolyte interface due to the electrochemical instability of common electrolyte systems in respect to the reduction potential of charged graphite, as discussed in previous chapters. Many researchers consider these reactions to be the major source for ageing of/at the anode (105) (108). By the fact that the SEI is not a homogenous film and has not the properties of a true solid electrolyte for lithium cations, other charged (anions, electrons, solvated cations) and neutral (solvents, impurities) species can still migrate through specific areas of the SEI and are reduced as soon as they get in contact with the surface of the charged electrode. These decomposition reactions seem to occur even in late stages of cycling, however to a lower extent and lower rate compared to the first cycle, leading to a small irreversible loss of capacity in each cycle, associated with a decrease of mobile lithium (105). The continuous growth of the SEI causes an increase of impedance und hence leads inevitably to power fade. Changes of the morphology or composition of the SEI can lead to higher impedances as well (105). Ageing of the cathode can influence the anode performance as well. On the condition that transition-metal ions get solved in the electrolyte and migrate or diffuse to the anode, the metal deposits at the anode, when the electrode potential is low enough. The most important reactions at the electrode/electrolyte interface are displayed in Figure 26.
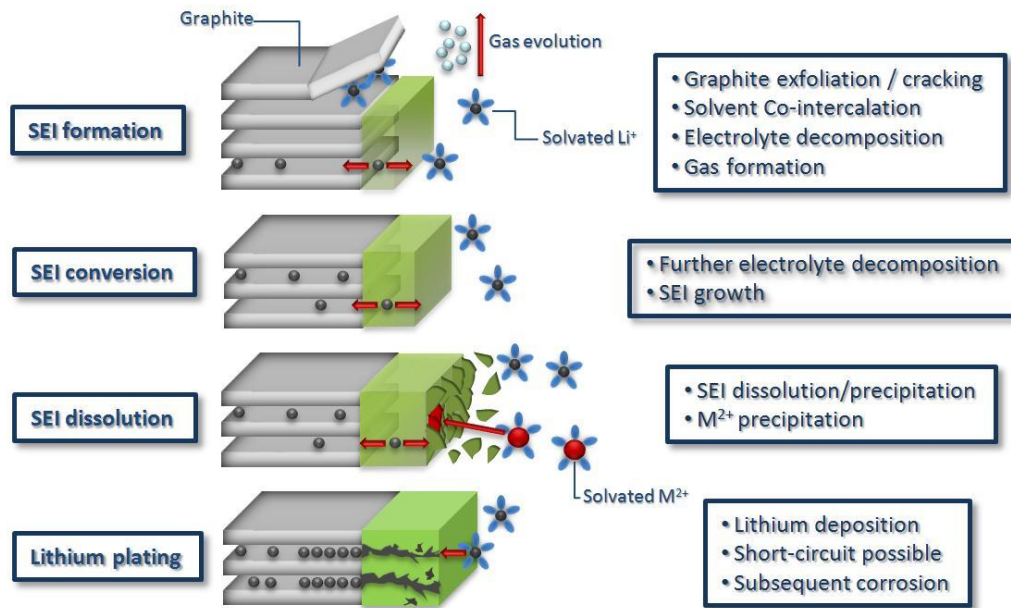
Figure 26: Changes at the anode/electrolyte boundary (redrawn) (105).

It has to be noticed that all of those ageing effects are temperature dependent and proceed faster at elevated temperatures, as it is the nature of chemical reactions. The solubility of certain SEI components in the electrolyte increases as well with higher temperatures and the film starts to break down. Hence, it can be assumed that neither usage nor storing of lithium ion batteries should happen at elevated temperatures (105).

Low temperatures, however, result in different challenges. Due to the fact that the intercalation potential of graphite is close to the potential of metallic lithium, lithium plating can occur under specific conditions. Those conditions include slow lithium ion diffusion into carbon or slow lithium ion diffusion in the electrolyte due to the low temperatures. Poor cell balancing, meaning an excess of cathode material or geometric misfits like oversized, overlapping cathodes can lead to lithium plating as well. Furthermore, mixed potential effects like locally different polarization enhance the probability of lithium deposition (105). Metallic lithium plating and lithium dendrite growth must be considered as parasitic reaction and accelerate not only the ageing rate but represent also a severe safety hazard for the reason that dendritic lithium can get in contact with the opposite electrode and causes an internal short-circuit. The major causes of anode ageing in lithium ion batteries, their effects and consequences as well as possible counter-measures are listed in Table 5.

Table 5: Lithium ion anode ageing causes, effects and influences (105)

Cause	Effect	Leads to	Reduced by	Enhanced by
Electrolyte decomposition (SEI - building + continuous side reaction)	Loss of lithium Impedance rise	Capacity fade Power fade	Stable SEI (additives) Rate decreases with time	High temperatures High SOC
Solvent co-intercalation, gas evolution and subsequent cracking formation in particles	Loss of active material Loss of lithium	Capacity fade	Stable SEI (additives) Carbon pre-treatment	Overcharge
Decrease of accessible surface area due to continuous SEI growth	Impedance rise	Power fade	Stable SEI (additives)	High temperatures High SOC
Changes in porosity due to volume changes, SEI formation and growth	Impedance rise Overpotential	Power fade	External pressure Stable SEI (additives)	High cycling rate High SOC
Contact loss of active material particles due to volume changes during cycling	Loss of active material	Capacity fade	External pressure	High cycling rate High DOD
Decomposition of Binder	Loss of lithium Loss of mechanical stability	Capacity fade	Proper binder choice	High SOC High temperatures
Current Collector Corrosion	Overpotential Impedance rise Inhomogeneous distribution of current and potential	Power fade Enhances other ageing mechanisms	Current Collector Pre-treatment	Overdischarge High DOD
Metallic lithium plating and subsequent electrolyte decomposition by metallic Li	Loss of lithium Loss of electrolyte	Capacity fade	Narrow potential window	Low temperature High cycling rates Poor cell balance Geometric misfits

2.2.5.2 Cathode Ageing Mechanisms

In analogy to the anode, cathode ageing depends on ageing of the active material, degradation or changes of electrode components, like conducting agents, binder or current collector, decomposition of the electrolyte components and surface film formation as well as interaction of ageing products with the negative electrode. Furthermore, degradation again depends on state of charge, cycling conditions and temperature. In contrary to the anode, however, decomposition is driven by an oxidation of the respective species. Due to the fact that the oxidation potential as well as the structure of common cathodes may vary (see chapter 2.2.2), depending for instance on the kind of transition-metal, several different ageing mechanisms are observed for diverse cathode materials (105).

Generally, it can be assumed that structural aspects have a major influence on the cycling behavior of cathodes, which is in contrast to graphite ageing, where structural changes within the compound are rather unusual. Phase transition can occur in almost every cathode material and although most of these transitions are theoretically reversible, they can cause micro-cracking and loss of contact of active material due to associated volume changes. These ageing effects can be reduced by doping the active material with, for instance, aluminum by the fact that the volume changes can be minimized this way (105).

The dissolution of transition-metal ions in the electrolyte is a big issue as well, because on the one hand these ions can precipitate and poison the anode and on the other hand the integrity of the cathode structure is threatened as well. The dissolution of metal ions is driven either by low potentials or catalyzed by the presence of HF (105).

The cathode/electrolyte interface is important in terms of power fade over time. As mentioned in chapter 2.2.3.3, cathode surface films predominantly consist of inorganic LiF and $Li_xPO_yF_z$, resulting from oxidation reactions of $LiPF_6$. This is particularly true for $LiFePO_4$, where the oxidation potential is not high enough to oxidize significant amounts of solvent molecules. The inorganic surface films, however, seems to have just a very limited influence on the electrode behavior at ambient temperature and the evolution deduced from EIS measurements suggests no influence of the surface layer but only a deterioration of the electrode, assigned to iron dissolution and loss of electrical contact within the electrode (109). However, if the cathode potential or the temperature is high enough to oxidize remarkable amounts of solvent molecules, an organic layer consisting of alkyl carbonates completes the surface film on the cathode and leads inevitably to a power fade. In contrast to the anode, this surface film cannot protect the electrolyte properly from further

oxidation (105). Beside this impedimental coated surface, enhanced gas evolution can be observed, when solvent molecules are oxidized to CO_2, CO, H_2 and alkenes (110) (111) (112). Due to the fact that the high cathode potential is decisive for electrolyte degradation, it can be assumed that these effects become dominant at high voltage cathodes as well as overcharge conditions.

2.2.5.3 Conclusion

M. Broussely concluded in *"Ageing Mechanisms and Calendar-Life Predictions in Lithium-Ion Batteries"* (104) that a good choice of active materials and additives can exhibit excellent cycling and calendar life. For example, lithium iron phosphate causes hardly any electrolyte oxidation at standard conditions, while the addition of VC can enhance the properties of the anodic SEI by far. Regarding to the negative electrode, the SEI growth is the main identified factor for ageing, resulting in lithium loss and impedance rise. The capacity loss can be modeled through a parabolic equation of corrosion in time, which is dependent of temperature, but not of SOC and hence a quite good prediction of calendar life seems possible. In contrary, electrolyte oxidation on the positive electrode is strongly dependent on the SOC, temperature and surface reactivity (104). Eventually it has to be noticed again that ageing mechanisms in lithium ion batteries are an incredibly complex system, especially for the reason that several different ageing mechanisms, influenced by various parameters, occur at the same time and produce the same observable data, which makes it very hard to distinguish even anode and cathode ageing in a commercial cell, not to mention single ageing effects on electrode level.

2.2.6 FROM SINGLE COMPONENTS TO LARGE HIGH-PERFORMANCE BATTERIES

Since all important components of a lithium ion battery have been discussed so far, the short general view on the overall battery will be given below. Generally, lithium ion cells are available in cylindrical, elliptical and prismatic shapes. Cell packages are usually aluminum or steel cans but also soft packaging, meaning a metalized plastic foil, has come into consideration. The big advantage of prismatic and elliptic cells is the higher packing density that can be achieved in modules of several batteries in contrast to cylindrical batteries. This can be advantageous in terms of heat dissipation. However, maintaining compressive force on the electrode to provide uniform contact is more difficult with prismatic cells (113).
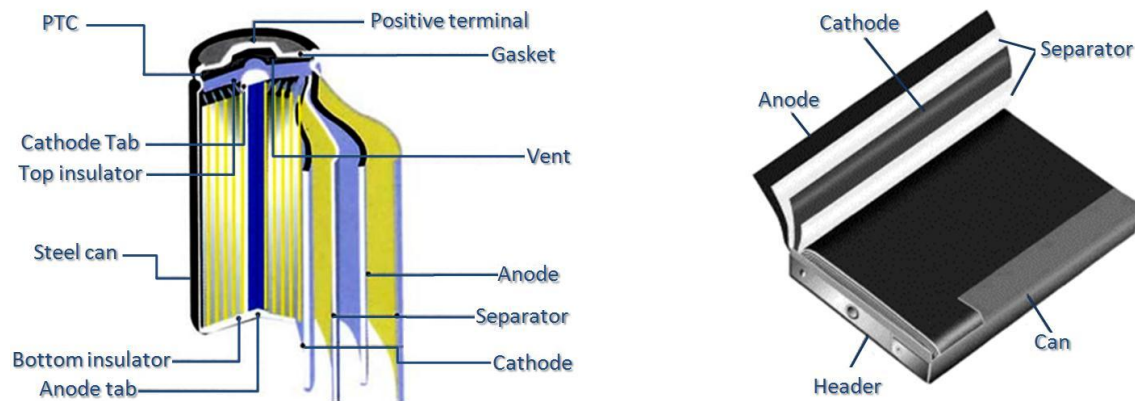
Figure 27: Schematic drawing of a cylindrical and prismatic lithium ion battery (114) (115) (edited).

As mentioned in chapter 1, lithium ion batteries for automotive applications are believed to get in the true sense of the word a driving force within the battery market. According to Horie et al. a energy of 133 Wh is needed per kilometer, hence a scale-up of common mobile phone or laptop batteries is inevitable (116). Basically, there is no difference between the technology implemented in small portable lithium ion cells and large cells. Electrode processing consist of coating metallic foils (Cu and Al) with a slurry containing active material, a dissolved binder in an appropriate solvent, and an electronic conductor. After drying, the electrode is calendered to the desired thickness/density. As a matter of fact, the thickness of the electrode determines the power that can be achieved (117). On the account that the lithium diffusion in the solid active material is the kinetically limiting step, the battery can be charged or discharged faster, if less active material is coated on the current collector, resulting in shorter diffusion pathways but also a worse ratio of active to inactive materials. This is a very interesting feature of lithium ion batteries due to the fact that batteries can be tailored for their purpose by varying just a few parameters.

Proper balancing of anode and cathode materials is of crucial importance for the performance of a battery. The cathode serves as lithium source in lithium ion batteries and due to the fact that a significant part of the mobile lithium is irreversibly lost during SEI formation, this loss has to be considered in the calculation for the total amount of cathode material. The anode, on the other hand, has to be oversized too, to exclude the possibility of lithium plating. Hence, it is a very thin line between providing an adequate safety and reducing costs and inactive parts, meaning areas of the electrode that do not participate in the electrochemical reaction, to a minimum.

Lithium ion batteries cannot be up scaled to any desired size. The usual cell range for large sized cells proposed by battery manufacturers is from 3 Ah (high power design) to 100 Ah (high energy design) (117). In some cases high direct currents accompanied with voltages of more than 300 V are required to drive an electric engine. Hence, many lithium ion batteries have to be connected in series

to achieve the required voltage and parallel to provide the desired capacity. A lithium ion battery pack, as it can be implemented into a vehicle, consists of modules and modules consist of single cells. This fact can lead to problems due to differences in capacity and/or impedance of individual cells. If, for instance, cells with identical capacity are charged in parallel, the cell with the lowest impedance will receive more current than the other cells, which is disadvantageous in terms of ageing. Temperature and voltage are electronically controlled for each module. A control of every cell would be advantageous but expensive and implements an increase of inactive materials as well. The electronic controls are usually linked to a local computer called the Battery Management System (BMS). The BMS protects the pack against abuse and communicates with other devices in the car (113).

In conclusion, it can be assumed that safety is a major parameter taken into account at the battery level and larger size of batteries or battery packs make this point even more crucial. In the following chapter safety hazards regarding lithium ion batteries will be particularly discussed (117).

2.2.7 SAFETY HAZARDS REGARDING LITHIUM ION BATTERIES

As shown in the previous chapters, lithium ion batteries provide highly energetic materials in combination with flammable organic electrolytes and although they are much safer than their closest relative, lithium metal batteries, they still can suffer premature failure, if subjected to conditions for which they never were designed. Any abuse, including heat disposure, overcharge, external short-circuit and mechanical damage can trigger spontaneous heat-evolving reactions, which can in turn end up in fire or even explosion. This is even more critical in regard to automotive applications, when several batteries can participate in hazardous reactions. To reduce the hazards of a lithium ion battery to a minimum, several safety tests have to be passed before they can be certified for the use by a consumer. The test matrix includes electrical tests such as external short-circuit, mechanical tests like nail penetration, crushing or dropping to the ground and environmental tests such as heating in a microwave oven, throwing into a hot liquid or leakage tests in a vacuum (118).

Assuming that no abuse conditions occur there are mainly two scenarios conceivable that are relevant to the safety issue and both are closely related to the ageing of the battery:

2.2.7.1 Heat Generation in LIBs

Firstly the heat generation in lithium ion batteries is of fundamental importance. Both reversible and irreversible heat generation have to be considered in this regard. Reversible heat generation occurs during discharging and can be explained by Equation 7. Conversely batteries remove heat from the environment during the charge step. Irreversible heat, however, is caused by internal resistance and hence linked with cycling conditions and cell ageing (119). Internal short-circuit, which can be traced back to contamination during processing, mechanical damage or lithium dendrites may cause massive heat generation as well. If the temperatures get too high, a so called thermal runaway can occur, which is described in literature as a three-stage process (111) (119).

The three stages of thermal runaway including the calorimetry profiles for a fully charged 18650 cell, containing a graphite anode and a $LiNi_{0.8}Co_{0.15}Al_{0.05}O_2$ cathode are shown in Figure 28.
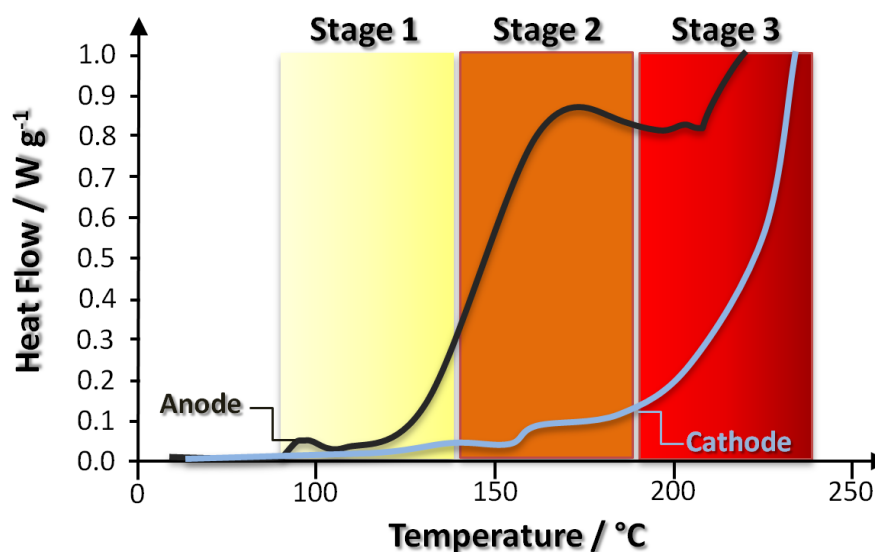
Figure 28: Calorimetry profiles at 100% SOC for a graphite anode and a $LiNi_{0.8}Co_{0.15}Al_{0.05}O_2$ cathode showing the anode/cathode onset reactions and three stages of thermal runaway (redrawn) (111).

According to Figure 28 following stages can be described:

- Anodic reaction starts at about 90° C and represents the rate-limiting step. As the temperature rises above 120° C, decomposition and solution of the SEI, respectively, follows, leading to reduction of the electrolyte at the charged negative electrode.

- Secondly exothermic reactions at the positive electrode start as the temperature rises over 140 °C. In case of cathode materials with the stoichiometry $Li_{1-x}MO_2$ (M = Co, Ni, Mn) oxygen starts to evolve rapidly.

- At the final stage, the positive electrode decomposes and the electrolyte gets oxidized at temperatures above 180°C. This is a high-rate exothermic process with a temperature rise as high as 100° C per min.

Furthermore, it has to be considered in this context that the design of state-of-the-art lithium ion batteries has an inherent drawback of poor heat dissipation (118). A sufficient cooling system stays one of the main challenges, especially for automotive battery packs.

As a matter of fact, lithium iron phosphate is thermally stable for its reactivity with the electrolytes is very low and no heat evolution is observed below 200° C. Hence, $LiFePO_4$ is probably the most exciting cathode material for large-sized lithium ion batteries in regard to the safety issue (118).

2.2.7.2 Gas Evolution in LIBs

Beside heat generation another safety hazard has to be mentioned, namely excessive gas evolution and cell overpressurisation caused by electrolyte decomposition. This effect may be triggered either by elevated temperature, but especially by overcharge conditions. As a matter of fact, gas evolution in lithium ion batteries can be mainly attributed to the oxidation of electrolyte at the positive electrode. Beside a massive amount of CO_2 and some CO, also highly flammable gases like H_2 and methane can be detected (112). With the use of $LiPF_6$, which serves as catalyst of the decomposition reactions due to the consequent presence of HF and PF_5 (see chapter 2.2.3.3), fluorinated organic compounds like highly toxic alkyl fluorophosphates ($OPF_2(OCH_2CH_3)$ or $OPF_2(OCH_2CH_3)_2$) have to be added to this list (119) (120). As a consequence, it should be assured that no gaseous compound is released at overcharge conditions.

2.2.7.3 Improving the Safety of LIBs

To prevent malfunctions in battery systems or at least to diminish its consequences, various safety mechanisms were developed. This does not have to concern only the battery chemistry but also safety or control devices outside. A rough classification can be made by distinguishing safety concepts for system hardware, system software and cell hardware.

Safety concepts at battery level (cell hardware) are subsequently listed.

- One promising approach is the installation of devices that aim to limit the current or ions passing through them and thus stop the (electro-) chemical reaction in case of a malfunction.

  - This includes for instance shut-down separators, which consist of two different polymers, mostly polyethylene and polypropylene. The separator is arranged as a PP/PE/PP trilayer, offering high-temperature stable PP layer and a PE layer, which melts at significantly lower temperatures and thus impedes the transfer of lithium ions through the separator (103).
  - Positive temperature coefficient (PTC) devices work by responding to increased currents passing through this element and cause a heating due to the Joule effect. This is translated into an increase on resistance of the device and therefore the current flow is stopped (119).
  - Shut-down additives are conceivable as well. On overcharge conditions they can either release gases, which in turn activate a current interrupter device, or get polymerized and thereby block ion transport through the electrolyte (118).

- The use of safer cathode materials like $LiFePO_4$ as well as non-flammable electrolytes (e.g. ionic liquids) are advantageous in terms of safety, but imply simultaneously a decrease in specific energy and ionic conductivity, respectively (118).

- A substitution of $LiPF_6$ as conducting salt could also significantly improves safety of lithium ion batteries, but as a matter of fact, safer conducting salts provide other important disadvantages by now (118).

- Another interesting approach is the use of so called redox-shuttles, which connote electrolyte additives that can be reversibly oxidized and reduced at characteristic potentials,

mainly in overcharge regions, and thus represent an intrinsic overcharge protection in lithium ion batteries (119).

- Finally, an integration of a safety vent is reasonable, allowing emerging gases to escape. Safety vents open in response to a sudden increase of the inner cell pressure. Nowadays, safety vents are back-up systems, meaning the release of gases from the cell to the environment is the last option and just necessary, if all other safety mechanisms fail (118).

3 Experimental

3.1 Introduction

Apart from energy density and costs, ageing and safety as well as their correlation remain one of the main challenges towards sustainable batteries for automotive applications. The possibilities to validate any ageing effects without destroying the cell are limited to the monitoring of capacity and power fade and the voltage/current characteristics, respectively. Electrochemical Impedance Spectroscopy (EIS) is another powerful tool to get information about ageing characteristics. A more precise knowledge of the processes inside industrially manufactured lithium ion batteries would be beneficial in any case but unfortunately the assembly of a conventional battery disallows a separate investigation of the positive and the negative electrode by the methods mentioned above. Instead, industrially manufactured lithium ion batters can be rated as a kind of black box during their cycle life. All effects like capacity fade or impedance rise can only be observed for the entire cell system. However, the distinction between anode and cathode characteristics would be very important to gain information about the kinetic and capacitive balancing of the system. Another point is to reveal the nature of both positive and negative electrode processes during battery cycling (121) and the attribution of ageing to the anode or cathode. Consequently, this work aims to reveal these effects by inserting a third electrode and hence gain a reference point for further investigations.

3.2 Characterization of an Industrially Manufactured Battery

A commercial cylindrical 32113 battery with a nominal capacity of 3.6 Ah and a nominal voltage of 3.3 V serves as standard bench mark system within this doctoral thesis (see Figure 29). The term 32113 refers to the dimensions of the battery, meaning a diameter of 32 mm and a length of 113 mm, respectively. The cell is produced and distributed by A123 systems and consists of an aluminum casing, containing tubular wound graphite and nano-scaled lithium iron phosphate electrodes. According to the manufacturer, the cell is designed for hybrid electric vehicles (HEV) applications and offers excellent calendar and cycle life (122).

Figure 29: Image of the investigated cylindrical 3.6 Ah- cells.

3.2.1 Constant Current Cycling of the Bench Mark System

First investigations include a constant current (CC) cycling study of the battery, which were performed at a Maccor Series 4000 battery tester. Therefore, the batteries were charged and discharged with a current of 3.6 A, which corresponds to the 1C current due to the nominal capacity of 3.6 Ah. The cells were cycled at ambient temperature (20° C) within the potential range of 2.4 V and 3.6 V, respectively.
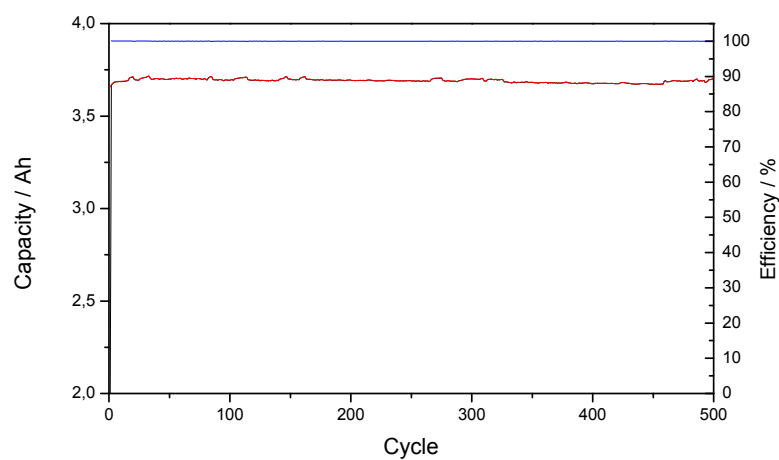
*Figure 30: Charge/Discharge characteristics (**black**/**red**) and efficiency (**blue**) of an A123 32113 cell at 1C current, cycled*

from 2.4 V to 3.6 V.

The CC cycling study shows an excellent cycling efficiency of nearly 100% for 500 cycles and no observable capacity fade, when cycled at ambient temperature. Beside the cycling study and the corresponding capacity or energy fade over time/cycles, also voltage profiles can be obtained by this kind of experiment.
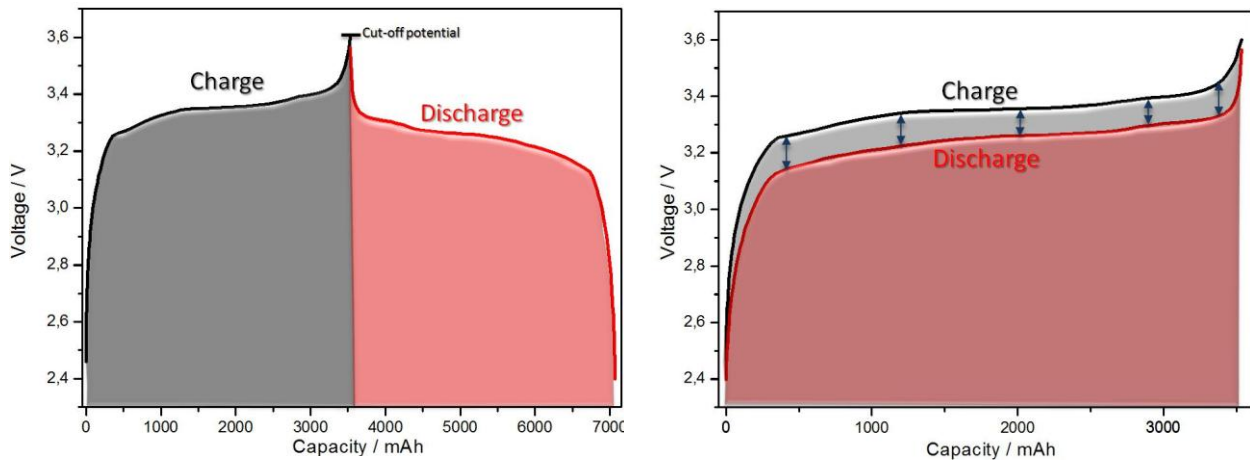
Figure 31: Voltage profiles of A123 32113 at 1C current, cycled from 2.4 V to 3.6 V.

Figure 31 shows the voltage profile of one cycle in this measurement. The charging curve is displayed by the black line, while the red line refers to the discharge curve. The overall energy that is needed to charge the cell and that can be obtained during discharge is displayed by the grey and bright-red areas beneath the voltage lines and corresponds to the integral of these potential curves. As can be seen in Figure 30 the energy efficiency differs from the capacity retention due to a so called hysteresis effect.

The term hysteresis is of Greek origin and means etymologically "coming behind" (123). By definition, hysteresis describes the characteristic of a system, in which a change in the direction of the independent variable leads to the dependent variable failing to retrace the path it passed in the forward direction. In other words, the dependent variable lags behind in an attempt to track the changes in the independent variable (124). Hence, the system exhibits a kind of "history dependence". In a system with hysteresis, prediction of the system's output is not possible, because the output depends not only in the given input but also on the internal state of the system (125). Hysteresis is a strongly nonlinear phenomenon, which occurs in many industrial, physical and economic systems (123). One of the best examples describing electrochemical hysteresis is the cyclic voltammetry, where the anodic and cathodic paths do not overlap due to kinetics, mass-transfer, and ohmic resistances (124). In terms of the observed voltage difference, hysteresis can be analogously explained by various overpotential effects and ohmic resistances, which lower or raise the potential

depending on the direction of current flow. It can be seen that hysteresis is no constant value but differs at various states of charge. In fact, it is obvious that hysteresis increase at very high or very low SOC, which is comprehensible due to the fact that charge-transfer overpotential and concentration overpotential are distinctive in this low/high SOC-regions (see Figure 11).

Voltage hysteresis is well known in NiMH-batteries, where the hysteresis is static. This means that that the hysteresis remains for a period of time that exceeds time constants of mass transport inside the electrodes significantly even after a charging or discharging current is switched off. As a consequence, the open-circuit voltage is independent on the state-of-charge as well as the preceding current rate (126). This point will be discussed later.

3.2.2 INVESTIGATIONS OF SINGLE ELECTRODES AFTER DISMANTLING THE BENCH MARK SYSTEM

The first attempt to get information about electrode kinetics and balancing of the A123 32113 included dismantling of the cell in an argon filled glove box (< 1 ppm H_2O, <1 ppm O_2). The separate investigation of cathode and anode materials of commercial cells via dismantling of cycled cells was reported by Aurbach et al (127) in 2002.

Within this doctoral thesis circular electrodes with a diameter of 12 mm were punched out of the gained electrode material and were electrochemically investigated in Swagelok test cells. This led to a total area of 1.13 cm^2 per electrode. A schematic drawing of a Swagelok© test cell is shown in Figure 32.
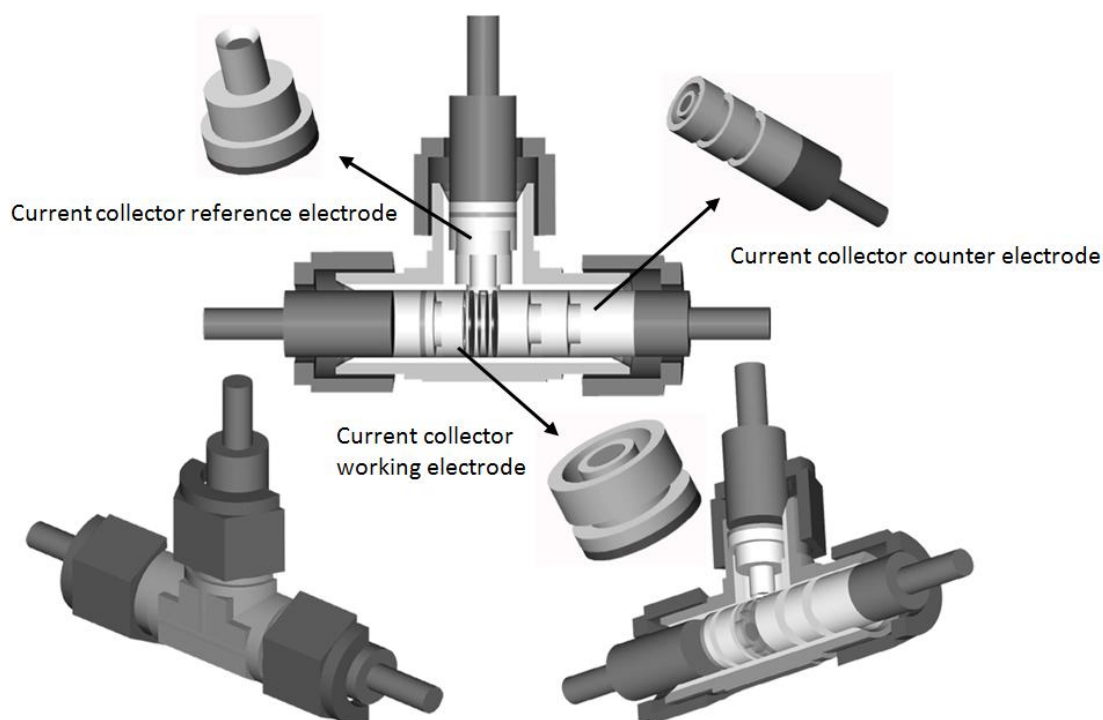
Figure 32: Schematic drawing of a Swagelok© test cell (drawing by S. Koller, edited by H. Kren).

This design allows an investigation of the electrode materials in a half-cell assembly meaning a counter-electrode and reference electrode consisting of lithium metal. This is important to get distinct information about anode and cathode behavior.

The electrodes were investigated by cyclic voltammetry (CV). The experiments were performed with a Potentiostat/Galvanostat (Adesys-Model 1612). Related parameters for the measurements are listed in Table 6.

Table 6: Parameters of cyclic voltammetry measurements.

	Anode	Cathode
Start Potential	OCV (approximately 3V)	OCV (approximately 3V)
Vertex Potential	0 V vs. Li/Li$^+$	4.2 V vs. Li/Li$^+$
End Potential	1.5 V vs. Li/Li$^+$	3.0 V vs. Li/Li$^+$
Scan rate	30 µV s^{-1}	30 µV s^{-1}

The results of these measurements are displayed in Figure 33.
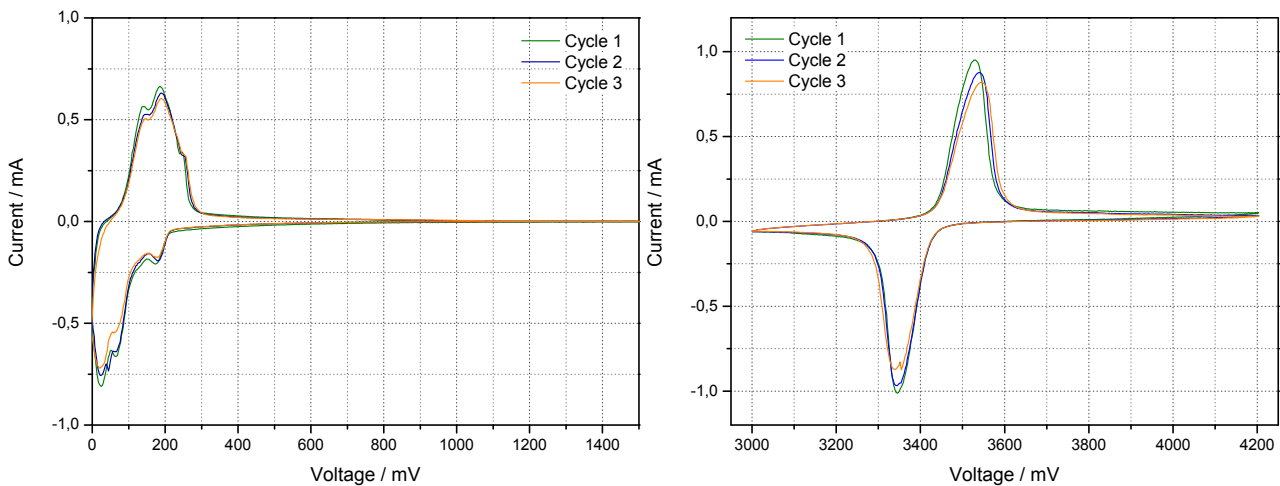
Figure 33: Cyclic voltammetric measurements for dismantled anode (left) and cathode (right) from A123 32113.

According to Figure 33, the electrodes provided good kinetics, which was indicated by sharp and high peaks in the cyclic voltammetry measurements. This was especially the case for the positive active material (right CV), where one sharp peak at about 3.5 V vs. Li/Li$^+$ represented the two-phase delithiation/lithiation of lithium iron phosphate, as it is described in literature. On the negative side (left CV), all four intercalation peaks of graphite could be identified during lithiation, while three peaks could be found during oxidation of the material, which is equal to the delithiation process. These observations are reasonable as well. The correlated data for capacities and reversibilities is listed in Table 7 and Table 8.

Table 7: Capacities and reversibilities of dismantled anode (obtained from CV-data).

Cycle	Charge Capacity [mAh]	Discharge Capacity [mAh]	Reversibility [%]
1	0.917	0.852	92.9
2	1.021	0.917	89.8
3	1.005	0.941	93.7

Table 8: Capacities and reversibilities of dismantled cathode (obtained from CV-data).

Cycle	Charge Capacity [mAh]	Discharge Capacity [mAh]	Reversibility [%]
1	1.003	0.898	89.6
2	0.892	0.867	97.2
3	0.859	0.847	98.6

As a result, the capacities of anode and cathode were similar at about 1 mAh per electrode, which indicated a similar load concerning the amount of storable charge. However, the reversibilities were as low as 90% for the anode and not higher than 98.6% for the cathode, which was in contrast to the data obtained in the cycling study done before (see Figure 30). Taking a closer look, the cyclic voltammetry measurement of the anode showed a slight current flow starting at about 700 mV vs. Li/Li$^+$. This could be related to a decomposition of electrolyte, meaning a further SEI formation. In contrast to the original first film formation, however, this process was not at all finished after the first cycle, but got even worse in the next cycle. As a matter of fact, the dismantling of the cell and possibly the temporary desiccation caused by lack of electrolyte presence seemed to damage the already existing surface films of the electrodes. This concerned especially the negative side, but also the positive electrode suffered from the conversion into the Swagelok© cell system.

In conclusion, the dismantling of the cells and subsequent investigations of the single electrodes may give information about electrode kinetics and approximate capacities, but the intervention in the electrodes environment is crucial and may lead to wrong results. Therefore, another method had to be found for separate investigations of anode and cathode.

3.3 IMPLEMENTATION OF REFERENCE ELECTRODES IN COMMERCIAL

LITHIUM ION BATTERIES

As described before, a separate observation of anode and cathode in a commercial lithium ion battery is hardly possible. In chapter 3.2.2 an option for a more precise knowledge of the electrode processes includes the dismantling of the battery and can be seen as a kind of post-mortem analysis.

Another approach that is reasonable in this regard is the implementation of a reference point into the cell system without dismantling the battery. This can be achieved by the insertion of a lithium-metal reference electrode into the original cell. Investigations of commercial 18650 cells by implementation of a lithium-metal reference electrode were reported by Wu et al. (128). Lithium-metal is a reasonable reference system in lithium ion batteries and provides a readily reproducible and stable potential. As mentioned in chapter 2.1.1 the use of lithium metal would additionally offer the advantage that the zero grade of the Li/Li^+ scale corresponds to the anode potential in fully charged state. However, the use of lithium reference electrodes requires special handling and storage and can only be used without the presence of water, oxygen or nitrogen (129). Hence, the opening of the cell in an inert atmosphere, insertion of the lithium-metal and the absolutely air-tight sealing afterwards is of crucial importance. Another point that will be discussed beforehand is the partial lithiation of the aluminum casing in the cell, which would have the advantage that a cell opening would not be necessary.

3.3.1 IN-SITU LITHIATION OF THE ALUMINUM CASING

The idea behind this approach was the possibility to build a lithium aluminum alloy and hence create a stable potential as a reference point for further measurements. However, this is linked to the condition that the casing is electronically conducting and furthermore provides a so-called "floating potential". This means that the casing is insulated from both electrodes, which is quite usual for lithium ion batteries because it minimizes the risk of an external short-circuit by a slight touch of a conducting object.

First of all it was tried to use the casing as a reference electrode without previous lithiation. Therefore, three cycles were recorded, using a current of 1C and cell voltage limits of 2.4 V and 3.6 V, respectively. In addition to the cell voltage the potentials between aluminum casing and anode as well as aluminum casing and cathode were measured. The results of this test are shown in Figure 34.
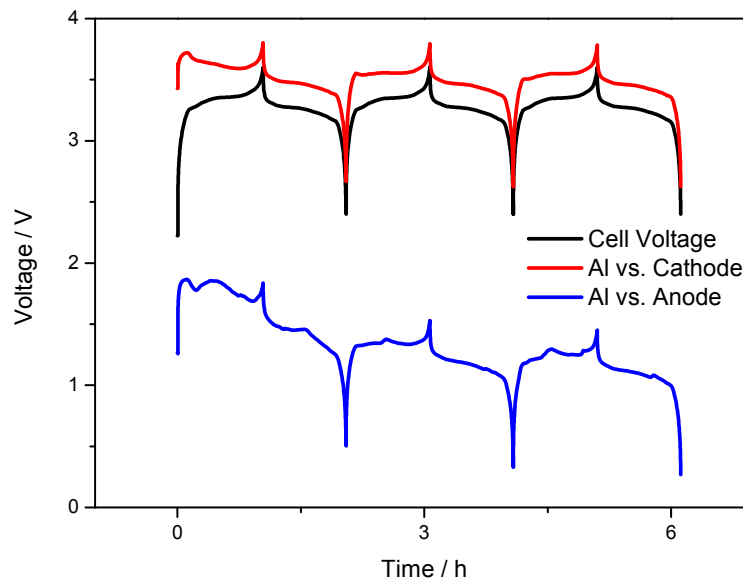
*Figure 34: Voltage profile of three cycles of A123 32113, cycling at 1C current, voltage limits from 2.4 V to 3.6 with cell voltage (**black**), casing vs. cathode (**red**) and casing vs. anode (**blue**).*

It is obvious in Figure 34 that the aluminum casing could not provide stable potentials, which could be seen by the potential drift from cycle one to cycle three. As a consequence the use of the ordinary casing as a reference in electrochemical measurements seemed to be inappropriate. This assumption gets even clearer when the difference between the measured anode and cathode potential, which should result in a calculated cell voltage, is drawn against the practically measured cell voltage.
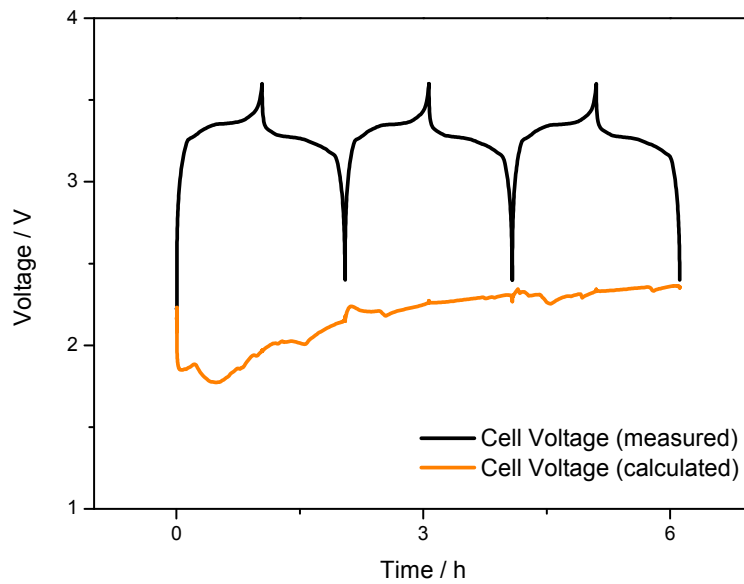
*Figure 35: Comparison of measured (**black**) and calculated (**orange**) cell voltage A123 32113, cycling at 1C current, voltage limits from 2.4 V to 3.6 V.*

Figure 35 reveals the inadequacy of this method to serve as reference system in lithium ion batteries. The reason for that can be probably found in polarization effects at the aluminum surface, leading to false values, especially for the anode potential.

The next step was the partial lithiation of the aluminum casing, which should ideally result in a stable potential and hence provide a better reference electrode. For this reason a fully discharged battery was connected in a way that the cathode served as lithium source as usual, but the casing served as negative pole/electrode. The build-up is schematically drawn in Figure 36.
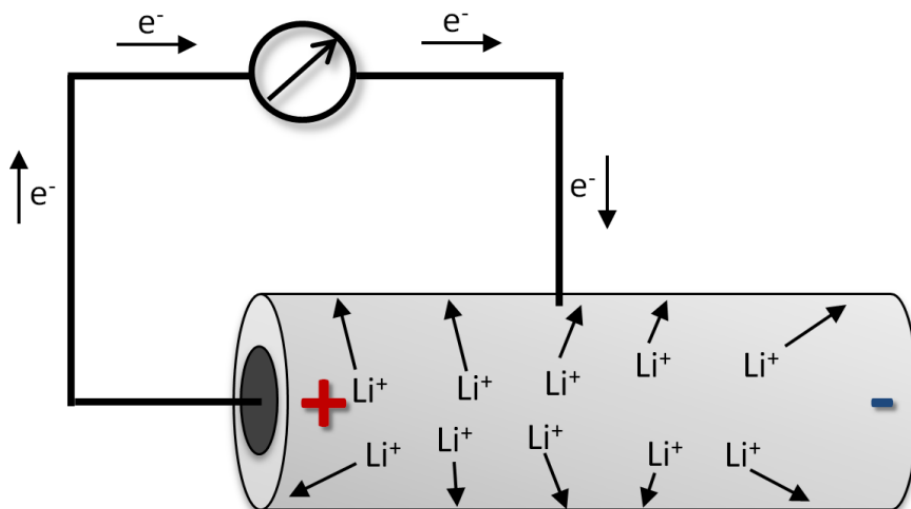
Figure 36: Schematic drawing of the lithiation of the aluminum casing.

Due to the fact that it was very hard to predict the velocity of the electrochemical lithiation of the aluminum, the reaction was not controlled in galvanostatic, but in potentiostatic mode, meaning that a potential of 3.6V between cathode and aluminum casing was applied by the Maccor 4000 series battery tester. The limiting conditions for this step were either 500 hours or 5% of the cells capacity, which is equal to 0.18 Ah.
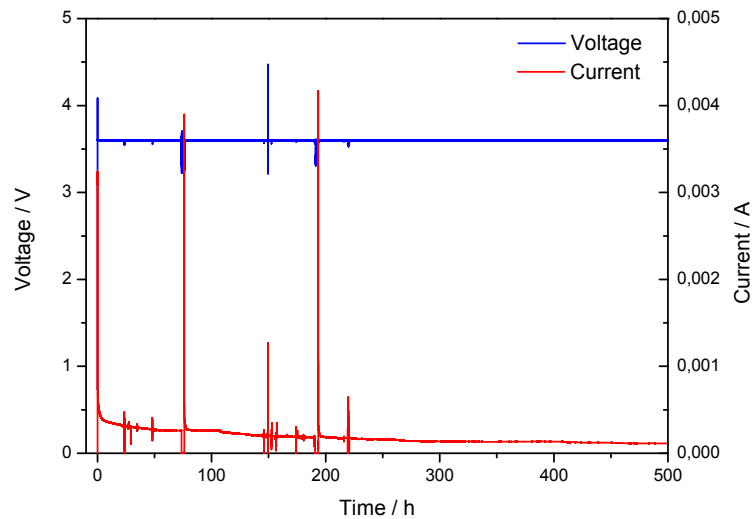
Figure 37: Voltage/Current characteristics of the lithiation of the aluminum casing.

Figure 37 displays the voltage/current characteristics of the lithiation step. Obviously, the lithiation occurred slow, providing a current flow of less than 1 mA over duration of 500 hours. After this timeframe, a charge of 91.5 mAh passed the external circuit, which was equal to about 2.5% of the total capacity. Furthermore, the characteristics showed partially aberrations in the current flow, which led consequently to deviant values in the voltage line. These aberrations may originate from lithium deposition, if the potential of specific areas drops below 0.1 V vs. Li/Li$^+$.

After lithiation the cell performed another three cycles with 1C current and voltage limits of 2.4 V and 3.6 V. The obtained data is displayed in Figure 38. For an unknown reason the voltage characteristics for the anode potential was not recorded properly and hence misses in the evaluation of this graph. However, again the potential lines for the cathode (red lines) are drifting to lower potentials, so no stable reference point could be obtained by this approach. For this reason an opening of the cell was inevitable to place a reference electrode in contact to the electrolyte.
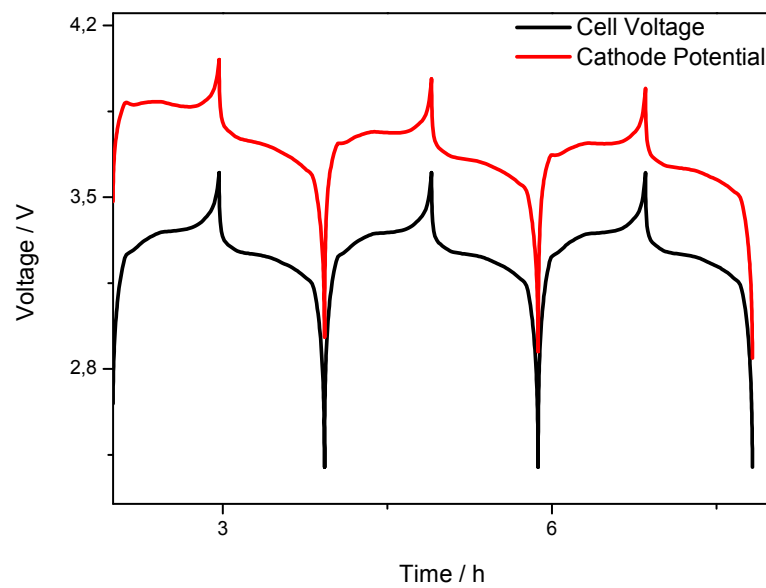
*Figure 38: Voltage profile of three cycles of A123 32113, including a lithiated casing, cycling at 1C current, voltage limits from 2.4 V to 3.6 with cell voltage (**black**), casing vs. cathode (**red**).*

3.3.2 LITHIUM METAL AS REFERENCE ELECTRODE IN LITHIUM ION BATTERIES

Due to the fact that the placement of a reference system without cell opening failed, another way had to be found in order to get separate information of cathode and anode potentials. On the account that lithium metal was chosen as the reference system two possibilities are conceivable to accomplish this aim.

In principle, those two possibilities differ from each other by the way the lithium metal is deposited on the current collector of the reference electrode. On the one hand, the lithium may origin from the lithium ion battery itself, which would be advantageous in terms of handling and preparation of the reference electrode. In this case it would be just necessary to insert a conducting copper wire into the battery and to ensure that this wire is in continuous contact with the electrolyte, while it is separated from the electrodes. Due to the fact that the cells provide safety vents, no drilling of the casing was necessary. Instead, a stranded copper wire was inserted via the small hole of the removed vent. The airtight sealing was guaranteed by multi-component epoxy glue, which reacted chemically and caused cross-links between its components even under argon atmosphere. The very simple build up is displayed in Figure 39.
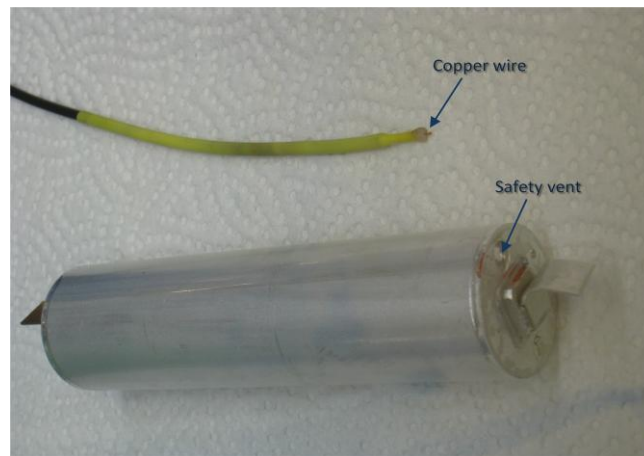
Figure 39: Copper wire and lithium ion battery with a safety vent as the starting ingredients of a reference electrode.

The deposition of lithium was done in the same way as the lithiation of the aluminum casing in chapter 3.3.1. Due to the fact that the estimation of an appropriate constant current was very hard, a constant voltage of 3.6 V was applied for one hour and lithium was deposited on the copper wire. This procedure was repeated for three times, while charge of 0.46 mAh passed the external circuit in total. Afterwards another three cycles at 1C charge/discharge were carried out. The voltage profiles of this measurement are shown in Figure 40.
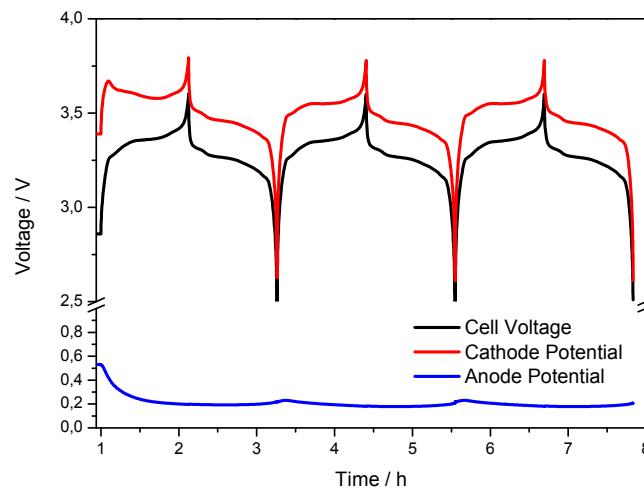
*Figure 40: Voltage profile of three cycles of A123 32113, including a copper wire with deposited lithium, cycling at 1C current, voltage limits from 2.4 V to 3.6 with cell voltage (**black**), lithium vs. cathode (**red**) and lithium vs. anode (**blue**).*

The obtained data revealed realistic behaviors for the potentials of cathode and anode. The intercalation plateaus of LiFePO$_4$ could be found at about 3.5V vs. Li/Li$^+$, which was in agreement

with the results of the cyclic voltammetry measurements in chapter 3.2.2. No voltage drift was observable between second and third cycle, while the first cycle differed a little due to higher potentials at anode as well as cathode. This was possibly the impact of an overpotential or polarization effect and concerned only the charging step. As a matter of fact, the voltage profile of the entire cell was strongly dependent on the cathode potential, while the anode potential was widely constant at about 0.2 V, which could be correlated with the first intercalation step in the left graph of Figure 33. This led to the conclusion that the anode in this A123 32113 cell was oversized in terms of capacity. In regard to the safety of the battery, this was beneficial, because the deposition of lithium on the anode should be completely suppressed by offering more active material than necessary. This point was of special importance for the design of batteries for automotive applications due to the fact that conditions, which could lead to augmented lithium plating, like high currents or low temperatures, were included in the demand profile of these battery systems. Of course this meant simultaneously an increase of more or less inactive material and hence a decrease of energy.

For verification of these data, the measured cell voltage was again plotted against the calculated difference of the recorded electrode potentials. The result is shown in Figure 41.
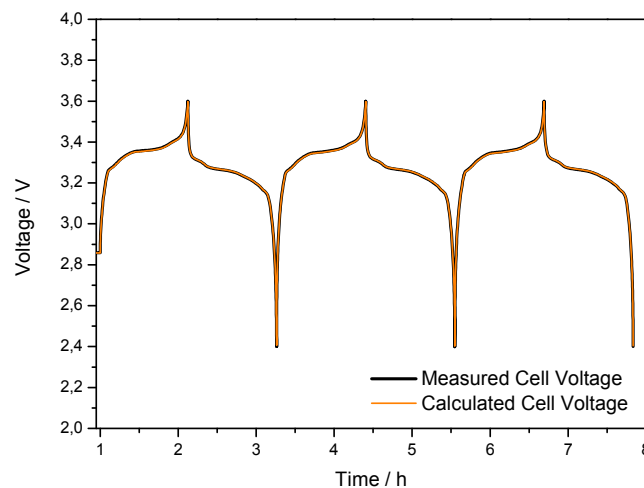
*Figure 41: Comparison of measured (**black**) and calculated (**orange**) cell voltage A123 32113, including a copper wire with deposited lithium, cycling at 1C current, voltage limits from 2.4 V to 3.6.*

Obviously, the measured and calculated voltage plots are nearly identical, which is an indication for the fact that on the one hand the lithium deposition was successful and on the other hand lithium metal provides a stable reference potential indeed. After this experiment the battery was dismantled and the stranded copper wire including the deposited lithium was investigated by scanning electron

microscopy (SEM). The investigation was performed on a TESCAN VEGA EasyProbe microscope at an accelerating voltage of 20 kV. Images of the stranded wire are shown in Figure 42.
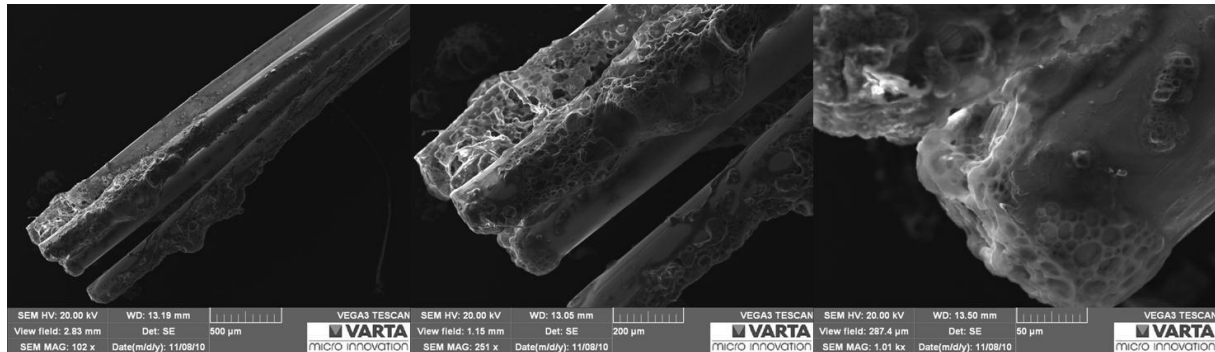
Figure 42: SEM investigations of lithium deposition on stranded copper wire.

The dismantling of the battery occurred under inert atmosphere but unfortunately, there was no possibility to keep this inert atmosphere during transfer of the wire to the microscope. For that reason it has to be mentioned that probably no metallic lithium could be found on the surface of the copper wire anymore. Instead various compounds, including LiOH, Li_2O or Li_3N, could originate from reactions with air. Additionally, these deposits were self-evidently covered with decomposition products of the electrolyte. It could be seen in the microscopic investigations that the deposition of lithium and these compounds, respectively, was rather uneven and this fact implied the risk of either dendritic growth of metallic lithium during preparation of the reference electrode or the generation of mixed potentials of lithium and copper, which could occur, if parts of the pristine copper surface got in contact with the electrolyte. Hence, it had to be concluded that the characterization of electrode materials by using lithium plated stranded copper wire as a reference electrode was risky regarding the reproducibility. For that reason another concept was developed to implement a lithium metal electrode into a commercial lithium ion battery.

Instead of using the cell's lithium and decreasing, even if marginally, the overall capacity of the battery by the depositing of mobile lithium on the copper wire, the other possibility was to bring in metallic lithium that was mechanically pressed on a current collector before. Again the airtight sealing required particular attention. For this purpose a special concept was developed to guarantee this permanent seal. Again the safety vent was used to open the battery without significant intervention. The reference electrode consisted of a steel current collector, which was shrouded by a polypropylene shell. Lithium metal was smoothly brought on one end of the steel pin. Gaskets and threads completed the reference electrode set. A cross section view of an A123 cell with and without

reference electrode as well as a schematically drawing of the implemented reference is shown in Figure 43.
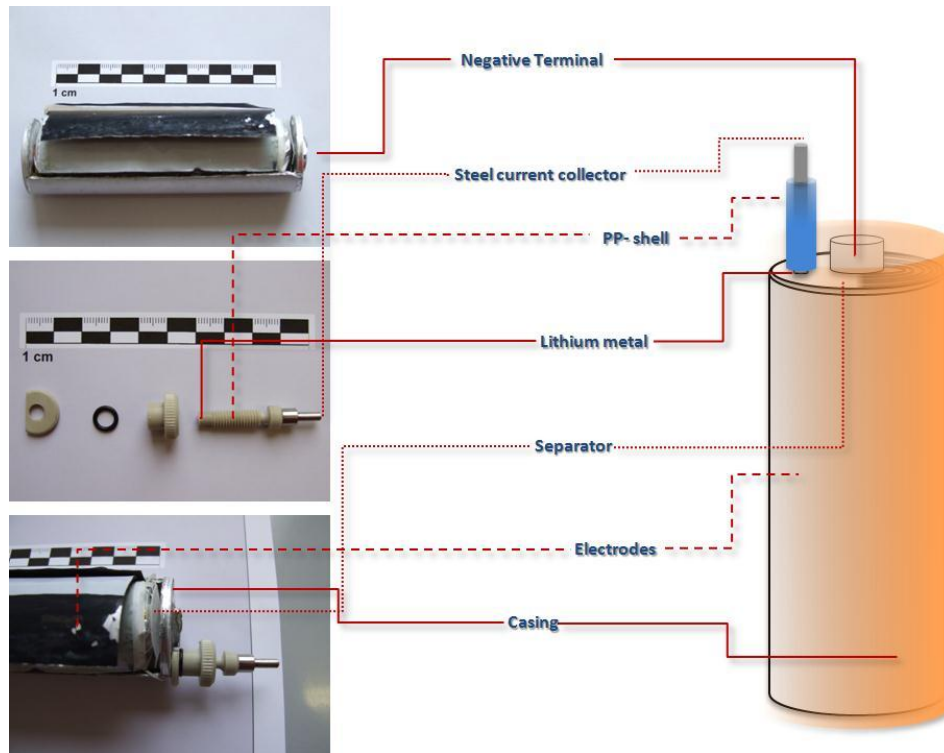
Figure 43: Cross section view of the implementation of a reference electrode in a commercial A123 32113 cell and a schematic drawing of the implemented reference electrode.

First of all, it was important to verify, that the implementation of the reference electrode had no influence on the behavior and performance of the battery, respectively. Hence, three cycles were recorded again.
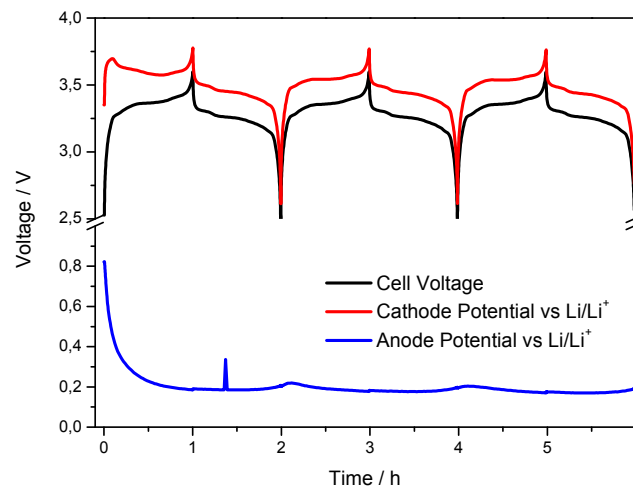
*Figure 44: Voltage profile of three cycles of A123 32113, including a reference electrode with metallic lithium, cycling at 1C current, voltage limits from 2.4 V to 3.6 with cell voltage (**black**), lithium vs. cathode (**red**) and lithium vs. anode (**blue**).*

In analogy to the measurements shown before, stable potentials could be obtained by implementation of a reference electrode consisting of metallic lithium. As a matter of fact, the first cycle differed again from the remaining two and showed significantly higher potentials for anode and cathode. The high anode potential at begin of the measurement could possibly be traced back to a self-discharge process due to the fact that the cell might have had a long time of storage before the electrochemical measurements were performed.
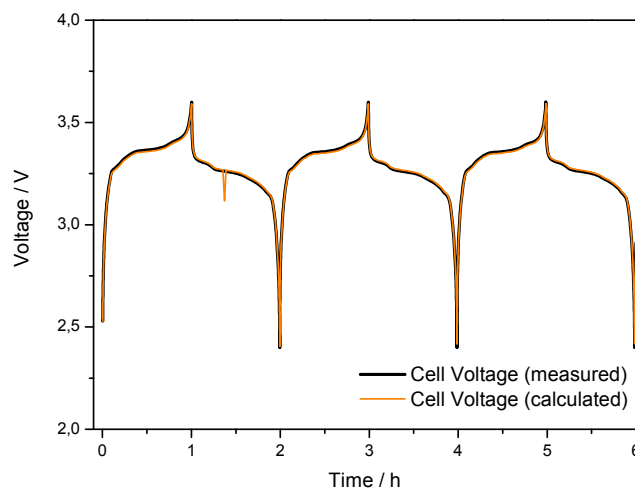
*Figure 45: Comparison of measured (**black**) and calculated (**orange**) cell voltage A123 32113, including reference electrode with metallic lithium, cycling at 1C current, voltage limits from 2.4 V to 3.6.*

Again the measured cell voltage was compared to the cell voltage that could be obtained by the difference of the measured electrode potentials and looking at Figure 45 the conformity of the voltage lines is obvious. The cycling performance of pristine systems and systems with reference electrodes may differ due to the temporary cell opening and insufficient sealing, so charge and discharge capacities as well as efficiencies were recorded for fifty cycles. Figure 46 shows the first fifty cycles of the measurement in Figure 30 on the left side, compared to fifty cycles of a cell with implemented reference electrode on the right side. As a result the capacity fading of the reference-containing system is negligible, while the efficiencies are just about 100 % for each cycle. So no difference to the pristine battery could be observed in any regard.
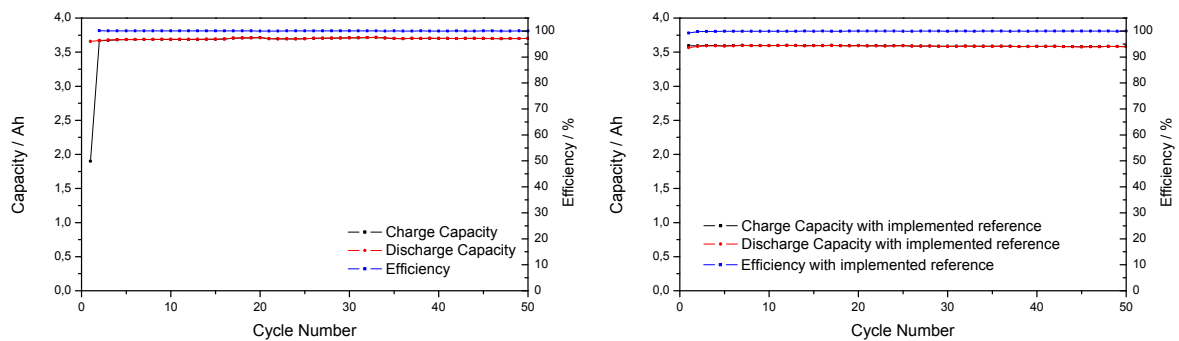
Figure 46: Comparison of charge/discharge characteristics (black/red) and efficiencies (blue) of two A123 32113 cells at 1C current, cycled from 2.4 V to 3.6 V without reference electrode (left side) and with implemented lithium reference electrode (right side).

Eventually it can be assumed that the insertion of reference points into commercial cells can turn out tricky, because several factors have to be considered. Especially the airtight sealing needs special attention in this regard. Deposition of mobile lithium from the cell, either on the aluminum casing or on an inserted copper wire did not lead to the desired results. Finally, the implementation of a lithium metal reference electrode, mechanically pressed on a steel current collector was successful and all subsequent measurements are accomplished by this system.

3.4 ELECTROCHEMICAL MEASUREMENTS WITH REFERENCE ELECTRODES

3.4.1 GALVANOSTATIC INTERMITTENT TITRATION TECHNIQUE

As far back as 1977 and hence long before the first lithium ion battery was introduced, Weppner et al. suggested the galvanostatic intermittent titration technique (GITT) to get electrochemical information about diffusion coefficients or the electrical and general lithium mobilities in Li_3Sb and Li_3Bi compounds (130). GITT measurements have remained a powerful tool in the characterization of batteries and its components until today. In principle, the experiment is comprised of several low current pulses (0.05 C), followed by a period of rest. Hence, it can be described as the combination of a coulometric titration and electrochemical relaxation measurements. A schematic drawing of a single current pulse and the correlating potential response is shown in Figure 47.
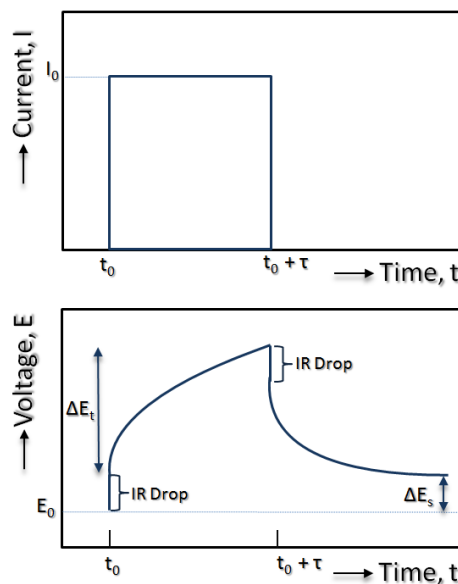
Figure 47: Illustration of a single current pulse (above) and the correlating potential response (below) (redrawn) (130).

By use of this method, it is possible to gain information of the system on load (during the current pulse) as well as at equilibrium conditions (during the relaxation phase) at different states of charge. At begin of the measurement the cell is in electrochemical equilibrium. Due to ohmic resistance and overpotential effects the voltage raises immediately as soon as the current pulse starts. During this charge/discharge step lithium ions are either inserted or extracted from the electrodes and a new stoichiometric composition is built. When the pulse is followed by the period of rest, the unevenly

distributed charge carriers (mainly lithium ions) start to homogenize over the entire available electrode material. The velocity of this relaxation is dependent on the velocity of lithium diffusion and results in a sloping of the potential. The diffusion coefficient of the involved species can be calculated by Equation 27 (131).

$$D = \frac{4}{\pi \cdot \tau} \left(\frac{V_M m_B}{S M_B} \right)^2 \cdot \left(\frac{\Delta E_s}{\Delta E_t} \right)^2$$

<div align="right">*Equation 27*</div>

D...   *chemical diffusion coefficient*
τ...   *time duration of the constant current pulse*
V_M...   *molar volume of the host material*
m_B...   *mass of the host material*
M_B...   *molar mass of the host material*
S...   *area of electrode/electrolyte interphase*
ΔE_S...   *change of steady state voltage during GITT step*
ΔE_T...   *total change of cell voltage during GITT step*

However, this equation is just valid in terms of very thin electrodes and on the condition that the change of volume and associated surface area are negligible. On the account that this is not the case for the industrially manufactured high-power battery, calculations of diffusion coefficients are not reasonable.

At the end of the diffusion process (when the potential is constant) a new equilibrium voltage is reached. This equilibrium voltage refers to the open-circuit voltage at the respective states of charge. Hence, the information that can be obtained by GITT measurements is mainly comprised of overpotential effects (depending on the change of voltage under load) and open-circuit or steady-state voltage at different states of charge. For a better understanding, a sequence of three consecutive current pulses and relaxation periods from a real experiment is shown in Figure 48.
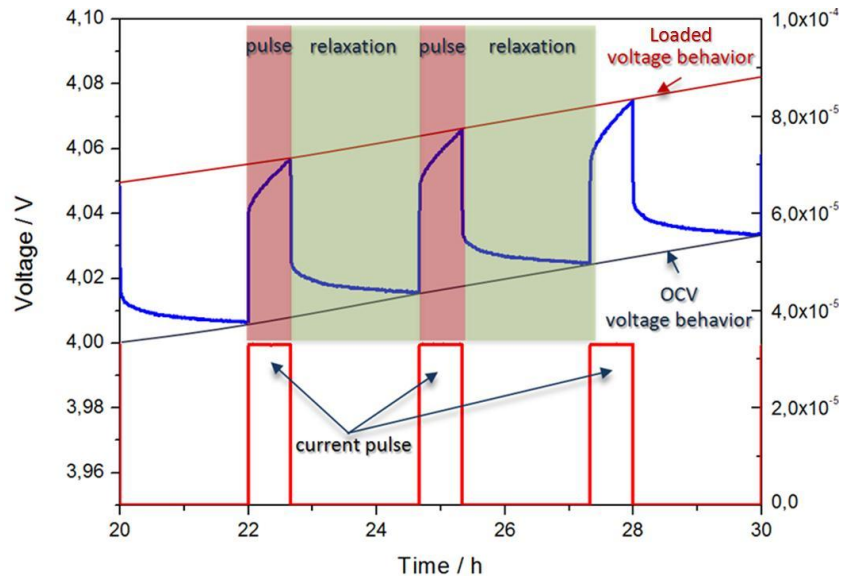
Figure 48: Sequence of three current pulses (red) in a GITT-experiment, leading to a voltage response (blue). The corresponding loaded (dark red) and open-circuit (dark blue) voltages are shown as well.

With the implementation of a reference electrode, the obtained voltage data could be expanded to anode and cathode potentials again. Hence, information about kinetic parameters as well as balancing of the electrodes could be gained. The following measurement setup was adopted from Weppner et al. (130) and was composed of 40 charge pulses with a current equal to 0.05 C, each lasting for 40 minutes or until a voltage of 3.6 V was reached. Every charge pulse was followed by a period of relaxation, which lasted 120 min each. Afterwards the process was reversed and 40 discharge pulses and rest periods were performed. The test program is again shown in Table 1.

Table 9: Test program for the following GITT measurement

	Count	Step	Cut-off condition
Charge	40 x	Current pulse (0.05C)	40 min or 3.6V
		Period of rest	120 min
Discharge	40 x	Current pulse (0.05C)	40 min or 2.4V
		Period of rest	120 min
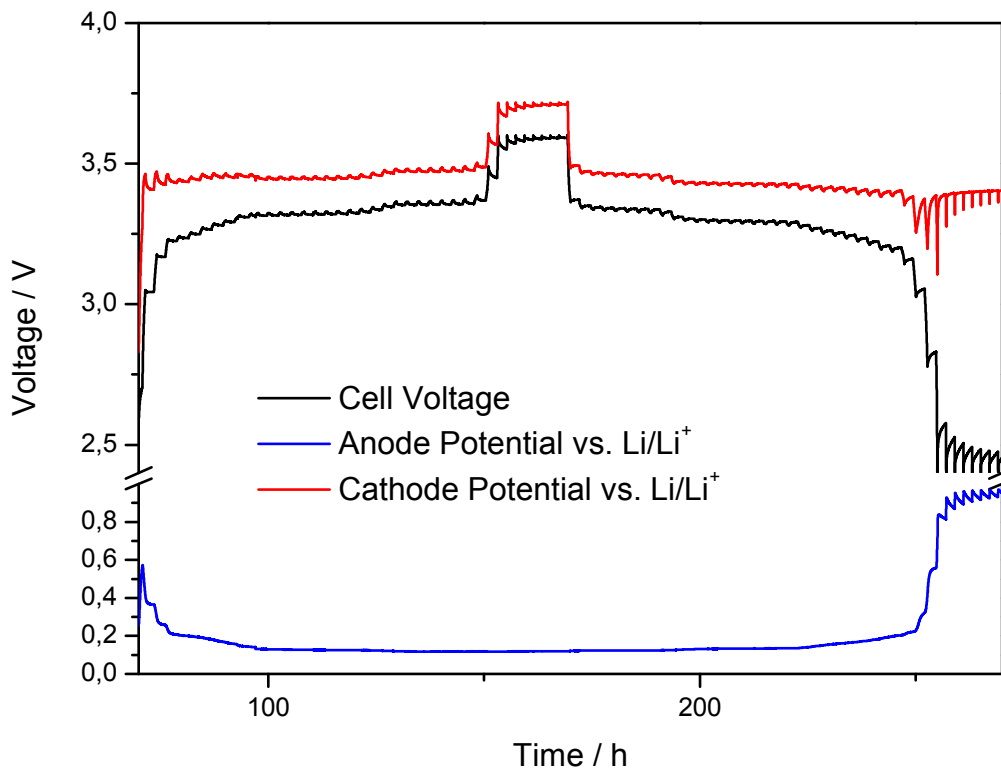
*Figure 49: Cell voltage (**black**), cathode potential (**red**) and anode potential (**blue**) in a GITT experiment.*

Figure 49 shows the potential lines of anode, cathode and as well as the cell voltage in the GITT experiment. It is obvious that the cathode potential (red line) was not only responsible for the behavior of the overall cell voltage but also for the voltage drop or rise within the period of relaxation. The fact that practically no overpotential or ohmic resistance was observable at the anode was an evidence to suggest that lithium ion uptake or release at the anode was much faster or at least less impeded than at the cathode. The voltage data could either be displayed against the time (like in Figure 49) or against capacity and state of charge, respectively (like in Figure 50). Both applications were valid and principally equal but in case that the x-axis describes the SOC, the OCV-line of battery could be determined very easily. Figure 50 shows this application. The consequential open-circuit voltage lines for the charge and the discharge process were displayed as well.
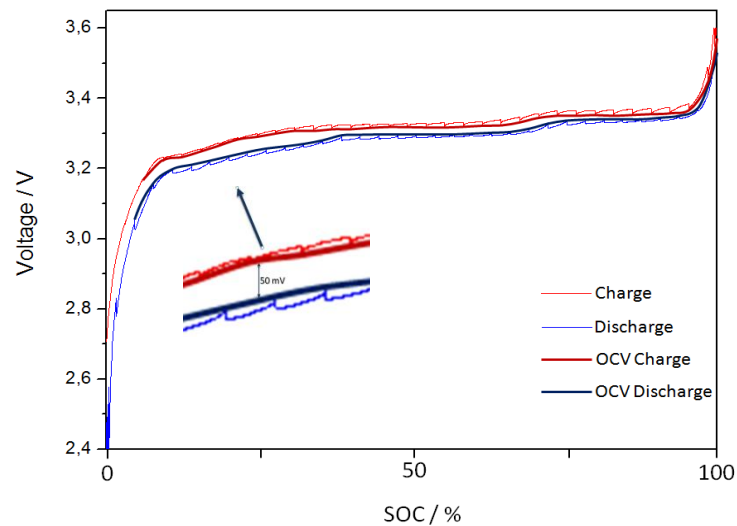
Figure 50: Charge and Discharge cell voltage lines and OCV-Charge and OCV-Discharge cell voltage lines during a GITT experiment.

The result of this experiment was unexpected. The analysis of the open-circuit curves clearly revealed a voltage hysteresis in the range of several mV up to about 50 mV. This was as much remarkable as the OCV should only depend on the state of charge, as well as on temperature and concentration of the involved species (see chapter 2.1.2) but not on the way these states are reached. Concretely, the voltage of a cell at exactly 50% SOC should have been decisive regardless of its charge or discharge background. To gain information about the origin of this hysteresis, the potential data of the graphite anode and the LFP cathode was compared (see Figure 51).
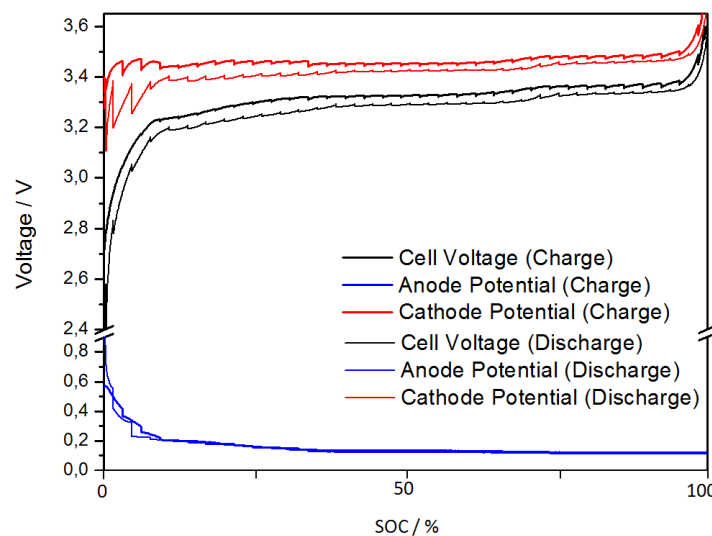
*Figure 51: Comparison of charge and discharge behavior in a GITT experiment with cell voltage (**black**), cathode potential (**red**) and anode potential (**blue**).*

Considering Figure 51, it was obvious that the hysteresis effect could be assigned to the cathode potential of the cell. Analogously to the overall cell voltage, OCV points of the charge and discharge branch differed. The difference was rather small in regions of middle and high SOC and relatively high at high depth of discharge. In contrast to that, the charge and discharge curve of the anode were even on load conditions nearly identical for a wide range of SOC, and differed just at high depth of discharge.

As mentioned in chapter 3.2.1 the phenomenon of static hysteresis is already known in Ni-MH battery systems. The characteristics of the Ni-MH hysteresis are in accordance with the domain theory that states that the electrode material is composed of clearly separated regions or domains each of which exhibits two or more metastable states. However, even in the NiMH-battery, this metastability is yet still a matter of scientific discussion (126). It is assumed that either changes during intercalation or phase separation are possible causes for the hysteresis effect in NiMH-systems (124). The expansion and contraction of the lattice structure during the intercalation and ejection processes are a possible cause for hysteresis as well. This assumption is based on the observed hysteresis of hydrogen permeation through palladium membranes due to changes in the lattice parameters within these membranes during the process (132).

Within the lithium ion battery community OCV hysteresis effects gained only little attention. Dahn described OCV hysteresis effects concerning half-cell investigations on hydrogen-containing anodes and led it back to an activating process that was necessary for this kind of active material but lowered the efficiency significantly (133). Considering Figure 51, this reason could be excluded in terms of the hysteresis phenomenon of the A123 32113 cell, because neither a hysteresis nor excessive overpotentials were observed at the anode.

Matsui et al. investigated the open-circuit voltage of $LiFePO_4$ olivine particles and observed voltage hysteresis at very high and low SOC, which they attributed to Li^+ diffusion kinetics. Extraordinary little Li^+ diffusion coefficients were proved by GITT experiments at very high and very low SOC. This led to the conclusion that the obtained OCV profile in this regions may not be in an equilibrium state due to the very slow kinetics (134). Although a small hysteresis could be observed over the entire voltage range, this small Li^+ diffusion, which is caused or accompanied by a small $LiFePO_4/FePO_4$ contact area within the particles, could be one main reason for the differences of the OCV curves during charge and discharge. Furthermore, the lattice parameters of the compound during the lithiation/delithiation exhibit a difference of about 0.5 Å (10.32 Å for $LiFePO_4$ vs. 9.77 Å for $FePO_4$) along the a-axis (78).

On its largest width, voltage hysteresis in the observed A123 32113 exhibited a value of about 50 mV (see Figure 50). By the fact that the cell was cycled in the range of 2.4 V to 3.6V, 50 mV would correspond to about 4% of the total voltage range and hence seemed to be undesirable but negligible up to a certain extent. However, the problem that occurs in terms of LiFePO$_4$ based electrodes is the very flat voltage curve, originating from the wide range of the LiFePO$_4$/FePO$_4$ two-phase region. As a matter of fact, the open-circuit voltage plays a key role in determination of the state of charge in automotive applications. Due to the fact that no other measured data is available beside the cell voltage and the capacity, it would be very advantageous, if the OCV could help to determine the exact position on the SOC-branch. The consequence of the obtained information concerning the OCV/SOC correlation is displayed in Figure 52, where two points of the performed GITT experiment are outlined.
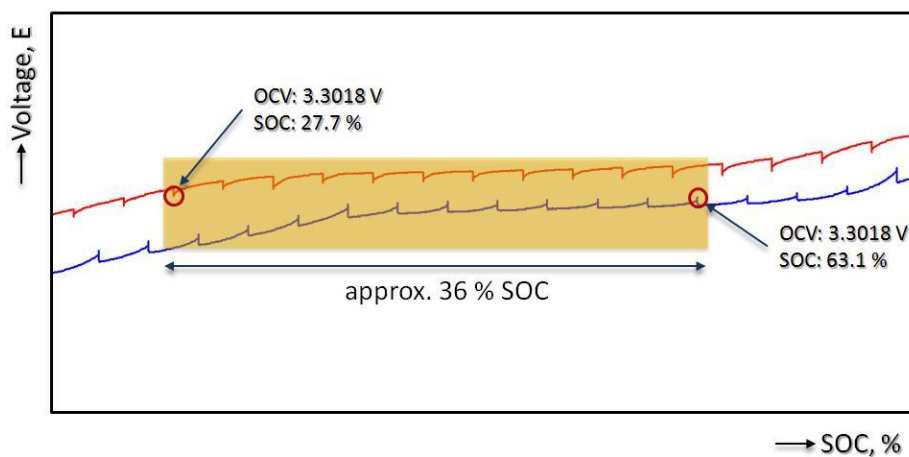
Figure 52: Two points of the GITT experiment with different SOC but equal OCV of 3.3018 V

This graph revealed the major problem with SOC determination via OCV. On the condition that the information about the "history" of the open-circuit voltage was lacking, a prediction of the state of charge or depth of discharge was mindless. In fact, a steady-state voltage of 3.3018 V could belong to a state of charge of 27.7%, when the cell was charged and 63.1 % when the cell was discharged, respectively. Practically, this means that the battery management system (BMS), which should control battery packs in automotives by monitoring their voltage, current, temperature etc., could be wrong by a value of up to 36% percent, when the SOC and therefore the remaining range of the vehicle is calculated by the use of the steady-state voltage. This, however, was a problem that could not be solved by implementation of a reference electrode due to the fact that the cathode potential suffered from the same hysteresis effect and the anode was oversized in regard to the overall capacity, so its potential curve was very flat over a wide range.

3.4.2 RATE CAPABILITY TEST

In the following, rate capability tests of a fresh A123 32113 cell were performed. One the one hand, these tests aimed to gain information about the voltages on load conditions, meaning the revealing of overpotentials and ohmic resistances, respectively, and furthermore, to get knowledge about the kinetic balancing of the A123 32113 cell.

It was reported that the placement of the reference electrode could have a direct impact on the accuracy of measurements, due to the fact that reference electrodes positioned in the electrolyte pool outside of the electrode are would reflect the potential field of the electrode nearest (135). For that reason a second reference electrode was implemented in this test via the second safety vent on the other side of the cylindric cell.
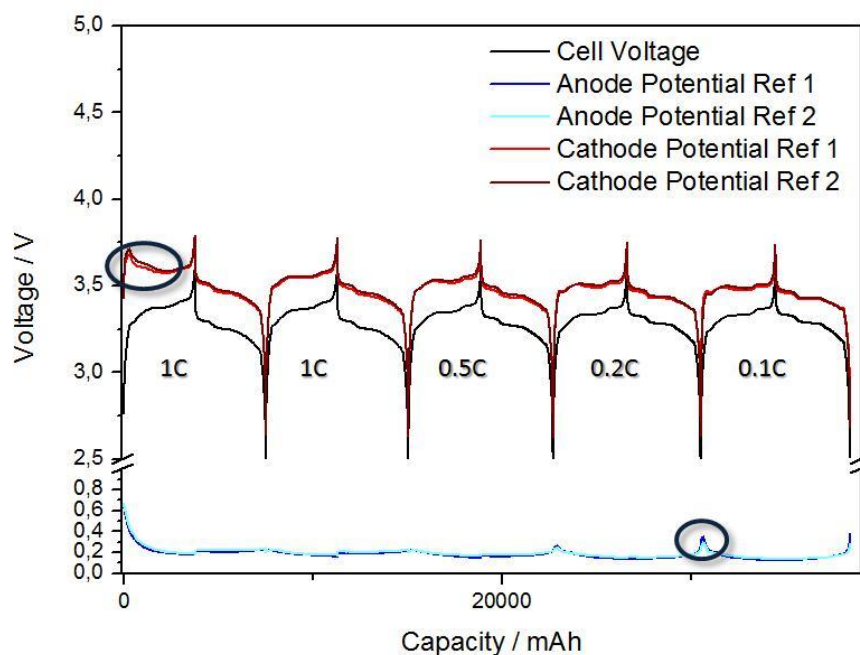
*Figure 53: Voltage profiles of A123 32113, cycling at different rates, voltage limits from 2.4 V to 3.6 with cell voltage (**black**), reference 1 vs. cathode (**red**), reference 2 vs. cathode (**wine**) and reference 1 vs. anode (**blue**) and reference 2 vs. anode (**light blue**).*

The rate capability test included six cycles, where the cell was charged and discharged with a current of 1C during the first and second cycle, 0.5C during the third, 0.2C during the fourth and 0.1C during the fifth cycle (see Figure 53). Eventually one cycle was performed with a c-rate of 0.01C, leading to a theoretical cycling duration of 100h for charge as well as discharge.

The insertion of a second reference electrode revealed that the cathode as well as the anode potential was not evenly distributed over the entire electrode material. Areas, which exhibit potential difference of more than 30 mV, are marked by a dark blue circle in Figure 53.

The origin of this potential distribution could be mainly found in two reasons. On the one hand the cell geometry could cause areas that are more loaded than others, due to the field lines of the electric field or, for instance due to oversized and hence overlapping areas, where the distance for lithium ion migration in the electrolyte is very long. On the other hand, uneven charge distribution could be caused by pronounced ageing of the cell. Especially the formation of surface films at the anode- but also at the cathode/electrolyte interphase lead to an impedance of charge transfer, as it was discussed in chapter 2.2.5. As mentioned in chapter 2.2.7, uneven charge distribution can lead to a safety hazard due to the possibility of lithium deposition at the anode surface. As a matter of fact, no conditions were observed within these measurements, at which lithium plating was possible.

In the following, the voltage lines for the overall cell, the anode and the cathode were separately displayed. Figure 54, Figure 55 and Figure 56 described the potential behavior during the charging and discharging step. According to these measurements, it was obvious that the cell potential as well as the cathode potential increased with higher currents during charge and lowered during discharge. This means in fact, that the hysteresis of the voltage curve got bigger at higher C-rates (more voltage was necessary during charge and less voltage was obtained during discharge) and the overall energy efficiency decreased significantly. However, one may think, this should be in analogy in case of the negative electrode. But as a matter of fact, the anode potential during charge was higher at 1C than at 0.01 C, which was the exact opposite of the expected behavior. This could only be explained by two reasons. First of all the deintercalation of lithium ions from the $LiFePO_4$ particles was obviously the speed limiting process at the charging step. Higher currents led to more ohmic resistance and thus caused higher potentials, whereas the ohmic resistance for the anode was still negligible. This however, would just explain the voltage behavior of the cathode. So secondly there had to be a kind of diffusion process inside the graphite that was responsible for the observed potential characteristics at the negative side. Concretely, it was assumed that the positioning of the reference electrode played an important role, due to the fact that the recorded potential was just valid for an edge region of the electrode wound. At very low current, the anode was able to distribute the charges evenly over the entire electrode, leading to significantly lower potentials in the edge region. Unfortunately, this placement is the only possibility to investigate spirally wound commercial batteries with the help of reference electrodes. A placement of the reference electrode in the middle and especially in between anode and cathode would be advantageous and was realized for pouch-bag cells in chapter 3.4.3.
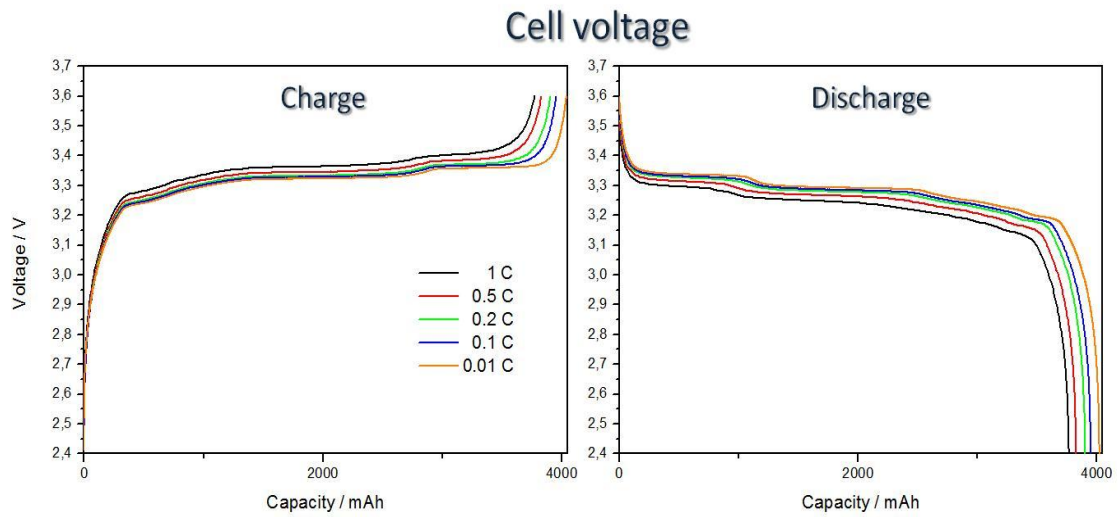
Cell voltage

Figure 54: Voltage profiles of the overall cell during charge and discharge at different C-rates.
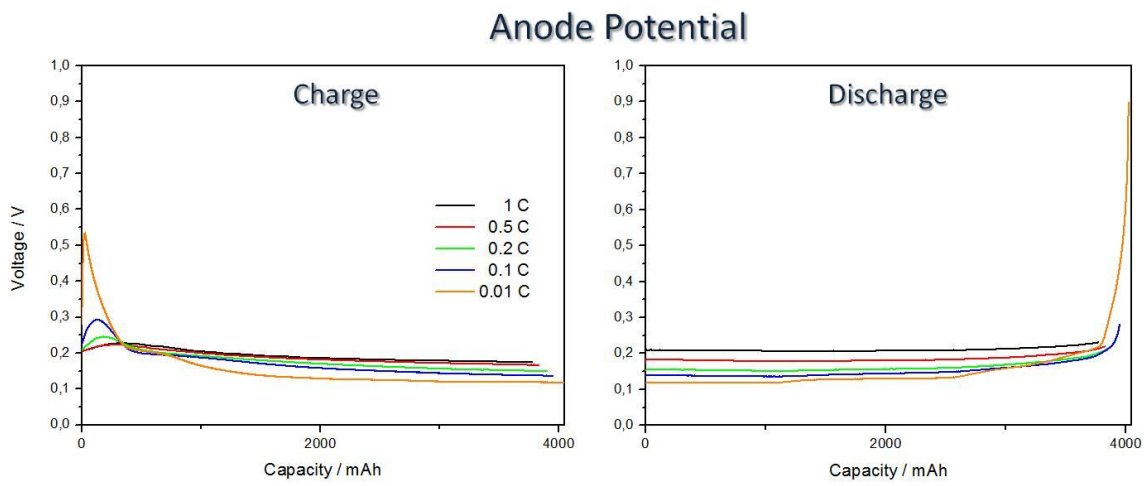
Anode Potential

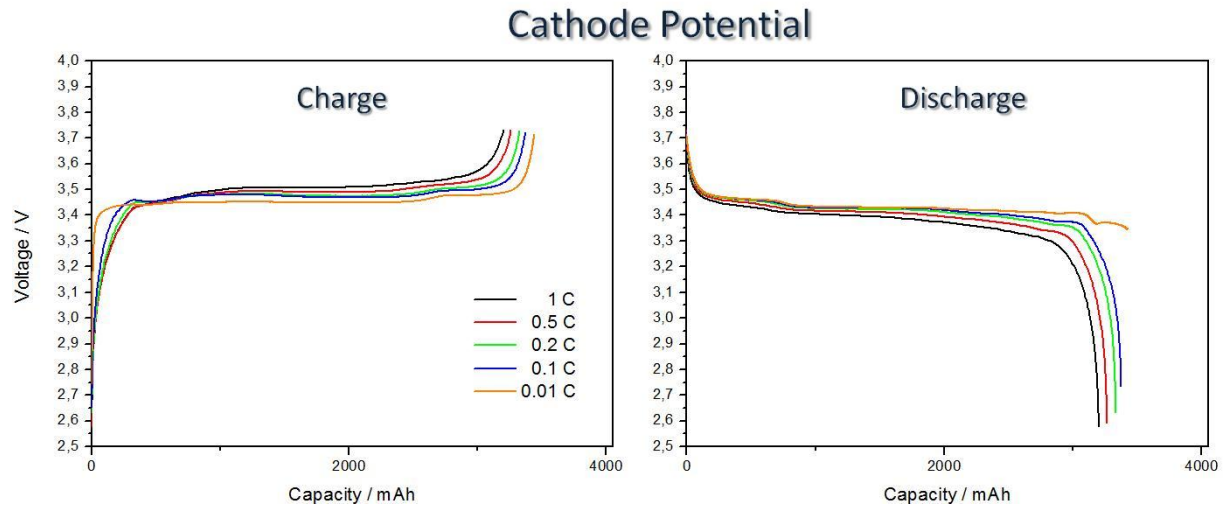*Figure 55: Anode potentials during charge and discharge at different C-rates.*
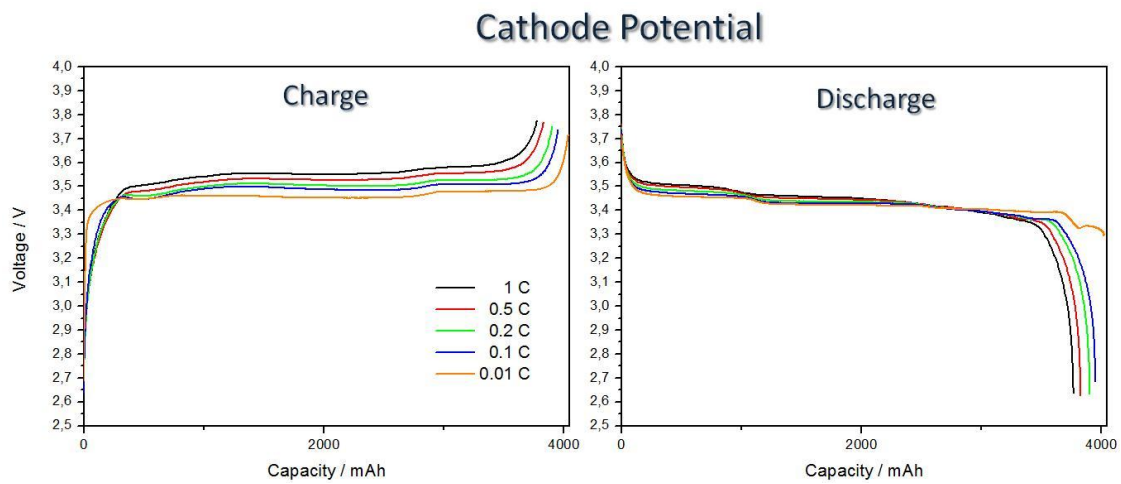
Cathode Potential

Figure 56: Cathode potentials during charge and discharge at different C-rates.

3.4.2.1 Ageing Effects and Rate Capability Tests

Due to the close cooperation with Magna E-car systems it was possible to obtain aged cells of the same cell type, which were used in practically relevant tests in an entire battery pack. Unfortunately, the exact measurement conditions were not available due to secrecy agreements but the operating time was approximately 2,000 hours at alternating charge and discharge currents. This led to loss of capacity of about 15% percent compared to its initial value.

In the following, the same rate capability test was performed with an aged A123 32113 battery. The measured data is displayed in the following Figure 57, Figure 58 and Figure 59.
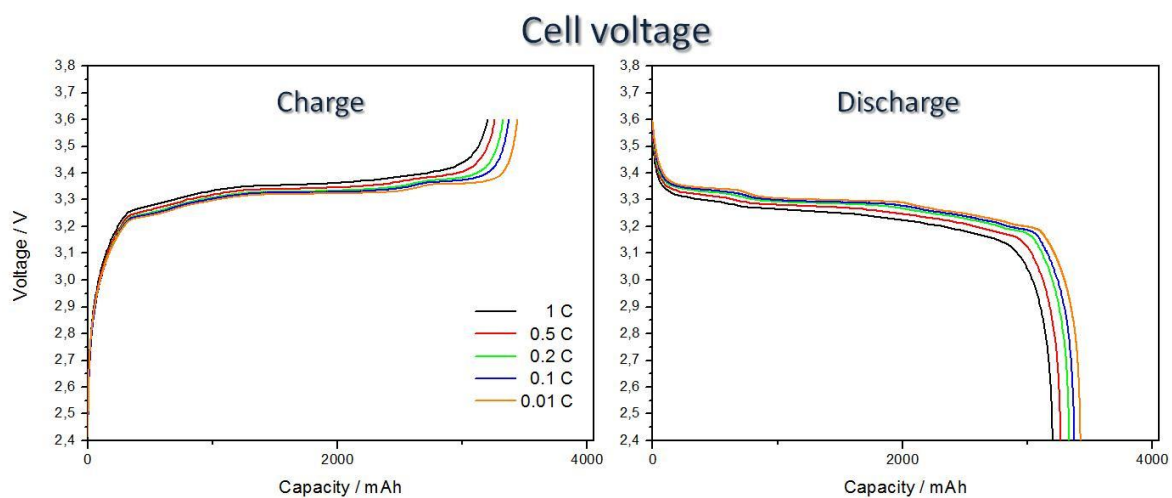
Figure 57: Voltage profiles of an aged cell during charge and discharge at different C-rates.
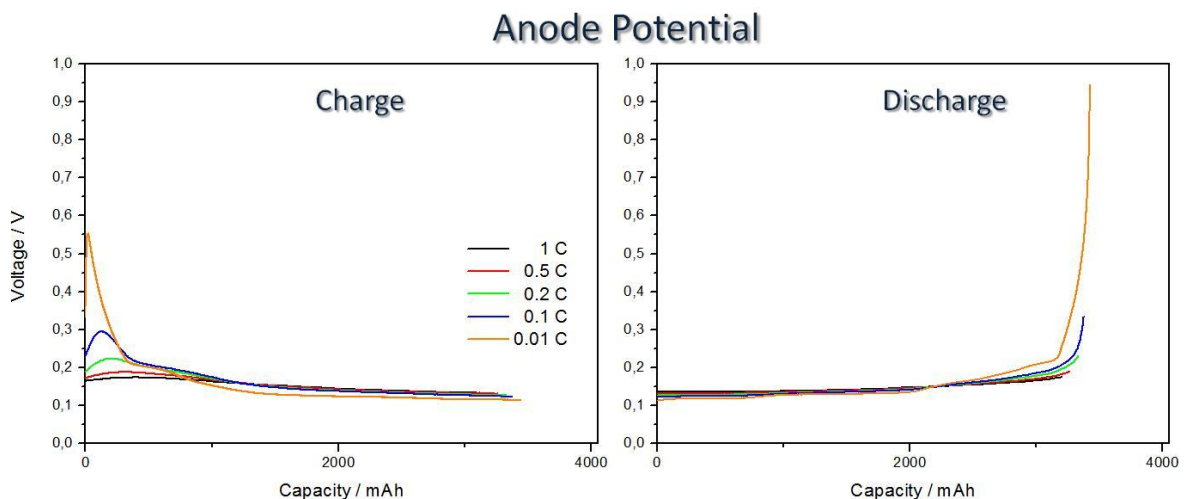
Figure 58: Anode potentials of an aged cell during charge and discharge at different C-rates.

Figure 59: Cathode potentials of an aged cell during charge and discharge at different C-rates.

This experiment revealed principally a similar behavior of the aged cell compared to the fresh cell in the previous measurement. Again the anode seemed to be kinetically favored, which led to higher cathode potentials, the higher currents were applied. The obtained capacity was logically lower than the previous one, which could be easily explained by the capacity fade caused by its pretreatment at Magna E-car systems. In the following the cell voltages of the new and the aged cell were compared during the charging steps (see Figure 60).
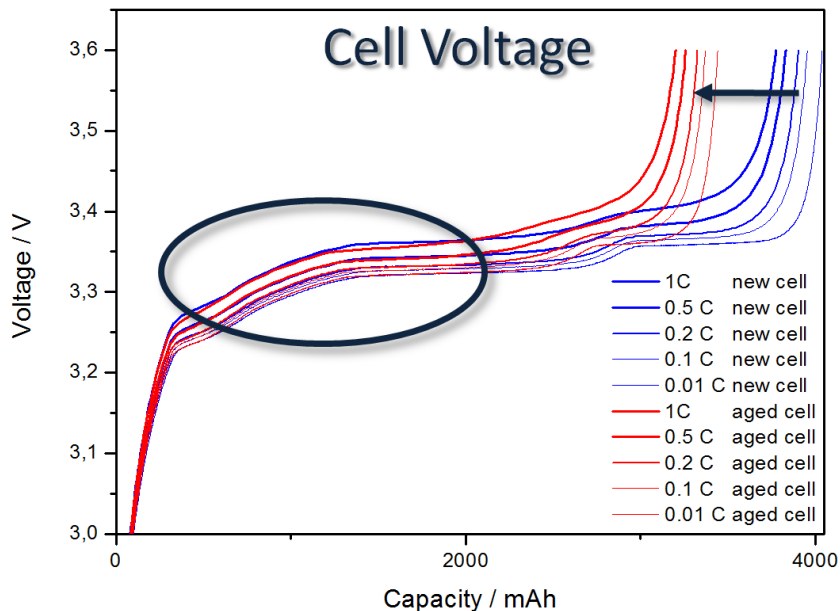
Figure 60: Cell voltage of the new and the aged cell during the charging steps of the rate capability test.

It could be obtained from Figure 60 that the potential lines were shifted in x-direction (see blue arrow), which can be easily explained by the observed capacity fade. However, the potential lines at lower states of charge (marked by the blue circle) are absolutely similar, which was an indication that the cell did not suffer a power fade. So the simple comparison of the cell voltage could reveal an observable loss of charge, meaning either the loss of lithium or the loss of active material (see Table 5), but not its reason.
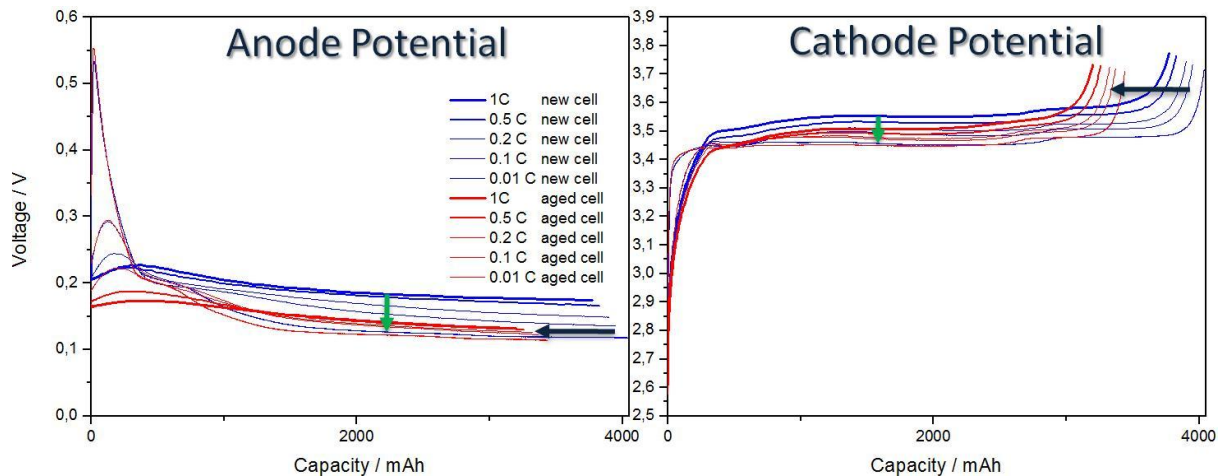
*Figure 61: Anode and cathode potential of the new (**blue**) and the aged (**red**) cell during the charging steps of the rate capability test.*

The comparison of the anode and cathode potentials of the new as well as of the aged cell, however, could help to interpret the observed behavior. Again, the blue arrows in Figure 61 marked the potential shift that was caused by the fact, that the capacity of the aged cell was lower than those of the new one. Additionally, a potential shift in y-direction was observable in both graphs, which was marked by a green arrow. As a matter of fact the anode potential during charging shifted to lower values, which is a clear indication of an impedance rise and overpotential effect, respectively. By considering Table 5, and on the assumption that no overcharge conditions could have caused a corrosion of the current collector, this could be only traced back to the continuous growth of the SEI with prolonged cycling. However, due to the fact that the cathode material limits the kinetics of the reaction, this growth of the SEI and simultaneous increase of impedance did not lead to the consequential power fade.

Concluding the results of these rate capability tests with inserted reference electrodes, it had to be noted that the anode seemed to be the mainly responsible origin of the cell ageing. Considering the potential shift of the anode potential, which was caused by an increase of impedance or overpotentials, it had to be assumed that the continuous growth of the SEI played a dominating role in terms of the capacity loss of the overall cell. However, it had to be mentioned that ageing of the

cathode was hard to determine by this method, because the impact of the anode ageing superimposed other ageing effects.

3.4.3 ELECTROCHEMICAL IMPEDANCE SPECTROSCOPY

All previously mentioned component steps of any electrochemical process, including ohmic resistance and all kinds of overpotentials, contribute to the total potential drop across the cell that could be observed within the so far performed measurements. For a ***direct current*** these effects can be represented by resistances, caused for instance, by the ohmic drop through the electrolyte or the inhibition of the charge-transfer through phase boundaries. However, if an ***alternating current*** flows, it becomes necessary to distinguish purely ohmic resistances from non-ohmic, complex and normally frequency-dependent resistances, which are often termed impedances (32).

With a given potential E at an electrode a stationary or not too fast changing state is adjusted to which belongs a current I. The superposition of a sinus-ac voltage U (ω) with the frequency **f** (ω =2πf) causes an ac-component current I (ω). If the amplitude of this voltage E is small enough, I (ω) can also be regarded as sinusoidal (136).

$$E = E_0 \cdot \sin(\omega \cdot t + \varphi_U)$$

<div align="right">*Equation 28*</div>

$$I = I_0 \cdot \sin(\omega \cdot t + \varphi_I)$$

<div align="right">*Equation 29*</div>

E…	*voltage*
E_0…	*voltage amplitude*
ω…	*angular frequency*
t…	*time*
φ…	*phase angle*
I…	*current*
I_0…	*current amplitude*

This point has to be considered in the view of the fact that the amplitudes higher than 25mV can cause polarization effects in electrochemical systems and the validity of Ohm's law and thus the linearity of the system gets lost. Precisely due to this linearity condition, the current amplitude I is proportional to R and the quotient E/I is consequently non-variant at given frequency. However, between the sinus-signals E (ω) and I (ω) appears a phase shift **φ** (see Equation 28 and Equation 29), whenever the current is not only dependent on the momentary value of the potential (like real

ohmic resistance) but also on previous values (136). The influence of the three most important resistances, namely the ohmic resistance, the inductance and the capacitance is illustrated in Figure 62.
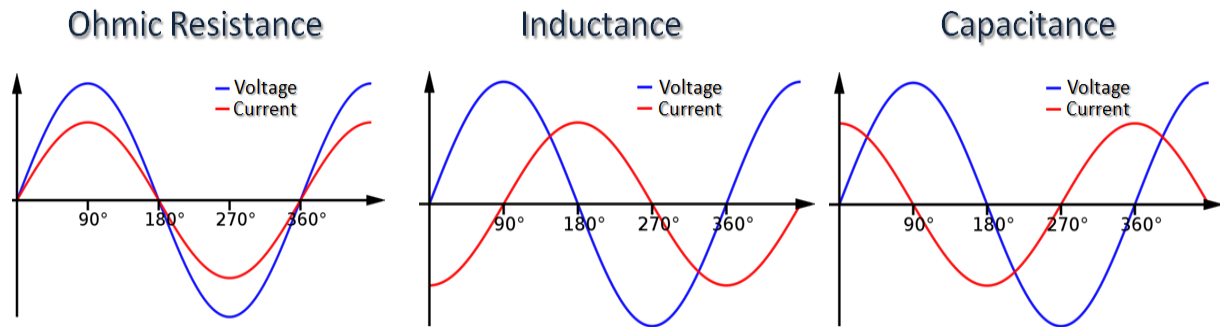
Figure 62: The three most important resistances during ac-measurements.

According to this illustration, the ohmic resistance causes no shift in the phase angle of the sinusoidal signal. Inductance or capacitance lead to a phase shift in the system, where either the current signal (for capacitive effects) or the voltage signal (for inductive effects) is lagging behind. In this context, inductance describes the ability to store energy by providing an electromagnetic field. But also fields outside the system can disturb the measurement. For that reason it is necessary to shield the measured cell from the environment to avoid disturbances caused by external devices. A Faraday cage is very suitable to protect the investigated system and therefore commonly applied during impedance measurements. Capacitance on the other hand, is already described in chapter 2.1.3.1 and means the formation of an electrochemical double layer, which can be observed by apparent charge consumption. Beside these two, also Warburg impedance, which is caused by diffusion kinetics, is common in electrochemical devices and leads to a phase shift in the impedance measurement.

In order to get an exact mathematical solution of the differentiation of Equation 28 and Equation 29, they are expanded into complex numbers. By description in the complex plane, the sinusoidal signals are sufficiently determined.

$$E = E_0 \cdot \sin(\omega \cdot t + \varphi_U) \longrightarrow \hat{E} = E_0 e^{i \cdot (\omega \cdot t + \varphi_E)}$$

<div align="right">*Equation 30*</div>

$$I = I_0 \cdot \sin(\omega \cdot t + \varphi_I) \longrightarrow \hat{I} = I_0 e^{i \cdot (\omega \cdot t + \varphi_I)}$$

<div align="right">*Equation 31*</div>

E...	*voltage*
$\hat{E}$...	*complex voltage*
E_0...	*voltage amplitude*
ω...	*angular frequency*
t...	*time*
φ...	*phase angle*
I...	*current*
$\hat{I}$...	*complex current*
I_0...	*current amplitude*

Using Euler's formula, these expressions can finally be divided in a real part and an imaginary part of the impedance, as shown in Equation 32.

$$e^{i \cdot (\omega \cdot t + \varphi)} = \cos(\omega \cdot t + \varphi) + i \cdot \sin(\omega \cdot t + \varphi)$$

<div align="right">*Equation 32*</div>

Due to the fact, that the relationship of voltage amplitude and current amplitude is linear and hence follows the ohmic law, the complex impedance **$\hat{Z}$** can be calculated by Equation 33.

$$\hat{Z} = \frac{\hat{E}}{\hat{I}}$$

<div align="right">*Equation 33*</div>

$\hat{Z}$...	*complex impedance*
$\hat{E}$...	*complex voltage*
$\hat{I}$...	*complex current*

$\hat{Z}$ is a complex number, and thus the frequency dependent $\hat{Z}_{(\omega)}$ can be displayed in two absolutely equivalent ways, namely by Cartesian coordinates (Equation 34) as well as by polar coordinates (Equation 35).

$$\hat{Z}_{(\omega)} = |Z| \cdot \cos\varphi + |Z| \cdot i \cdot \sin\varphi$$

$$\hat{Z}_{(\omega)} = |Z| \cdot e^{i \cdot \varphi}$$

$\hat{Z}$ ...   *complex impedance*
ω...   *angular frequency*
ϕ...   *phase angle*

The analysis and interpretation of impedance measurements occurs by graphic representation of Equation 34 and Equation 35. The graph following Equation 35 is called Bode plot and displays the frequency dependence of either the impedance or the phase angle.
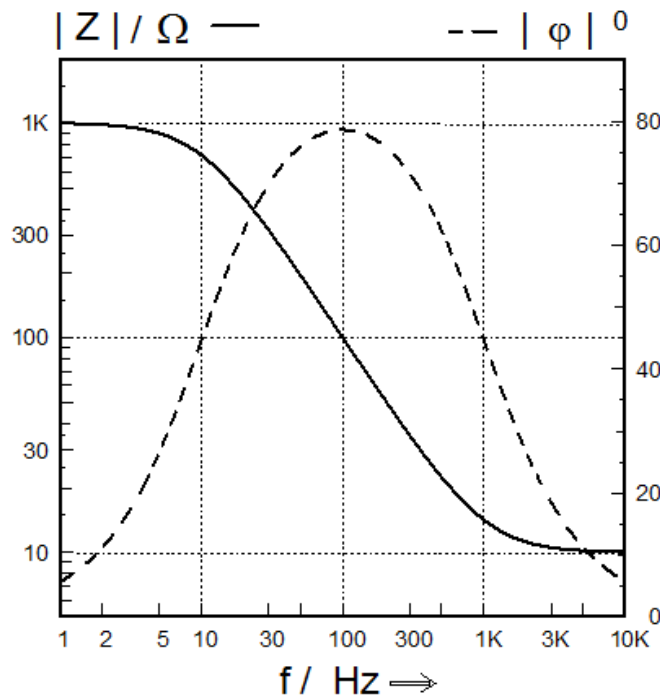
Figure 63: Bode plot, originating from polar coordinates (137).

The second graphic representation is called Nyquist plot and originates consequently from the Cartesian coordinates of the impedance measurement. Here the real part of Equation 34 is plotted against the associated imaginary part. A simple example for a Nyquist plot is shown in Figure 64.
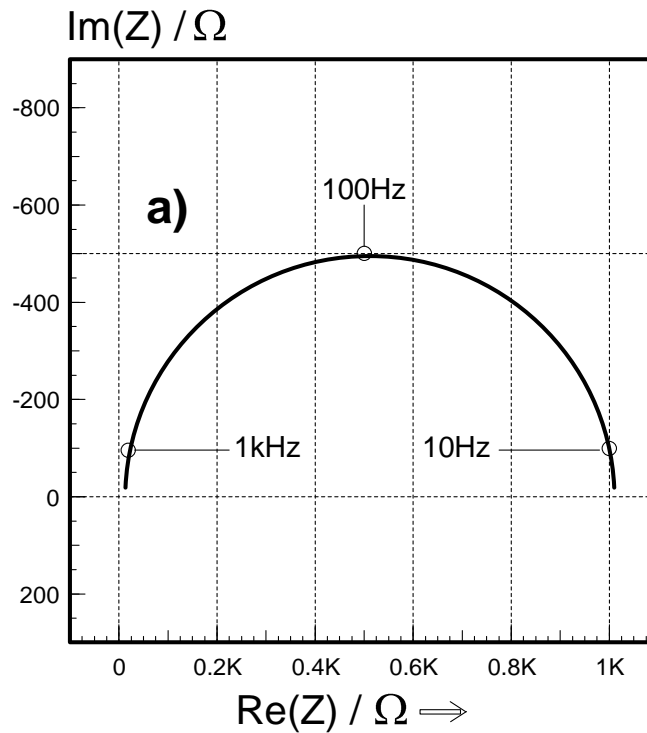
Figure 64: Nyquist plot, originating from Cartesian coordinates (137).

Within the lithium ion battery community impedance measurements are mostly displayed by the Nyquist plot. The main difference compared to the Bode plot, is the fact that phase angle and absolute value of impedance are combined in one graph (and split into real and imaginary part), while the graphical information about the frequency dependence gets lost. Furthermore, the opposite of the imaginary part is generally plotted on the ordinate axis, so that the capacitive loops appear in the upper quadrants (138).

One final aim of an impedance measurement is the creation of a so called equivalent circuit diagram. Equivalent circuits are very common in electrical engineering and science and refer to a theoretical circuit that retains all of the electrical or electrochemical characteristics of a given circuit (139) and can therefore help to simplify analysis, comparison and modeling by computational methods. The most significant equivalent circuit symbols are given in Figure 65.
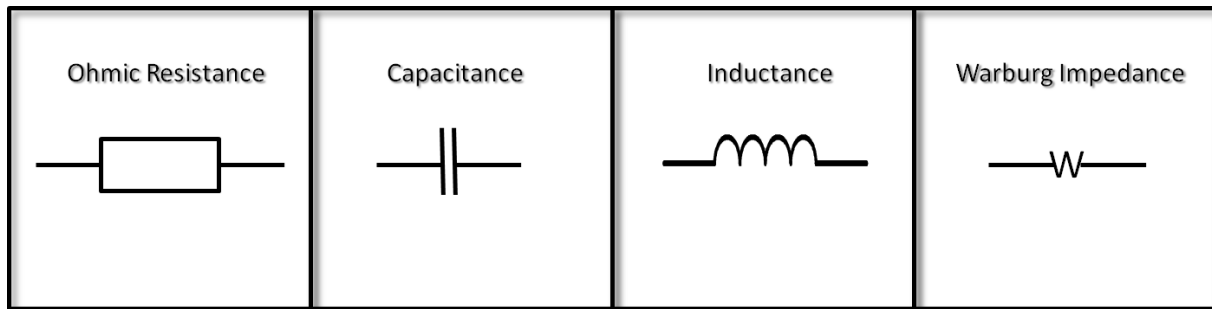
Figure 65: Different types of equivalent circuit symbols for the most common impedances in LIBs.

By using these symbols practically any obtained Nyquist or Bode plot could be translated into an equivalent circuit diagram. A summary of the most common curve shapes in Bode or Nyquist plots, their relating equivalent circuit diagrams and their origin in the battery are displayed in Figure 66.
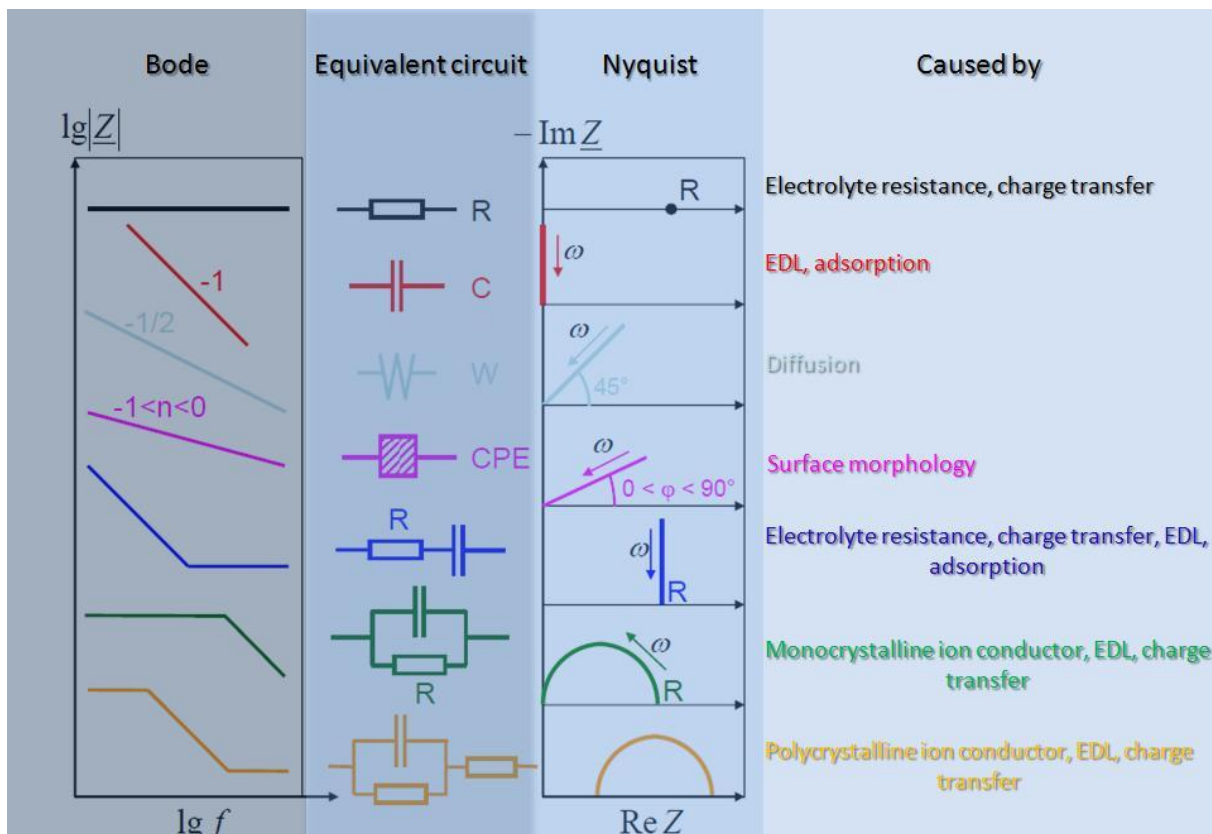
Figure 66: Bode/Nyquist curve shapes and their associated equivalent circuits as well as their origin (140).

Batteries are dynamic systems and impedance spectroscopy can be used for analyzing the dynamic behavior of batteries (138) (141). At low frequencies (below 1 Hz), mass transport effects can be observed, whereas higher frequencies are caused by charge-transfer reactions, double-layer formation and inductive effects. An idealized model of a battery, investigated by impedance spectroscopy is shown in Figure 67.
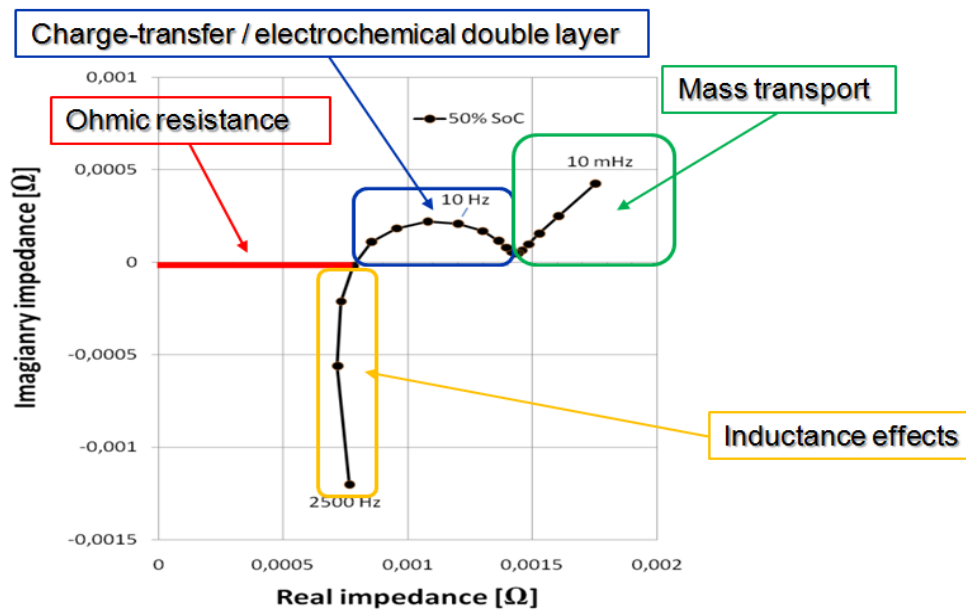
Figure 67: Idealized impedance spectrum of a battery (142).

In this context, it is important to mention that the impedance of a cell corresponds to the sum of all real or imaginary resistances. In practice, this means that the overall impedance of a commercial cell consists of resistance, capacitance and inductance of anode, cathode and electrolyte. Consequently, the impedance spectrum, shown in Figure 67, originates from the influence of all battery components. The differentiation of these impedances is again difficult in a two-electrode arrangement and hence a system with an implemented reference electrode could provide more precise information about the origin of the overall cell impedance.

In a battery the shape and value of the resistance in the impedance spectrum can be strongly affected by solvents, particle sizes, thickness of the electrodes or stack pressure and hence the geometry of the cell (143). Ageing can also have a main influence on the ohmic resistance and the impedance of the system, which can be mainly explained by the formation and growing of surface films on both, the anode and the cathode, as described in chapter 2.2.5. Various investigations were carried out to obtain impedance spectra of electrodes in lithium ion batteries. However, most these investigations aimed either to get information about the electrode/electrolyte interface in half cells (144) (145) (146) (147) or to investigate full cell impedance behavior for the determination of the state of charge or overall ageing effects (138).

Three-electrode arrangements in commercial cells, however, attracted less attention. This could be mainly attributed to the fact that the placement as well as the airtight sealing of reference electrode in industrially manufactured cells is still a main challenge. Three-electrode impedance measurements

were carried out by Dollé et al in 2001, using self-made carbon and lithium cobalt oxide electrodes and lithium-metal and lithium titanate ($Li_4Ti_5O_{12}$) reference electrodes, where the reference was placed exactly in between the working and the counter-electrode (148). Song et al. adapted this build-up and presented three-electrode measurements of a prismatic pouch cell, using a lithium-metal reference, attached on a conducting wire, which was inserted under inert atmosphere (143). The same build-up was used by Nagasubramiam in commercial 18650 cells from Sony (149). However, in all of these measurements, it was necessary to protect the opened cell from air, either in a glass jar (149) or by additional sealing in a hermetic plastic bag (143) (148), to accomplish measurements outside of the glove box and its inert atmosphere.

With the reference arrangement, shown in Figure 43, it was possible to seal the commercial A123 32113 itself without the need of an additional casing, which is in contrast to all measurements shown in literature before. The following impedance measurements were performed on a Biological VMP3 Potentiostat with implemented impedance spectroscopy option. The device is shown in Figure 68.
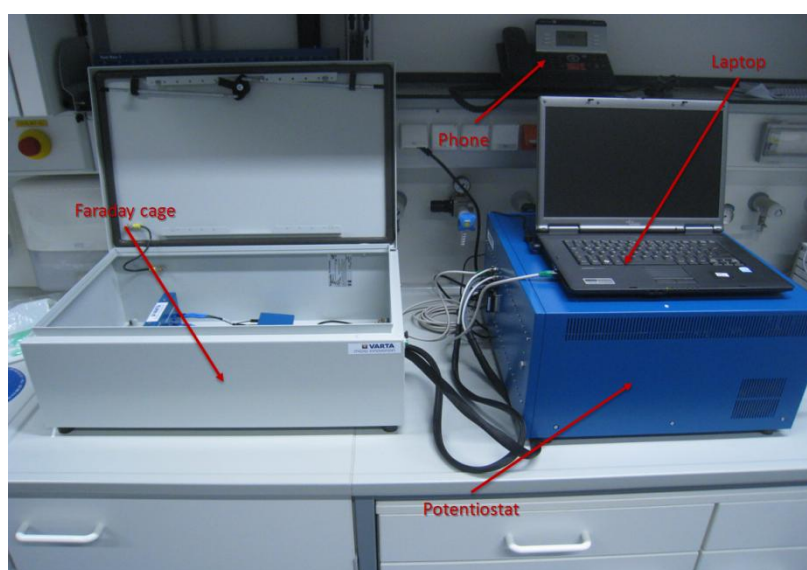
Figure 68: VMP3 measuring station with Faraday cage.

For the impedance measurement the A123 32113 cell was charged to an SOC of 20% and the impedance was recorded for 67 frequencies between 100 kHz and 20 mHz, which consisted of ten data points for the each of the first six decades and seven data points for the last low frequency decade. The cell was measured in a two-electrode arrangement to obtain the overall cell impedance and in a three-electrode arrangement to get information of the anode and cathode impedance, respectively. The associated impedance spectra are displayed as a Nyquist plot in Figure 69.
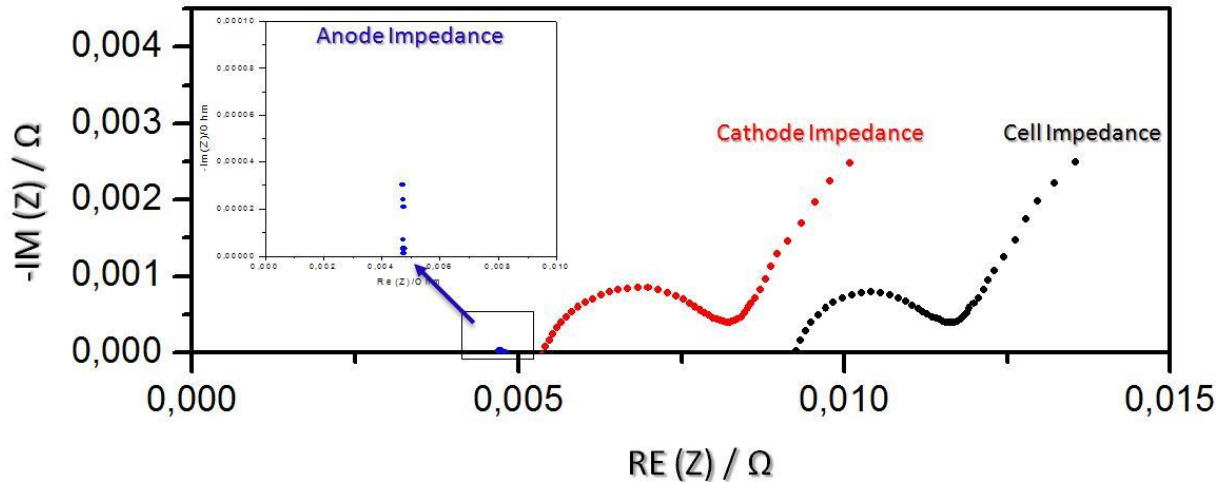
*Figure 69: Impedance spectra of the A123 32113 cell (**black**), its anode (**blue**) and its cathode (**red**) at 20% SOC.*

These impedance measurements revealed a lot of important information. First of all, it had to be noticed that the overall ohmic resistance of the cell was very low, which was essential for the use as a high-power battery in automotive applications. The total ohmic resistance could be obtained by the point of intersection between x-axis and impedance spectrum, which implicated that the imaginary part of the impedance was equal to zero. For this cell the overall resistance amounted to 9.3 mΩ, while a majority of this resistance could be attributed to the cathode resistance (5.3 mΩ). This was in accordance with data from literature, because lithium iron phosphate is a bad electronic conductor by nature, and hence it was reasonable that the cathode participated strongly in the overall ohmic resistance even after carbon-coating of the LFP-particles. However, really remarkable was the anode behavior that could be describe as a straight line, intercepting the x-axis at about 4.7 mΩ. By taking a look on Figure 66, it got obvious that this curve shape was caused by a small ohmic resistance and capacitive impedance, which are connected in series in the equivalent circuit diagram. But due to the fact that no ion conduction was measurable (which would had led to a semicircle in the Bode plot), it had to be assumed that the anode did not take part in the electrochemical reaction, but served just as electrochemical double layer. This, of course, could not be the whole truth.

The reason for this observation was supposed to be due to the geometry of the cell. As a matter of fact, the observed measurement data related always to the anode area that is nearest to the lithium metal reference electrode. The anode material, however, is oversized to impede the plating of metallic lithium at high SOC and/or low temperatures. As a consequence, the negative electrode overlapped the positive at the edge region of the wound and hence created an area, where the diffusion pathways from the cathode through the electrolyte to the anode were very long. This was already observable during the rate capability test in chapter 3.4.2. Impedance spectroscopy is a very fast measurement method, meaning most of the frequencies were scanned in ms up to several

seconds and hence the time was too short to cause a lithiation of the graphite in these edge regions. As a consequence, the only measureable component was the electrolyte/electrode interface, which behaved like a capacitor and led to the observed Nyquist curve shape.

To verify the cell geometry as the main cause for this, another measurement setup had to be found, where the reference electrode could have been placed in between the electrode stack. Unfortunately, this was not possible for the cylindrical cell type due to the fact that there was high pressure on the electrodes and for this reason no space left for the reference. Hence, another cell type was chosen to prove the validity of the previously recorded data. For the reason of availability the so called C-Cell of the company EnerDel was selected as a comparator (see Figure 70). This pouch-bagged battery consisted of a carbonaceous anode combined with a manganese spinel cathode, providing an overall capacity of 1.7 Ah.
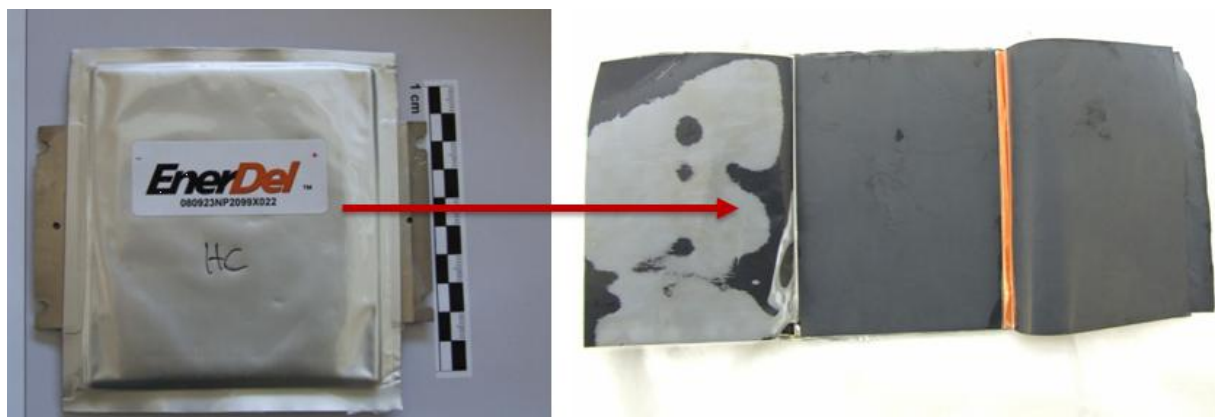
Figure 70: Image of the investigated EnerDel C-Cell.

To implement a reference electrode into this cell type, the procedure of insertion had to be slightly adapted. It was important to prevent bulging of the electrode stack, which would have led to areas of low reactivity, when the straight anode/separator/cathode arrangement got lost. Hence, the reference electrode had to be as flat as possible. An isolated nickel wire served as current collector and a small amount of metallic lithium was brought on its top. The whole operation was made under inert atmosphere and finally the cell was sealed analogously to the A123 32113 cell type. The following impedance measurements are displayed in Figure 71. The procedure and settings remained the same as in the previously showed impedance spectra.
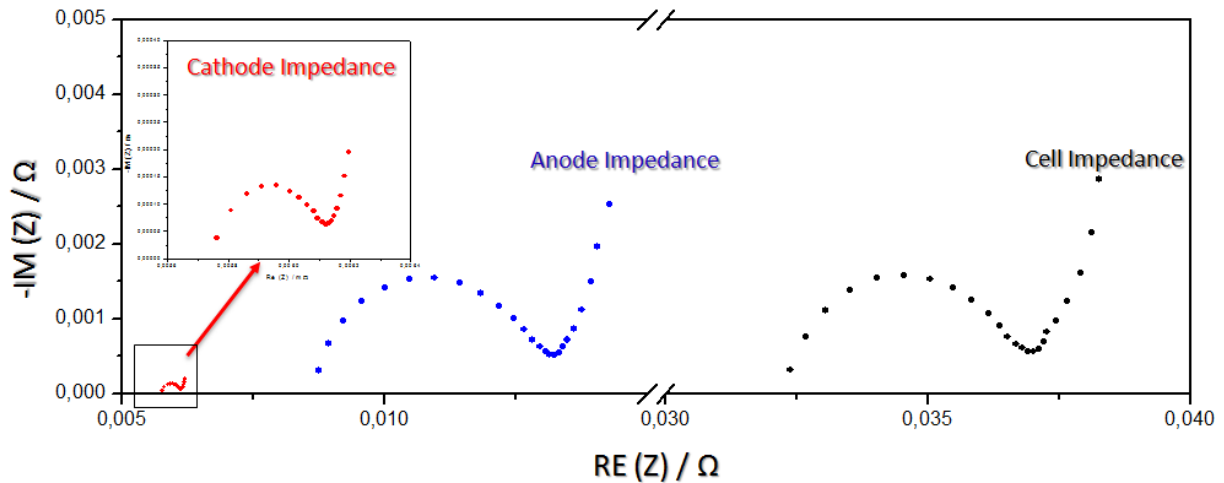
*Figure 71: Impedance spectra of the EnerDel C-Cell (**black**), its anode (**blue**) and its cathode (**red**) at 20% SOC.*

The impedance measurements of the EnerDel C-cell revealed that anode as well as cathode provided a semicircle, as could be seen in Figure 71. This was in good agreement with data shown in literature. However, in contrast to the LFP-based A123 cell, the overall cell impedance was significantly higher, resulting in an ohmic resistance of 32.3 mΩ, while the anode was responsible for the major part of the cell's impedance. The cathode impedance on the other side caused a very small semicircle, which was an indication for a very good electronic and ionic conductivity. Additionally, it was supposed that the smaller semicircle is caused by a relatively small electrolyte/electrode interface due to larger lithium manganese oxide particles.

This experiment proved that the placement of the reference electrode was crucial to get the correct data for the impedance measurement. If it was possible to place the electrode centered and in between the electrodes, correct semicircle for anode as well as cathode could be obtained. Due to the knowledge that the recorded anode impedance was a consequence of the positioning in the electrolyte pool outside of the electrode stack and hence the reflection of the potential field of the anode edge (which was nearest to the reference), the anode data did not attach importance within the next experiment.

3.4.3.1 Ageing Effects and EIS

Of course, electrochemical impedance spectroscopy is excellently suited for the determination of ageing effects in lithium ion batteries. Most ageing effects, especially the growth of electrode/electrolyte surface films cause a change of the overall as well as the electrode's impedance. In the following the same cell, which performed rate capability tests in chapter 3.4.2,

was investigated by EIS. Once again procedure and settings remained the same as in previously showed impedance spectra.
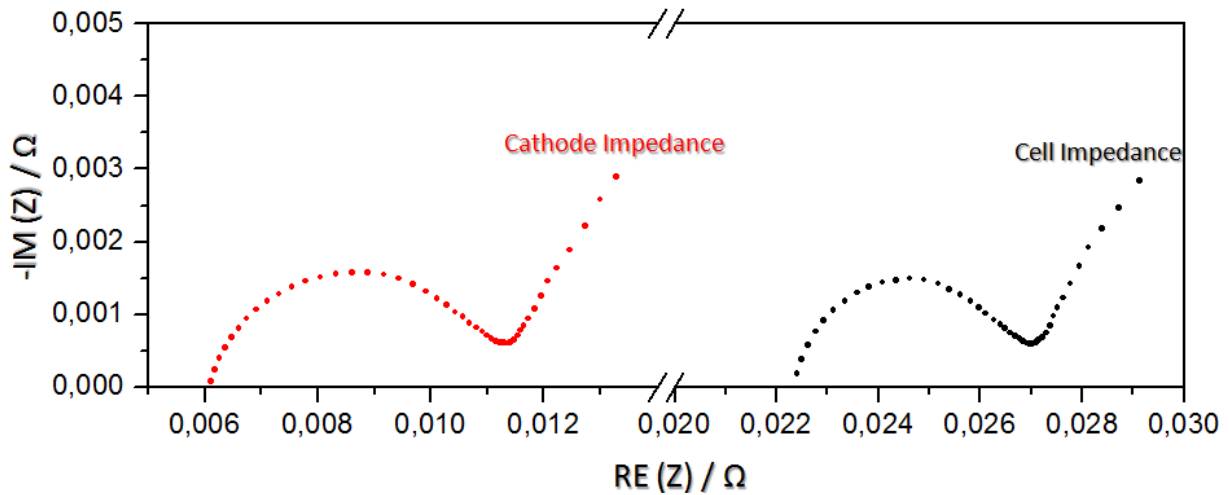
*Figure 72: Impedance spectra of the aged A123 32113 (**black**) and its cathode (**red**) at 20% SOC.*

The impedance spectra of the aged cell and its cathode were displayed in Figure 72. The shape of the semicircles was similar to the new cell. The ohmic resistances, meaning the interception of the branches and the x-axis, changed slightly from 5.3 mΩ to 6.1 mΩ for the LFP cathode, which is in very good agreement with assumptions made in literature. Due to the low redox-potential of lithium iron phosphate, the surface film on the cathode was mainly composed of inorganic oxidation products, originating from the decomposition of the conducting salt. On that account, it could be assumed that the lack of decomposed organic molecules resulted in an only marginally higher ohmic resistance. The overall cell resistance, however, increased significantly from 9.3 mΩ to 22.4 mΩ. For the reason that the cell impedance could be obtained by summing up all impedances of the system, this increase had to be correlated to an increase of the anode resistance. Unfortunately, the anode resistance was not directly available from the measurement. But the observed impedance behavior confirmed the assumptions made in chapter 3.4.2.1, where the anode was determined as the major participant in the cell ageing.
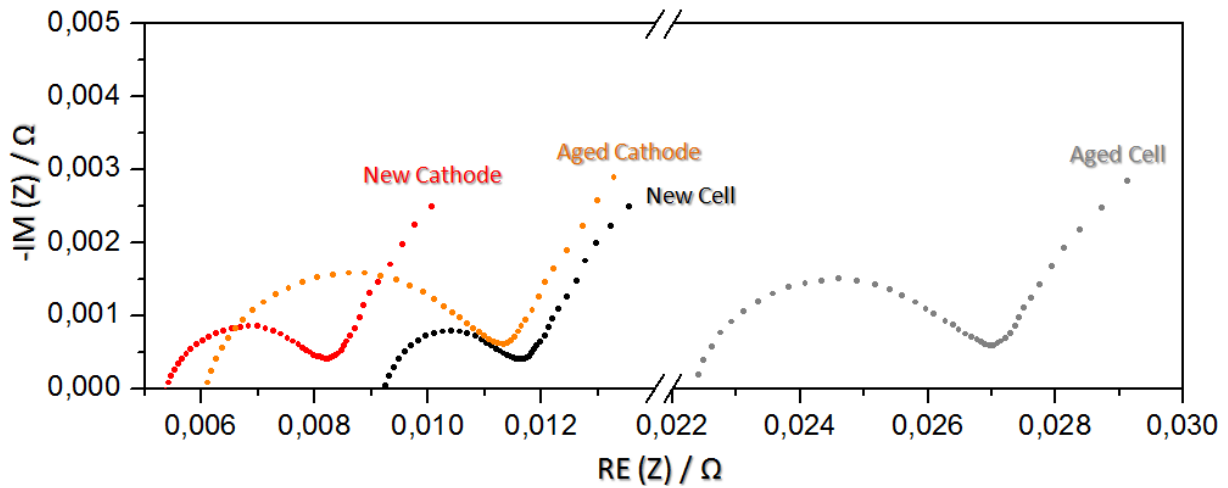
Figure 73: Comparison of the impedance spectra of the aged and the new A123 32113 cell at 20% SOC.

For a better comparison the obtained cell and cathode impedance spectra were once again displayed in one plot (see Figure 73). It was obvious from this graph that not only the real part of the impedance, meaning the ohmic resistance, changed during prolonged cycling, but also the imaginary part. This increase, elucidated by the bigger radius of the first semicircle, had to be related to the electrode/electrolyte interface of the cathode, or more precisely to the double-layer capacitance of this interface. Hence, a change of the morphology of the particle surface could be assumed. Simultaneously, the angle of the beginning second semicircle is almost identical for all four impedance measurements. This slope could be associated with diffusion kinetics within the electrolyte, and on that account, it had to be noticed that the electrolyte did not suffer any restrictions due to prolonged cycling so far.

4 CONCLUSION

While lithium ion batteries dominate the battery sector by now in terms of consumer electronics, their use in automotive applications has only just begun. However, the required improvement of energy and power density makes a substitution of common NiMH batteries by lithium ion systems inevitable in future. Simultaneously, the issue of cell ageing and safety, respectively, is more relevant than ever. The image of the lithium ion battery suffered definitely from media-hyped pictures of burning or even exploding laptops. Although state-of-the-art lithium ion batteries provide a number of safety concepts, including shut-down separators, PTCs or safety vents, it is undeniable that the placement of dozens of batteries with energy contents several hundred times higher than common laptop batteries, presents certain risks in driving vehicles.

Unfortunately, a battery can be regarded as a kind of black box, where only a few parameters can be measured without dismantling of the cell. This includes applied current, cell voltage and temperature. However, processes (especially cell ageing) within a lithium ion battery are very complex and unique for every single battery and therefore a valid model for cycle or calendar life prediction is very hard to achieve.

On that account, it would be advantageous to have an additional sensor within the system that helps to monitor the potential of the positive and negative electrode as well. By this presupposition it would be possible to gain information about the kinetics and balancing of the system and thus to optimize the battery. On the other hand, it would be feasible to identify conditions where undesired side reaction could occur. To be more precise, it would be very auxiliary to have knowledge about the anode potential in order to prevent deposition of metallic lithium and at the same moment to monitor the cathode potential in order to prevent electrolyte decomposition at highly oxidative electrode potentials. Finally, from a scientific point of view, the determination of aging effects either on the anode or on the cathode can't be distinguished in a normal battery system.

The aim of this doctoral thesis was the implementation of such a sensor, videlicet a third electrode, in an industrially manufactured and commercially available battery, namely the cylindrical A123 32113 cell. This third electrode was used as reference point and allowed the investigation of the interaction of anode and cathode and differentiation of ageing effects by electrochemical and most notably non-destructive methods.

First of all, a suitable and preferably non-polarizing reference electrode had to be found. Lithium metal was soon established as the system of choice, which could be easily explained by the fact that

it provided a stable potential over a long period of time. Furthermore, it was beneficial relating to lithium ion batteries because by its use the reference electrode represented the zero grade of the Li/Li$^+$ scale, which was widely used to describe electrode potentials within the lithium ion battery community.

First measurements were made to prove the accuracy of the system (see Figure 45 and Figure 46). The obtained data were consistent and in the following further investigations aimed to monitor the nature of positive and negative electrode behavior.

On the one hand, GITT-experiments (Figure 49) revealed that the cell voltage was strongly influenced by the cathode potential, whereas hardly any overpotential effect was observable at the anode side, which led to the insight that the negative electrode was not only oversized in terms of capacity, but also provided faster kinetics than the positive electrode. Furthermore, a static hysteresis effects was observed, which could be attributed to the cathode as well. The reason for this hysteresis could be probably assigned to different Li$^+$ diffusion kinetics in LiFePO$_4$/FePO$_4$. As a matter of fact, this voltage hysteresis was undesired, because it impeded the determination of the state of charge by the steady-state voltage. This problem could admittedly investigated by a three-electrode system, however, SOC determination was neither possible by using the electrode potentials, because the cathode was the origin of the voltage hysteresis, so the use of the cathode potential for SOC determination was not feasible. On the other hand, the anode potential did not change over a wide SOC anyway due to its over-dimensioning and thus could not reveal SOC information too.

In the following, ageing effects of lithium ion batteries were investigated. For that reason, rate capability test as well as electrochemical impedance spectroscopy experiments were performed and the results of new cells and aged cells with a cycle life of about 2,000 hours were compared.

The rate capability tests, shown in Figure 54 - Figure 61, revealed that the overall ageing of the cell could be mainly attributed to the ageing of the anode. The data clearly indicated that the recorded loss of capacity went side by side with an increase of overpotential at the negative side, which led to an obvious voltage shift towards lower anode potentials. However, a power fade was not observed, which could be explained by the fact that the cathode still was the kinetically limiting factor in the battery.

This proposition was confirmed by the conducted three-electrode impedance measurements, displayed in Figure 69 - Figure 71. From these experiments it was obvious that the ohmic resistance of the LFP cathode changed slightly from 5.3 mΩ to 6.1 mΩ, whereas the overall cell resistance increased significantly from 9.3 mΩ to 22.4 mΩ. Due to the cell geometry and the associated reference electrode placement the anode resistance was not directly available from the

measurement, but as a matter of fact, this increase of cell resistance had to be correlated to an increase of the anode resistance for the reason that the cell impedance could be obtained by summing up all impedances of the system. By considering Table 5 this impedance rise could be assigned to the continuous growth of the solid electrolyte interphase. Furthermore, a bigger radius for the first semicircle of the cathode impedance was observable, which had to be correlated with a change of the surface morphology of the LFP particles.

In conclusion, the developed experimental arrangement successfully allowed to characterize the investigated system by the implementation of a lithium metal reference electrode. Not only could this setup reveal the origin of static hysteresis in LFP-based lithium ion batteries, but also determine ageing effects and attribute them to one of the both electrodes. In the investigated system, the negative electrode could be revealed as the main origin of cell ageing. This could be assigned to the continuous growth of the solid electrolyte interphase for the most part.

In terms of safety and SOH-prediction such a reference system would be advantageous in any large-sized lithium ion battery. Although an implementation of a reference point during processing by the manufacturer itself would be preferable, the introduced reference system could be also subsequently implemented in industrially manufactured cells without a great deal of time and effort.

5 APPENDIX

5.1 LIST OF ABBREVIATIONS

18650...	cylindrical cell with a diameter of 18 mm and a length of 65 mm
32113...	cylindrical cell with a diameter of 32 mm and a length of 113 mm
1C...	current that accomplishes full charge/discharge in one hour
AC...	alternating current
BMS...	battery management system
CC...	constant current
CV...	cyclic voltammetry
DC...	direct current
DEC...	diethyl carbonate
DOD...	depth of discharge
E...	voltage
EC...	ethylene carbonate
EDL...	electrochemical double layer
EIS...	electrochemical impedance spectroscopy
EUCAR	European Council for Automotive R&D
EV...	electric vehicle
GITT...	galvanostatic intermittent titration technique
HEV...	hybrid electric vehicle
I...	current
LFP...	lithium ion phosphate
LIB...	lithium ion battery
NaCMC...	sodium carboxymethylcellulose
NHE...	normal hydrogen electrode
NiMH...	nickel-metal hydride
OCV...	open circuit voltage
PC...	propylene carbonate
PE...	polyethylene
PHEV...	plug-in hybrid electric vehicle
PP...	polypropylene
PTC...	positive temperature coefficient
PVdF...	polyvinylidendifluoride
R...	resistance
SBR...	styrene butadiene rubber
SEI...	solid electrolyte interphase
SEM...	scanning electron microscopy
SOC...	state of charge
SOH...	state of health
VC...	vinylencarbonate
Z...	impedance

5.2 LIST OF FIGURES

5.3 LIST OF TABLES

5.4 REFERENCES

1. http://en.wikipedia.org/. [Online] http://en.wikipedia.org/wiki/Energy_and_society.

2. http://www.grida.no. [Online] http://www.grida.no/climate/ipcc_tar/slides/ppt/02.01.ppt.

3. http://www.tecson.de/historische-oelpreise.html. [Online]

4. http://www.eucar.be. [Online] http://www.eucar.be/affordability-and-
competitiveness/publications/EUCAR%20FOCUS%202009_Web.pdf.

5. http://ec.europa.eu/. [Online] http://ec.europa.eu/research/energy/pdf/expert_workshops.pdf.

6. http://en.wikipedia.org/. [Online] http://en.wikipedia.org/wiki/Gasoline.

7. http://www.eucar.be/. [Online] http://www.eucar.be/energy-and-
environment/publications/The%20Electrification%20of%20the%20Vehicle%20and%20the%20Urban
%20Transport%20System.pdf.

8. http://en.wikipedia.org. [Online] http://en.wikipedia.org/wiki/Baghdad_Battery.

9. http://scienceworld.wolfram.com. [Online]
http://scienceworld.wolfram.com/biography/Galvani.html.

10. http://en.wikipedia.org. [Online] http://en.wikipedia.org/wiki/Voltaic_pile.

11. **H. Berg,** Johann Wilhelm Ritter. *Review of Polarography.* **2008**, Vol. 54, 2.

12. http://en.wikipedia.org. [Online] http://en.wikipedia.org/wiki/History_of_the_battery.

13. http://de.wikipedia.org. [Online] http://de.wikipedia.org/wiki/Bleiakkumulator.

14. **A. J. Salkind, J. J. Kelley, A. G. Cannone.** [book auth.] D. Linden. *Handbook of Batteries.* **1995**, 24.

15. http://en.wikipedia.org. [Online] http://en.wikipedia.org/wiki/Nickel-cadmium_battery.

16. **W. Schalkwijk, B. Scrosati.** *Advances in Lithium Ion Batteries.* **2002**.

17. **L.F. Nazar, O. Crosnier.** Anodes and Composite Anodes: An Overview. [book auth.] G. Pistoia G.
Nazri. *Lithium Batteries - Science and Technology.* **2004**.

18. **J.B. Goodenough, K. Mizushima.** *GB 11953/79* United Kingdom, **1979**.

19. **K. Matsuki, K. Ozawa.** *Lithium Ion Rechargeable Batteries.* **2009**.

20. http://batteryuniversity.com. [Online]
http://batteryuniversity.com/learn/article/global_battery_markets.

21. **W. Tillmetz,** http://www.fvee.de. [Online]
http://www.fvee.de/fileadmin/publikationen/Workshopbaende/ws2010-1/ws2010-
1_09_Tillmetz.pdf.

22. **G. Hambitzer, K. Pinkwart, C. Ripp, C. Schiller.** Thermodynamics and Mechanistics. [book auth.] J.O. Besenhard. *Handbook of Battery Materials.* **1999**.

23. http://www.iwr.de. [Online] http://www.iwr.de/news.php?id=17259.

24. http://www.allaboutbatteries.com/. [Online] http://www.allaboutbatteries.com/battery-markets.html.

25. **C. Pellet,** *HEV, P-HEV& EV Market* ***2010****.*

26. **M. Anderman,** http://www.advancedautobat.com/press/05-30-11_cars21-header02.html. [Online]

27. **D. Linden,** Basic Concepts. *Handbook of Batteries.* **1995**.

28. http://de.wikipedia.org/. [Online] http://de.wikipedia.org/wiki/Daniell-Element.

29. **P. Atkins,** *Physikalische Chemie.* s.l. : Wiley-VCH, **2001**.

30. http://en.wikipedia.org/. [Online] http://en.wikipedia.org/wiki/Standard_electrode_potential_(data_page).

31. http://en.wikipedia.org/wiki/. [Online] http://en.wikipedia.org/wiki/Open-circuit_voltage.

32. **C. Hamann, A. Hamnett, W. Vielstich.** *Electrochemistry.* **1998**.

33. **M. Winter, R.J. Brodd.** *Chemical Reviews.* **2004**, 104, pp. 4245-4270.

34. **Pohlmann, Ludwig.** http://userpage.fu-berlin.de/. [Online] http://userpage.fu-berlin.de/~lap/PCIII_EC_4.pdf.

35. http://www.chemgapedia.de. [Online] http://www.chemgapedia.de/vsengine/vlu/vsc/de/ch/13/vlu/echemie/grundlagen/echemie_grundlagen.vlu/Page/vsc/de/ch/13/pc/echemie/grundlagen/doppelschichtmodell.vscml.html.

36. http://de.wikipedia.org/. [Online] http://de.wikipedia.org/wiki/Ionenst%C3%A4rke.

37. http://en.wikipedia.org/. [Online] http://en.wikipedia.org/wiki/Capacitance.

38. **L. Kaltenböck,** Diploma Thesis. **2010**.

39. http://en.wikipedia.org/. [Online] http://en.wikipedia.org/wiki/Electrical_resistance.

40. **H. Ebert,** *Elektrochemie.* **1979**.

41. http://www.ecochemie.nl/. [Online] http://www.ecochemie.nl/export/Homepages/Autolab/download/Applicationnotes/Appl022.pdf.

42. **M.Winter, K.C. Moeller, J.O. Besenhard.** Carbonaceous and Graphitic Anodes. [book auth.] G. Pistoia G. Nazri. *Lithium Batteries - Science and Technology.* **2004**.

43. **K. Nishio, N. Furukawa.** Practical Batteries. [book auth.] J.O. Besenhard. *Handbook of Battery Materials.* **1999**.

44. **B. Scrosati, J. Garche.** *Journal of Power Sources.* 2010, 195, pp. 2419–2430.

45. **Y. Hamon, T. Brousse, F. Jousse, P. Topart, P. Buvat, D.M. Schleich.** *Journal of Power Sources.* 2001, 97-98, pp. 185-187.

46. **A. Manthiram,** Materials Aspects: An Overview. [book auth.] G. Pistoia G. Nazri. *Lithium Batteries - Science and Technology.* 2004.

47. **J.B. Goodenough, Y. Kim.** *Chem. Mater.* **2010**, 22, pp. 587-603.

48. **M. Winter, J.O. Besenhard, M. E. Spahr, P. Novak.** *Advanced Materials.* 10, **1998**.

49. **S. Koller, M. Schmuck.** Lecture. *Primäre und wiederaufladbare Lithium-Batterien.* Graz Univerity of Technology : s.n., **2009**.

50. **N. S. Hochgatterer, M. R. Schweiger, S. Koller, P. R. Raimann,T. Wöhrle, C. Wurm, M. Winter.** *Electrochemical and Solid State Letters.* 2008, 11,pp. A76-A80.

51. **Z. Ogumi, M. Inaba.** Carbon Anodes. [book auth.] B. Scrosati W. A. van Schalkwijk. *Advances in Lithium Ion Batteries.* **2002**.

52. **K. Kinoshita,** Carbons. [book auth.] J.O. Besenhard. *Handbook of Battery Materials.* **1999**.

53. **S. J. Harris, A. Timmons, D. R. Baker, C. Monroe.** *Chemical Physics Letters.* 2010, 485, pp. 265-274.

54. **J.R. Dahn,** *Physical Review B.* 44, **1991**, pp. 9170-9177.

55. **D. Aurbach, B. Markovskya, I. Weissmana, E. Levia, Y. Ein-Elib.** *Electrochimica Acta.* **1999**, 45, pp. 67-86.

56. **M. Winter, J.O. Besenhard.** *Chemie in unserer Zeit.* **1999**, 6, pp. 320-332.

57. **J. Wolfenstine, J. Allen.** *Journal of Power Sources.* **2005**, 142.

58. **G. Ceder, G. Hautier, A. Jain, S.P.Ong.** *Materials Research Bulletin.* **2011**, 39.

59. **M. M. Thackeray,** The Structural Stability of Transition Metal Oxide Insertion Electrodes for Lithium Batteries. [book auth.] J.O. Besenhard. *Handbook of Battery Materials.* **1999**.

60. **B. L. Ellis, K. T. Lee, L. F. Nazar.** *Chem. Mater.* **2010**, 22, pp. 691-714.

61. http://en.wikipedia.org/. [Online] http://en.wikipedia.org/wiki/File:Lithium-cobalt-oxide-3D-polyhedra.png.

62. **M. S. Whittingham,** Lithium Batteries and Cathode Materials. *Chem. Rev.* **2004**, 104, pp. 4271-4301.

63. **J.B. Goodenough,** *Journal of Power Sources.* **2007**, 174, pp. 996-1000.

64. **M. M. Thackeray,** *Journal of Electrochemical Society.* **1995**, 142.

65. **J.W. Fergus,** *Journal of Power Sources.* **2010**, 195, pp. 939-954.

66. **M. M. Thackeray, W.I.F. David, P.G. Bruce , J.B. Goodenough.** *Materials Research Bulletin.* **1983**, 18, pp. 461-472.

67. **L. Chen, J. Schoonman.** *Solid State Ionics.* **1993**, 67.

68. **T. Ohzukua, R. J. Brodd.** *Journal of Power Sources.* **2007**, 174, pp. 449–456.

69. **Q. Luo, T. Muraliganth and A. Manthiram,** *Solid State Ionics.* **2009**, 180, pp. 703-707.

70. **K. S. Nanjundaswamy, A. K. Padhi, J. B. Goodenough, S. Okada, H. Ohtsuka, H. Arai and J. Yamaki.** *Solid state ionics.* **1996**, 92, pp. 1-10.

71. **A. K. Padhi, K. S. Nanjundaswamy, J. B. Goodenough.** *Journal of Electrochemical Society.* **1997**, 144, pp. 1188-1194.

72. **S. Okada, J. Yamaki.** Iron-Based Rare-Metal-Free Cathodes. [book auth.] K. Ozawa. *Lithium Ion Rechargeable Batteries.* **2009**.

73. **C. Masquelier, S. Patoux, C. Wurm, M. Morcrette.** Polyanion-based positive electrode materials. [book auth.] G. Pistoia G. Nazri. *Lithium Batteries - Science and Technology.* **2004**.

74. **M. M. Thackeray,** *Journal of Power Sources.* **2001**, 97-98,pp. 7-12.

75. http://www4.nau.edu/. [Online] http://www4.nau.edu/meteorite/Meteorite/Images/OlivineStructure.jpg.

76. **J. B. Goodenough,** Oxide Cathodes. [book auth.] B. Scrosati W. A. van Schalkwijk. *Advances in Lithium Ion Batteries.* 2002.

77. **D. Morgan, A. van der Ven, G. Ceder.** *Electrochemical and Solid-State Letters.* **2004**, 7, pp. A30-A32.

78. **C.V. Ramana, A. Mauger, F. Gendron, C.M. Julien, K. Zaghib.** *Journal of Power Sources.* **2009**, 187,pp. 555–564.

79. **A. Yamada, S. C. Chung, K. Hinokuma.** *Journal of Electrochemical Society.* **2001**, 148, pp. A224-A229.

80. **N. Ravet, Y. Chouinard, J.F. Magnan, S. Besner, M. Gauthier, M. Armand.** *Journal of Power Sources.* **2001**, 97-98, pp. 503-507.

81. **G. Arnold, J. Garche, R. Hemmer, S. Ströbele, C. Vogler, M. Wohlfahrt-Mehrens.** *Journal of Power Sources.* **2003**, 119-121, pp. 247–251.

82. **M. Nazri,** Liquid Electrolytes: Some Theoretical and Practical Aspects. [book auth.] G. Pistoia G. Nazri. *Lithium Batteries - Science and Technology.* **2004**.

83. **S. Hossain,** Rechargeable Lithium Batteries. [book auth.] D. Linden. *Handbook of Batteries.* **1995**.

84. **M. Schmuck, S. Koller.** *Lecture. Primäre und wiederaufladbare Lithium-Batterien.* **2007**.

85. **G. E. Blomgren,** *Journal of Power Sources.* **2003**, 119–121, pp. 326–329.

86. http://msds.chem.ox.ac.uk. [Online]
http://msds.chem.ox.ac.uk/LI/lithium_hexafluorophosphate.html.

87. **K. Xu,** *Chem. Rev.* **2004**, 104, pp. 4303-4417.

88. **J. Barthel, H.J. Gores.** Liquid Nonaqueous Electrolytes. [book auth.] J.O. Besenhard. *Handbook of Battery Materials.* **1999**.

89. **J. Yamaki,** Liquid Electrolytes. [book auth.] B. Scrosati W. van Schalkwijk. *Advances in Lithium Ion Batteries.* **2002**.

90. **Q. Zhu, Y. Song, X. Zhu and X. Wang.** *Journal of Electroanalytical Chemistry.* **2007**, 601, pp. 229-236.

91. **P. Verma, P. Maire, P. Novak.** *Electrochimica Acta.* **2010**, 55, pp. 6332-6341.

92. **E. Peled,** *Journal of Electrochemical Society.* **1979**, pp. 2047-2051.

93. **E. Peled, D. Golodnitsky and J. Penciner.** The Anode/Electrolyte Interface. [book auth.] J.O. Besenhard. *Handbook of Battery Materials.* **1999**.

94. **R. Imhof, P. Novak.** *Journal of Power Sources.* **1998**, 145, pp. 1081-1087.

95. **E. Peled, D. Bar Tow, A. merson, A. Gladkich, L. Burstein, D. Goldonitsky.** *Journal of Power Sources.* **2001**, 97-98, pp. 52-57.

96. **G. Ardel, D. Golodnitsky, E. Peled.** Journal of Electrochemical Society. **1997**, 144.

97. **M. Winter, J. O. Besenhard.** *Chemie in unserer Zeit.* **1999**, 6, pp. 320-332.

98. **M. Broussely, , a, Ph. Blanchardb, Ph. Biensanb, J. P. Planchata, K. Nechevc and R. J. Staniewiczc.** *Journal of Power Sources.* **2003**, 119-121, pp. 859-864.

99. **D. Aurbach, A. Schechter.** Advanced Liquid Electrolyte Solutions. [book auth.] G. Pistoia G. Nazri. *Lithium Batteries - Science and Technology.* **2004**.

100. **S.K. Martha, E. Markevich, V. Burgel, G. Salitra, e. Zinigrad, B. Markovsky, H. Sclar, Z. Pramovich, O. Heik, D. Aurbach, I. Exnar, H. Buq, T. Drezen, G. Semrau, M. Schmidt, D. Kovacheva, N. Saliyski.** *Journal of Power Sources.* **2009**, 189, pp. 288-296.

101. **K. Edström, T. Gustrafsson, J.O. Thomas.** *Electrochimica Acta.* **2004**, 50, pp. 397-403.

102. **W. Böhnstedt,** Separators. [book auth.] J.O. Besenhard. *Handbook of Battery Materials.* **1999**.

103. **P. Arora, Z. Zhang.** Battery Separators. *Chemical Reviews.* **2004**, 104, pp. 4419-4462.

104. **M. Broussely,** Aging mechanisms and calendar life predictions in lithium ion batteries. [book auth.] B. Scrosati W.A. van Schalkwijk. *Advances in Lithium Ion Batteries.* **2002**.

105. **J. Vetter, P. Novak, M.R. Wagner, C. Veit, K.-C. Möller, J.O. Besenhard, M. Winter, M. Wohlfart-Mehrens, C. Vogler, A. Hammouche.** *Journal of Power Sources.* **2005**, 147, pp. 269-281.

106. **Y. Wang, X. Guo, S. Greenbaum, J. Liu.** *Electrochemical and Solid-State Letters.* **2001**, 4, pp. A68-A70.

107. **R. Spotnitz, J. Franklin.** *Journal of Power Sources.* **2003**, 113, pp. 81–100.

108. **D. Aurbach, E. Zinigrad, Y. Cohne, H. Teller.** *Solid State Ionics.* **2002**, 148, pp. 405-416.

109. **N. Dupré, J. Martin, J. Degryse, V. Fernandez, P. Soudan and D. Guyomard.** *Journal of Power Sources.* **2010**, 195,pp. 7415-7425.

110. **R. Imhof, P. Novak.** *Journal of Electrochemical Society.* **1999**, 146, pp. 1702-1706.

111. **D.P. Abraham, E.P. Roth, R. Kostecki, K. McCarthy, S. MacLaren, D.H. Doughty.** *Journal of Power Sources.* **2006**, 161, pp. 648–657.

112. **T. Ohsaki, T. Kishi, T.i Kuboki, N. Takami, N. Shimura, Y. Sato, M. Sekino, A. Satoh.** Overcharge reaction of lithium-ion batteries. *Journal of Power Sources.* **2005**, 146, pp. 97–100.

113. **R. Spotnitz,** Scale-up of Lithium Ion Cells and Batteries. [book auth.] B. Scrosati W. A. van Schalkwijk. *Advances in Lithium Ion Batteries.* **2002**.

114. http://www.gebattery.com.cn/. [Online]. http://www.gebattery.com.cn/geb/Upload/image/Cylindrical%20Battery/cb1.jpg.

115. http://www.technick.net. [Online] http://www.technick.net/images/guide_bpw2/c03_04.gif.

116. **H. Horie,** Research and Development Work on Advanced Lithium-Ion Batteries for High-Performance Environmental Vehicles. [book auth.] K. Ozawa. *Lithium Ion Rechargeable Batteries.* **2009**.

117. **M. Broussely,** Lithium-Ion Batteries for EV, HEV and other industrial Applications. [book auth.] G. Pistoia G. Nazri. *Lithium Batteries - Science and Technology.* **2004**.

118. **P.G. Balakrishnan, R. Ramesh, T. Prem Kumar.** *Journal of Power Sources.* **2006**, 155, pp. 401-414.

119. **D. Lisbona, T. Snee.** *Process Safety and Environmental Protection.* **2011**.

120. **C. L. Campion, W. Li, W.B. Euler, B. L. Lucht, B. Ravdel, J. F. DiCarlo, R. Gitzendanner, and K. M. Abraham** *Electrochemical and Solid-State Letters.* **2004**, 7, pp. A194-A197.

121. **Q. Wu, W. Lu, J. Prakash.** *Journal of Power Sources.* **2000**, 88, pp. 237-242.

122. http://www.a123systems.com/. [Online]. http://www.a123systems.com/products-cell-32113-cylindrical-cell.htm.

123. http://euclid.ucc.ie/hysteresis/. [Online] http://euclid.ucc.ie/hysteresis/node3.htm.

124. **V. Srinivasan, J. W. Weidner, J. Newman.** *Journal of Electrochemical Society.* **2001**, 148, pp. A969-A980.

125. http://en.wikipedia.org/. [Online] 2011. http://en.wikipedia.org/wiki/Hysteresis.

126. **M. Thele, O. Bohlen, D. U. Sauer, E. Karden.** *Journal of Power Sources.* **2008**, 175, pp. 635–643.

127. **D. Aurbach, B. Markovsky, A. Rodkin, M. Cojocaru, E. Levi, H. Kim.** *Electrochimica Acta.* **2002**, 47, pp. 1899-1911.

128. **Q. Wu, W. Lu, J. Prakash.** *Journal of Power Sources.* **2000**, 88, pp. 237-242.

129. **D. P. Abraham, S. D. Poppen, A. N. Jansen, J. Liu, D. W. Dees.** *Electrochimica Acta.* **2004**, 49, pp. 4763–4775.

130. **W. Weppner, R.A. Huggins.** *Journal of Solid State Chemistry.* **1977**, 22, pp. 297-308.

131. **X.H. Rui, N. Ding, J. Liu, C. Li, C.H. Chen.** *Electrochimica Acta.* **2010**, 55, pp. 2384-2390.

132. **K. Ta, J. Newman.** *Journal of Electrochemical Society.* **1999**, 146, pp. 2769-2779.

133. **T. Zheng, J.R. Dahn.** *Journal of Power Sources.* **1997**, 68, pp. 201-203.

134. **H. Matsui, T. Nakamura, Y. Kobayashi, M. Tabuchi, Y. Yamada.** *Journal of Power Sources.* **2010**, 195, pp. 6879-6883.

135. **A. N. Jansen, D. W. Dees, D. P. Abraham, K. Amine, G. L. Henriksen.** *Journal of Power Sources.* **2007**, 174, pp. 373–379.

136. **H. Göhr,** Thaler's IM& Owners Manual. *About contribution of certain electrode processes to the impedance.*

137. **W. Strunz,** bscw-izs.izs.fhg.de. [Online] bscw-izs.izs.fhg.de/pub/bscw.cgi/d673118/Vortrag%20Impedanz.ppt.

138. **F. Huet,** *Journal of Power Sources.* **1998**, 70, pp. 59-69.

139. http://en.wikipedia.org/wiki. [Online] http://en.wikipedia.org/wiki/Equivalent_circuit.

140. **G. Fafilek,** *Impedanzspektroskopie.* **2008**. Impedanzspektroskopie.

141. **A. Jossen,** *Journal of Power Sources.* **2006**, 154, pp. 530–538.

142. **J.L. Jespersen, A.E. Tønnesen, K. Nørregaard, L. Overgaard, F. Elefsen.** *World Electric Vehicle Journal .* **2009**, 3.

143. **J.Y. Song, H.H. Lee, Y.Y. Wang, C.C. Wan.** *Journal of Power Sources.* **2002**, 111, pp. 255-267.

144. **D. Aurbach, B. Markovsky, M.D. Levi, E. Levi, A. Schechter, M. Moshkovich, Y. Cohen.** *Journal of Power Sources.* **1999**, 81-82, pp. 95-111.

145. **C.R. Yang, J.Y. Song, Y.Y. Wang and C.C. Wan.** *Journal of Applied Electrochemistry.* **2000**, 30, pp. 29-34.

146. **D. Aurbacha, B. Markovsky, I. Weissman, E. Levi, Y. Ein-Eli.** *Electrochimica Acta.* **1999**, 45, pp. 67-86.

147. **K. Sawai, R. Yamato, T. Ohzuku.** *Electrochimica Acta.* **2006**, 51, pp. 1651–1655.

148. **M. Dolle, F. Orsini, A. S. Gozdz, J. Tarascon.** *Journal of Electrochemical Society.* **2001**, 148, pp. A851-A857.

149. **Nagasubramanian, G.** *Journal of Power Sources.* **2000**, 87, pp. 226-229.